Contributions to Mineralogy and Petrology

Fe3+ partitioning systematics between orthopyroxene and garnet in mantle peridotite xenoliths and implications for thermobarometry of oxidized and reduced mantle rocks

--Manuscript Draft--

Manuscript Number:	CTMP-D-14-00145R1
Full Title:	Fe3+ partitioning systematics between orthopyroxene and garnet in mantle peridotite xenoliths and implications for thermobarometry of oxidized and reduced mantle rocks
Article Type:	Original Paper
Keywords:	Ferric iron; Orthopyroxene; Garnet; Mantle xenoliths; Thermobarometry
Corresponding Author:	Paolo Nimis Università di Padova Padova, ITALY
Corresponding Author Secondary Information:	
Corresponding Author's Institution:	Università di Padova
Corresponding Author's Secondary Institution:	
First Author:	Paolo Nimis
First Author Secondary Information:	
Order of Authors:	Paolo Nimis
	Alexey Goncharov
	Dmitri A. Ionov
	Catherine McCammon
Order of Authors Secondary Information:	
Abstract:	We have investigated the partitioning of Fe3+ between orthopyroxene (Opx) and garnet (Grt) in well-equilibrated mantle xenoliths using Mössbauer spectroscopy. The samples cover a wide range of P-T conditions (2.1-6.6 GPa, 690-1,412 °C) and geothermal gradients, and are thus representative for Earth's upper mantle in both on-craton and off-craton continental settings. Garnet has Fe3+/Fetot ratios of 0.03-0.13 and Fe2O3 contents of 0.24-1.00 wt%. Orthopyroxene has, on average, lower Fe3+/Fetot ratios (0.01-0.09) and Fe2O3 contents (0.05-0.63 wt%). In low-pressure, high-temperature samples, however, Opx is systematically richer in Fe2O3 than the coexisting Grt. The Fe3+ Opx/Grt partition coefficient (DFe3+ Opx/Grt) shows no obvious relationship with temperature, but increases with decreasing pressure and with increasing NaOpx. The observed Opx/Grt Fe3+ systematics imply that the Opx-Grt Fe-Mg exchange thermometer is not robust against redox changes if total Fe is treated as Fe2+. An approximate evaluation of errors on T estimates due to redox effects predicts negligible deviations for strongly reduced conditions (< 65 °C), but potentially large deviations (> to >> 100 °C) for strongly oxidized conditions, especially at very high pressure and when both P and T are calculated by iteration.
Response to Reviewers:	Our replies to the Reviewers' specific comments are listed here and introduced by the notation "R -". Reviewer #1 I) The role of clinopyroxene Among mantle minerals clinopyroxene should not be neglected since it is the phase that most incorporates Fe3+ among mantle minerals… R - We have added Mössbauer data for Cpx in nine of our xenoliths (the others were either two small-sized or contained too little Cpx to obtain sufficient separates). The results are now briefly described in the “Mössbauer analysis” section, presented in new Table 5, and discussed in the “Results” section. Since the aim of the paper is

investigating Opx–Grt relationships, only the aspects that may have some bearing on the incorporation of Fe3+ in Opx and Grt are discussed in detail.

As an example some confusion arises at P. 12, L. 1-13, where the authors wrote that "the Fe3+ opx/grt partition coefficient shows no relationship with T and a roughly negative correlation with P ... in contrast with data of clinopyroxene-garnet pairs..." This comparison is useless without considering all the phases that may incorporate Fe3+ at equilibrium.
R - We have added a two-plot Figure (now Fig. 5a,b) which summarizes the Fe3+ partitioning behavior of Cpx vs. Grt and Opx.

Why lherzolites sample from Dariganga are the only ones with lnDFe3+(opx/grt)>0 (Fig. 3), whereas harzburgites not?
R - The Dariganga xenoliths are not the only ones with significant modal abundances of Cpx. To avoid confusion, we have added a new Table (now Table 1) with main petrographic and compositional features of our xenoliths and clarified the text where needed. Clearly, the abundance of Cpx cannot account for the systematic displacement of the off-craton Dariganga samples from the on-craton samples in terms of Opx/Grt Fe3+ distribution.

II) Redox conditions versus oxygen fugacity
…I profit to make a general comment that might go beyond the goal of this work…
…Tens of works use to claim that oxygen fugacity decreases with pressure when compared with FMQ buffer, due to stabilisation of the skiagite component in garnet…
…the habit to compare fO2 with FMQ buffer…is trivial…because FMQ buffer will never occur in peridotite rocks [and]…the commonly used equilibrium skiagite = fayalite + ferrosilite + O2 of Gudmundsson and Wood (1995), which involves only Fe-bearing phases, shows a slight negative slope with pressure while FMQ has a positive slope…
R - As admitted by the reviewer, these interesting aspects go beyond the goal of the present work, as our aim is not to revisit redox estimates for mantle peridotites. We only use the available estimates to bracket the redox conditions expected to be relevant for lithospheric mantle sections, and the same method used to estimate the redox conditions (Stagno et al. 2013) is used backward to calculate model Fe3+/Fetot ratios in Grt. Ours is a 'relative' approach (see Appendix for details) and thus the effect of possible systematic inaccuracy in fO2 estimates is minimal.

It must be said that Gudmundsson and Wood themselves specified that the Fe3+/Fetot in orthopyroxenes of upper mantle composition can be neglected in the calculation of FeSiO3 activity only if this is less than 0.05 (Page 64 of the cited work)… This point should be stressed in the manuscript in order to strengthen the importance of considering the Fe3+ content in orthopyroxene, which seems to be above 5% in many mantle peridotites, as a further variable in the calculation (I would say estimate) of fO2 in these systems.
R - Gudmundsson and Wood (1995) stated something different. The correct quotation is "Mössbauer data (Dyar et al. 1989; Wood, unpublished) show that the Fe3+/SFe of orthopyroxenes of upper mantle composition is only about 0.05, an amount which can be neglected in the calculation of FeSiO3 activity." However, the suggestion of including a discussion of the potential implications of our data on fO2 calculations is valuable. We have added a paragraph in the "Conclusions" section. It appears that even if some of our Opx are richer in Fe3+ than commonly assumed, the bias on redox calculations should still be negligible.

Minor comments:

P. 3, L. 6-11: The citation of Frost and McCammon 2008 about "distribution of ferric iron in mantle minerals" is not appropriate (see comment I). In this work the authors reviewed the various oxybarometers referring only to the Fe3+ content in spinel, garnet, perovskite, etc. in the use of redox equilibria involving one Fe3+-bearing phases.
R - Ok, deleted.

P. 3, L. 13-30: It should be specified that here only the subcratonic mantle is considered here as "upper mantle sections", otherwise other works should be cited for oceanic mantle and supra-subduction mantle.

R - Ok, text changed.

P. 7-8: relative to Mossbauer analyses, given the accuracy of the data reported, it should be useful write a sentence to demonstrate the absence of possible exsolutions of magnetite in orthopyroxene which is not rare in this kind of rocks, in order to exclude that the Mossbauer analyses (bulk) also include magnetite in the Fe3+ measurements.
R - Ok, sentence added justifying the absence of exsolutions.

P. 15, L.15: "the following expression ... as a function of P and Na2O (Fig. 4). I do not understand the link between this statement and Figure 4. Is the reference wrong and related to Figure 3c? Otherwise this should be better explained.
R - Ok, text clarified.

P. 16, L. 11-20: I do not completely agree with this section, unless clinopyroxene is absent in the association, as well as the statement at 26-28 that "opx may represent the most important Fe3+ carrier in the mantle" (see comment I).
A more complete discussion of this issue is now provided, considering the modal proportions of minerals, crystalchemical considerations on Opx, and the new Cpx Fe3+ data.
R - We still maintain that opx may represent one of the most important Fe3+ carriers in Earth's lithospheric mantle, if the larger contribution of off-craton mantle sections is considered. Indeed, in our Dariganga samples, Opx IS the most important Fe3+ carrier!

P. 17, L. 18: "then temperature estimates may be affected by changes in redox conditions", redox conditions of the orthopyroxene (see comment II).
R - See reply to comment II.

P. 23, L. 22-24: as far as I know, Stagno et al. (2013) only consider the Cr-bearing garnet end-member in the reciprocal reactions used to calculate activity coefficients, but the equilibrium they propose to be used in the calculation of fO2 (their equilibrium 3 calculated using their equation 6) Cr is not considered in the exchange equilibrium between grossular and andradite. Their oxybarometer is not sensitive to the Al and Cr contents in garnet.
R - Since the activities are used in fO2 calculations, the oxybarometer is sensitive also to Cr and Al. We have clarified this point in the text.

Reviewer #2: General comments
My major complaint with this paper is that it is truly a shame that the authors did not also measure the Fe3+/Fe2+ for the clinopyroxenes in their samples - that would have been invaluable, and I hope the authors plan to do so in future.
R - Cpx data for nine samples were added and their relationships with Grt and Opx were discussed.

Specific comments
Page 6, line 33: Doucet et al (2013) missing from reference list
R - Ok, added.

Page 8, lines 18-20: More information on the "special holder to avoid asymmetry of the spectra" would be very helpful, especially in light of the later comment suggesting preferred orientation was a problem in the Canil and O'Neill study (page 9, lines 40-43).
R - Ok, text changed.

In general, more information on the fitting of the orthopyroxene spectra would be good - there is no way for the reader to judge whether the hyperfine parameters determined in this study compare well or poorly to previous work, or to get any indication of whether the authors are interpreting the ferric iron to be in tetrahedral or octahedral coordination.
R - Ok, more detailed fitting approach added in the "Mössbauer analysis" section and sentence added that ferric iron is octahedral.

Page 9. Line 1: Woodland and Ross (1994) missing from reference list.

R - Ok, added.

If the Fe3+/SigmaFe (Corrected) values in Table 3 are the result of applying this model for the recoil-free fractions in garnet, it would be good to note that in a footnote to the table.
R - Ok, done.

It would also be of interest to see how much this correction shifts the fO2 calculated with the Stagno et al. oxybarometer, given the ~25% reduction in the calculated Fe3+/SigmaFe.
R - A sentence was added in the Appendix.

Page 12, line 49 - are the hyperfine parameters observed consistent with this assumption (or the one on page 14 about tetrahedral coordination)?
R - Ferric iron in Opx is essentially octahedral according to hyperfine parameters and we added a sentence stating this. However, the possibility that undetectable amounts of Fe3+ also enter the thetrahedral site cannot be excluded. We have emphasized in the text that these amounts, if any, should be minor.

Late Reviewer #3

A) Considering that the measurement of Fe3+ in opx forms the basis for this manuscript, it is important that the approach for fitting the opx spectra is adequately discussed. The fitting strategy is presented on p. 8 without any real discussion of existing literature, for example, Luth & Canil (1993), Canil & O'Neill (1996) and Woodland et al. (2006). For example, an apparent asymmetry in a spectrum can be caused by different factors. Preferred orientation can indeed be a cause, as mentioned in the text. The authors indicate that their samples were specially prepared to avoid such effects, but they don't explain what was so special about their method. However, spectral asymmetry can arise from other effects such as nextnearest-neighbor effects. In fact this was invoked for garnet, but apparently the authors do no accept this possibility for opx, even though such effects have been described for cpx and opx since the 1970's.
R - More detailed fitting approach added in the "Mössbauer analysis" section.

The errors provided in the data table are only those related to the fitting process and do not capture the true sum of errors. Errors for opx are usually considered to be about ± 0.01, but are potentially higher for opx, due to peak overlap and the relatively small contribution from Fe3+. Catherine McCammon can provide more information about this aspect.
R - This is correct; hence we used only two doublets for Fe2+ where peak overlap is minimized. Errors for opx would be higher in the case of fixing parameters of the Fe3+ doublet, as was done in Canil & O'Neill (1996).

What are the uncertainties in the hyperfine parameters? Too many decimals are reported in the Mössbauer data tables.
R - Ok, Tables changed accordingly.

It is claimed without any explanation that opx in a sample from Canil & O'Neill (that was refit for this study) contained 8% cpx contamination. Considering that opx and cpx yield practically identical spectra and hyperfine parameters, it is strange that the present authors can detect such contamination. In fact I would maintain that this interpretation is incorrect. i) opx and cpx are easy to distinguish (one is bright green, the other not) when producing the separates for analysis. ii) This particular sample, FRB 1350, is yields a very low equilibration temperature. It is to be expected that the cation ordering will be different and more extreme at low T. This may yield a spectrum where the high velocity components of Fe2+ have more distinct hyperfine parameters, producing essentially separate peaks rather than just one broad asymmetric peak.
R - Ok, we agree. On renewed examination of the spectrum the hyperfine parameters of the contaminating phase fit to olivine, not cpx. We adjusted the text accordingly. Equation (6) was also modified according to the revised Fe3+/Fetot ratio of Opx FRB1350. The regression statistics have slightly improved.

It is stated in the text that refitting of the opx spectra from Canil & O'Neill (1996) yielded similar results compared to the original results. However, a look in figure 3 reveals significantly different results. (see below). This must be assessed.
R - No. We stated that "We obtained similar results to Canil and O'Neill (1996) using their fitting approach." and then "the Opx spectra were re-fitted". We then only state that "the change in Fe3+/Fetot values from our reprocessing of the Canil and O'Neill (1996) data compared to their original values is minor and does not alter the general conclusions presented in their paper." But this does not mean that there is no change.

B) Investigating the partitioning of Fe3+ between opx and garnet was the stated goal of this manuscript. The authors suggest that, while no temperature dependence on DFe3+ is observable, that a correlation with pressure is apparent. From the data presented, I find this unconvincing. The claimed pressure dependence relies only on the position of the dataset from Dariganga, for which the opxs have distinctly different compositions compared to the rest of the data. Consideration of the Dariganga data is inconsistent, however. These data are also anomalous in terms of the temperature vs DFe3+ plot, but here nothing is made of the difference. In addition, it is clear in Fig. 2 that the Dariganga locality is very anomalous in terms of P-T conditions. It is difficult to lump together the Dariganga samples equilibrated at ~2 GPa (and high T) with the other samples all equilibrated at 4-6 GPa (and lying on plausible mantle geotherms).
R - We totally disagree with this comment. Dariganga is different but not anomalous, it records P-T conditions that are very typical of off-craton mantle sections. Earth's lithospheric mantle is not made only of cratons. To stress this further, we have emphasized in a number of places in the text and in Fig. 2 the off-craton imprint of Dariganga vs. the on-craton imprint of the other xenoliths.
However, we accept that the description and interpretation of the relationships between DFe3+ and P-T-X deserved some clarification as well as some more caution. We have significantly expanded the text in the "Results" section and added the following comment in the "Discussion" section: "The good agreement between measured and calculated lnDFe3+ Opx/Grt (Fig. 6) suggests that most of the observed variability can effectively be explained by the influence of P and NaOpx on Opx/Grt Fe3+ partitioning."
In addition, with the revised Fe3+/Fetot ratio of Opx FRB1350 (see above) the P-dependency of lnDFe3+ becomes even clearer (see Fig. 3b).

In addition, I find it interesting that the original data from Canil & O'Neill indeed show a P- and T-dependence for DFe3+ and are even more or less consistent with the Dariganga data in both Fig. 3a and 3b. A comment needs to be made about this.
R - This suggestion does not make much sense, inasmuch as we refitted Canil & O'Neill's data in order to improve their accuracy. There is no point to stick with the original data.

In terms of the data presented, the dashed line in Fig. 3b has no real significance (i.e. a P-dependence is not consistent with the data. In Fig. 3c, it is unclear what is meant by residual ln DFe3+, why not just plot ln DFe3+ like for the other diagrams?
R - We do not agree that that regression 'has no real significance'. A regression is a regression and has some residuals. And we show that these residuals do not appear to be simply due to random scattering but show some dependency on Na in Opx. This way of presenting the data is more effective than an additional lnD vs Na plot, in which most of this information would be masked by the concomitant independent effect of P. We have tried to clarify the text to better explain the rationale of our analysis. We have also added in the 'Discussion' section that "the good agreement between measured and calculated lnDFe3+ (Fig. 6) suggests that most of the observed DFe3+ variability can effectively be explained by the influence of P and NaOpx on Opx/Grt Fe3+ partitioning."

It is also better to use cations pfu rather than wt % Na2O, especially when differences in composition are apparent. Why is the correlation between Fe3+ and Na considered to be a "second-order" compositional control? What would be first order? Why weren't the crystal chemical effects of Fe3+ incorporation in opx first discussed in terms of opx chemistry instead of going directly into the partitioning behavior?
R - We think the last comment was a valuable suggestion and have added a two-plot figure (now Fig. 4a,b) to show compositional relationships in Opx. They further support

	our hypothesis that Na may have a minor, but significant role in controlling Fe3+ partitioning in Opx. We have provided an alternative expression for lnDFe3+ (modified equation 6) which considers cations pfu only. C) The discussion of Fe3+ incorporation in terms of Al exchange is reasonable, but the arguments are not clear. As suggested, Al-substitution in opx can occur through different mechanisms. It would have been interesting to see a plot of Al vs Fe3+ (here the Al not involved in Tschermaks substitution). If there is no relationship here, then the above arguments need to be reconsidered. Also, the relatively large amounts of Al in the Dariganga opxs should be discussed in this regard. R - The relationships with Al are now discussed in the 'Results' section and illustrated in the new Fig. 4a. We do not think that a plot of Fe3+ vs 'Al not involved in Tschermaks substitutions' would be very informative: what we have is a set of samples equilibrated under very different P-T conditions and most of the Al variability is due to P-T variations rather than to a simple Fe3+-Al substitution; moreover, allocation of cation species such as Cr and Ti to Tschermaks-type vs Na-bearing components is not straightforward and would require subjective assumptions. D) The authors test the importance of Fe3+ incorporation on thermobarometric calculations (p.18 and appendix). This is a useful exercise. However, the range of fO2 values chosen to make the test makes no petrological sense. It is not reasonable to take a worldwide range (which is related to many different situations) and assume that such a range could apply to a single locality or even a single sample. The assumed range is far beyond what one might call a worst-case scenario. This needs to be reassessed with a smaller range in conceivable fO2 values. My feeling is that it ends up making little difference in the P-T calculations, considering the overall uncertainties, particularly when applying such an empirical thermometer as Nimis & Grütter (2010). This is already apparent in Fig. 7. Obviously what is important is that systematic differences between oxidized and more reduced domains could produce artefacts that might lead to false conclusions about the local geotherm. It would also be of interest to know what degree of oxidation is required to cause a significant "bias" in the calculated temperature and that the application of the opx-garnet thermometer should be avoided for samples where strong metasomatism is suspected.Is there evidence from other studies that the required high fO2 values are realistic for the localities mentioned here? R - We do not agree with this comment. Our goal was not to consider possible redox changes for 'a specific locality', but to investigate the possible effect of redox conditions in general, within the overall fO2 range of mantle rocks. In common practice, thermobarometry is done without even knowing the redox conditions, and we know from Fig. 7 (now Fig. 8) that these may be very different for different localities AND also for different xenoliths from one single locality. Here we explore what could be the maximum potential bias on commonly obtained P-T estimates. We do not aim to simulate 'realistic redox changes for a specific locality'. I was also surprised to see choice of samples used for this test. Of the 5 samples listed, only one was actually from this study. FRB 1350 from Canil and O'Neill (1996) was used, but this was the one sample the authors singled out as having contamination in the opx sample used for Mössbauer (which probably not the case; see above). The remaining 3 samples are not documented at all. So how do we know that the Na content of opx was reliable? or that the Fe3+ contents were determined in the same way as in this study? R - The chosen samples are ideal in that (i) they show excellent agreement between T estimates using internally-consistent thermometers (including one that is sensitive to redox variations), and (ii) they record apparent redox conditions which are 'average' compared to other mantle xenoliths. Our other samples do not meet the second criterion. We have further clarified these points in the text (see Appendix). We also note that (i) any possible inaccuracy in Opx Fe3+ data for these samples does not affect our calculations at all, and (ii) since the aim of this exercise is to assess 'relative' variations in final P–T estimates, possible small interlab discrepancies in Fe3+/Fetot ratios for Grt extracted from the literature and from this work cannot significantly alter our conclusions. We have added a sentence at the and of the Appendix to emphasize this point. As for sodium uncertainties, yes they might be a problem, as we had already admitted in the text: "The above exercises contain a significant degree of uncertainty, which derives from uncertainties in the oxybarometer of Stagno et al. (2013), which is used to

readjust the Fe3+/Fetot in the Grt, in the calibration of dependency of DFe3+ on P and NaOpx, in the determination of Na2OOpx in the test samples, and in the mechanisms of incorporation of Fe3+ in Opx and its effects on the activity of Al-components. Nonetheless, the results cast doubts on the reliability of many existing thermobarometric estimates…". And finally, at the end of the Conclusions: "An experimental verification of Fe3+ partitioning systematics, e.g., by high-resolution Mössbauer analysis of Opx–Grt pairs re-equilibrated under controlled P–T–O2 and with varying Na2O contents, would be desirable to derive a more robust evaluation…"

Minor comments
P.6. Doucet 2013, 2014 are not in the refernce list
R - Ok, added.

P.7. Was there any loss of Na due to the long counting times and high beam current? Were any precautions taken to prevent Na loss?
R - We added a sentence in which we explain that this has not been a problem. We observed no systematic decrease in measured Na contents using the longer times and higher currents.

P.15. What is the point of eq. 6? Weight percent is a poor variable to use. Why not cations pfu? That is more thermodynamically relevant.
R - We have provided an alternative expression for lnDFe3+ (modified equation 6) which considers cations pfu only.

P.15. following from eq.4 it might be better to cast the partitioning of Fe3+ on an equal number of oxygen's basis. i.e. either a 6 or 12 oxygen basis for both phases.
R - Ok. We have cast all formulas to a common 4-cation basis.

P.15. line 47. Na partitioning being favored by high T? Partitioning between opx and garnet?
R - No, between opx and cpx. We have clarified the text.

P.16. should give the exchange equilibrium for the mass action equation (8).
R - Ok, added.

P.19. line 26. So what is "strongly oxidized"? how high? Are these realistic values?
R - See our reply to point D above.

P.20 line 23. What started out as a "rough" P-dependence for DFe3+ has now become a "significant" dependence. This is not fair statement here, especially considering the comments made above.
R - Agreed. Text changed.

P.20. line 35. Why is it stated here "at least 9%" (Fe3+/Fetot). This gives the false impression that much more Fe3+ can be expected although there is no such evidence presented here. Evidence from spinel peridotites argues that Fe3+/Fetot ratios are always low in opx (Woodland et al. Lithos, 2009).
R - We are showing for the first time that Opx can contain significant Fe3+, but we cannot maintain that 9% is the maximum possible value. So we see no problem with our sentence. However, the sentence was slightly changed to clarify that we are only considering garnet-facies Opx here.

Figure 4. This figure doesn't tell me much, other than eq. 6 more or less fits the data. But we knew this already from the quoted R-value of the fit. More interesting would be to plot the calculated DFe3+ in Fig 3c.
R - The R-value alone does not allow one to properly judge the quality of the fit, as it does not discriminate between the presence e.g. of any anomalous data and any unresolved non-linearity in the measured vs calculated values. Therefore we have kept the Figure. We do not understand the second suggestion: if it is a plot of calculated DFe3+ vs. Na2O, we do not understand what this could tell us, since Na2O is already considered in the regression.

Figure 5. These 2 diagrams are essentially the same as those in Fig. 3 except with a change in scale for the y-axis. Are they really necessary?

	R - This is true, but the first pair shows a parameter that is commonly used in studies on the Fe3+ distribution (most people would expect to see it in plots), whereas the second pair (now Fig. 7) shows a parameter that quantifies the robustness (or non robustness) of thermometric estimates vs redox conditions (which is the basis for our evaluation of thermometric implications). And the distribution of the data in the two pairs of plots are not identical anyway. So we think it is worth keeping both Figures.We agree, however, that the second plot vs T is useless, so we have only kept the plot vs P in the new Fig. 7.

Fe^{3+} partitioning systematics between orthopyroxene and garnet in mantle peridotite xenoliths and implications for thermobarometry of oxidized and reduced mantle rocks

Paolo Nimis[1,*], Alexey Goncharov[2], Dmitri A. Ionov[3], Catherine McCammon[4]

[1] Dipartimento di Geoscienze, Università di Padova, Italy

[2] Institute of Earth Sciences, Saint-Petersburg State University & IPGG RAS Saint-Petersburg, Russia

[3] Géosciences Montpellier, CNRS-UMR 5243 - Université Montpellier II, 34095 Montpellier, France

[4] Bayerisches Geoinstitut, Universität Bayreuth, D-95440 Bayreuth, Germany

*: Corresponding author

e-mail: paolo.nimis@unipd.it

tel: +39-0498279161

fax: +39-0498279134

Abstract We have investigated the partitioning of Fe^{3+} between orthopyroxene (Opx) and garnet (Grt) in well-equilibrated mantle xenoliths using Mössbauer spectroscopy. The samples cover a wide range of *P*–*T* conditions (2.1–6.6 GPa, 690–1,412 °C) and geothermal gradients, and are thus representative for Earth's upper mantle in both on-craton and off-craton continental settings. Garnet has Fe^{3+}/Fe_{tot} ratios of 0.03–0.13 and Fe_2O_3 contents of 0.24–1.00 wt%. Orthopyroxene has, on average, lower Fe^{3+}/Fe_{tot} ratios (0.01–0.09) and Fe_2O_3 contents (0.05–0.63 wt%). In low-pressure, high-temperature samples, however, Opx is systematically richer in Fe_2O_3 than the coexisting Grt. The Fe^{3+} Opx/Grt partition coefficient ($D_{Fe^{3+}}^{Opx/Grt}$) shows no obvious relationship with temperature, but increases with decreasing pressure and with increasing Na^{Opx}. The observed Opx/Grt Fe^{3+} systematics imply that the Opx–Grt Fe–Mg exchange thermometer is not robust against redox changes if total Fe is treated as Fe^{2+}. An approximate evaluation of errors on *T* estimates due to redox effects predicts negligible deviations for strongly reduced conditions (< 65 °C), but potentially large deviations (> to >> 100 °C) for strongly oxidized conditions, especially at very high pressure and when both *P* and *T* are calculated by iteration.

Keywords Ferric iron, Orthopyroxene, Garnet, Mantle xenoliths, Thermobarometry

Introduction

Studies of the distribution of ferric iron in mantle minerals have provided important insights into the redox state and geochemical processes in the Earth. Measured Fe^{3+}/Fe_{tot} ratios in garnet and spinel from xenoliths have been used to derive oxygen fugacity profiles for several upper mantle sections (e.g., Luth et al. 1990; Luth and Canil 1993; Woodland and Peltonen 1999; Woodland and Koch 2003; McCammon and Kopylova 2004; Lazarov et al. 2009; Yaxley et al. 2012; Creighton et al. 2009, 2010; Goncharov and Ionov 2012; Goncharov et al. 2012). These data are of paramount importance for our understanding of processes involving volatile-bearing metasomatic fluids and melts active in the lithosphere today and during its evolution, including those involved in diamond formation and Earth's degassing (Woodland and Koch 2003; Shirey et al. 2013; Stagno et al. 2013).

A large number of Fe^{3+} analyses are now available for garnet, pyroxenes and spinel, which are the most important carriers of Fe^{3+} in the upper mantle. The contents and distribution of Fe^{3+} among these minerals are controlled by crystal-chemical constraints and *P–T* conditions and are affected by partial melting and metasomatism (Frost and McCammon 2008). It was recognized that in sub-cratonic mantle sections garnet Fe^{3+}/Fe_{tot} ratios and garnet/clinopyroxene Fe^{3+} partition coefficients tend to increase with temperature (Woodland and Koch 2003; Canil and O'Neill 1996; Woodland 2009). In addition, owing to stabilization of the $Fe^{2+}{}_3Fe^{3+}{}_2Si_3O_{12}$ ("skiagite") component in garnet with pressure, oxygen fugacity has been shown to be driven to lower values relative to the FMQ buffer with increasing depth (Gudmundsson and Wood 1995).

Despite the large amount of data on Fe^{3+} distribution in mantle rocks, specific information on the partitioning of Fe^{3+} between orthopyroxene (hereafter Opx) and garnet (hereafter Grt) is still very scarce. Predictive theoretical modeling of this partitioning is hampered by the lack of accurate thermodynamic data for Fe^{3+}-bearing Opx. Empirical modeling is also problematic due to the paucity of analytical data for Opx. To our knowledge, reliable partitioning data for Opx–Grt pairs are restricted to a set of eight mantle xenoliths, which were analyzed by conventional Mössbauer spectroscopy by Canil and O'Neill (1996), and two compositionally zoned Opx–Grt pairs from metasomatized xenoliths, which were analyzed by high-spatial-resolution Mössbauer spectroscopy by McCammon et al. (2001). Two additional pairs were reported for orogenic garnet peridotites by Malaspina et al. (2012), who used complementary analytical techniques for the determination of ferric iron, i.e., flank-method electron probe micro-analysis (EPMA) for Grt and electron energy-loss spectroscopy for Opx.

Nimis and Grütter (2010) showed that the distribution of Fe^{3+} between Opx and Grt in Canil and O'Neill's (1996) xenoliths is dependent on equilibrium *P*–*T* conditions, implying a significant effect of mantle redox state on Opx–Grt Fe–Mg-exchange thermometry. Unfortunately, the strong correlation between *P* and *T* in these samples did not allow discrimination of the net effects of *P* and *T* on Fe^{3+} partitioning. More recently, Matjuschkin et al. (2014) performed experiments in the CFMAS peridotitic system at 5 GPa and 1,100–1,400 °C under strongly oxidized conditions and measured Fe^{3+} contents in the garnets with the flank method. These authors observed a marked improvement of Opx–Grt temperature estimates using the Harley (1984) Fe–Mg exchange thermometer

when the significant Fe^{3+} contents in the garnets were accounted for and suggested that Fe^{3+}/Fe_{tot} ratios in the coexisting orthopyroxenes should be comparatively small.

To gain a better insight into the partitioning systematics of ferric iron between Opx and Grt under conditions relevant to Earth's upper mantle, we have undertaken a Mössbauer study of Opx–Grt pairs in well-equilibrated xenoliths from both on-craton and off-craton mantle sections, covering a wide *P*–*T* field. The results provide new indications on the mechanisms of incorporation of Fe^{3+} in Opx and have significant implications for mantle thermobarometry.

Materials and methods

Sample selection, microstructures and compositions

The samples used in the present work were selected among well-studied peridotite xenoliths to cover a range of *P*–*T* conditions representative of garnet-facies lithospheric mantle in cratonic and off-craton regions (Table 1). All selected samples show well-equilibrated microstructures. We avoided using samples showing significant alteration or any evidence of chemical disequilibrium, such as significant compositional variations in any minerals, poor consistency between thermometric estimates using independent, mutually-consistent thermometers (cf. Nimis and Grütter 2010) or poor consistency between fO_2 estimates using independent, garnet-based and spinel-based oxybarometers (cf. Goncharov and Ionov 2012).

The selected off-craton peridotites (N = 6) are from the Barun-Yargait eruption center within the Late Cenozoic Dariganga alkali basaltic field in SE Mongolia (Ionov et al. 1999; Ionov 2002). The peridotites are fertile to moderately refractory garnet lherzolites (2.7–3.9 wt% Al_2O_3 in whole-rocks) containing 54–66% olivine, 19–27% Opx, 6–13% clinopyroxene (hereafter Cpx) and 4–11% Grt; one sample (BY-18) contains accessory spinel (Table 1). They are coarse- to medium-grained rocks with protogranular textures. The grain size is similar for all silicate minerals. The mineral grains typically have curved boundaries and irregular shapes. Pyroxenes show no optical zoning or unmixing. Garnets have thin kelyphite rims. No volatile-bearing minerals (mica, amphibole, apatite) or silicate glass have been found. Veined peridotites or pyroxenite xenoliths are very uncommon in the whole xenolith suite. The peridotites are fresh and have positive loss on ignition (LOI) values, indicating that the gain of mass due to oxidation of FeO to Fe_2O_3 on heating is greater than the loss of volatiles introduced by alteration.

The selected cratonic peridotites (N = 12) are from the Udachnaya-East kimberlite pipe in the central Siberian craton. The samples are a subset of the xenolith collection described by Doucet et al. (2013, 2014), Goncharov et al. (2012) and Ionov et al. (2010), and were collected in the 420–640 m depth range in the diamond mine pit from unusually fresh kimberlites. Details on petrographic features, major and trace element compositions of whole-rocks and minerals, and oxygen fugacity estimates can be found in the quoted papers. The rocks range in composition from Cpx-bearing harzburgite to lherzolite to Opx-bearing wehrlite (Table 1), and show no or little alteration (commonly with positive LOI). Four samples (U29, U64, U283, U501) are coarse (undeformed), seven (U70, U183, U267, Y-10, Y-19, 87/70, 87/97) are sheared and one (U10) is

transitional (incipient deformation with ≤10% of olivine as neoblasts). One of the coarse xenoliths (U283) contains accessory spinel.

Chemical analysis

Major element compositions of minerals used in the present study were determined by wavelength-dispersive spectroscopy electron microprobe analysis at different laboratories. The minerals were analyzed in grain mounts or thin sections. Samples from Dariganga were analyzed at Macquarie University (Sydney) with a Cameca SX-50 instrument at 15 kV voltage and 20 nA current, using natural and synthetic oxide and silicate minerals as standards and the PAP matrix correction. Analyses for U-series samples from Udachnaya are the same as those reported in Ionov et al. (2010) and were obtained at the Laboratoire Magmas et Volcans (Clermont-Ferrand) on a CAMECA SX-100 using 15 kV voltage, 15 nA current and counting times of 10–20 s for peaks and 5–10 s for background; standards were natural and synthetic minerals; the ZAF correction was applied. The other samples from Udachnaya were analyzed or re-analyzed at Padova IGG-CNR with a CAMECA SX-50 and at Clermont-Ferrand with a CAMECA SX-100 using higher currents (20 kV, 40 nA) and longer counting times for Al, Cr, Ca and Na in pyroxenes (40 s peak, 40 s background) in order to minimize propagation of analytical errors on thermobarometric estimates and optimize the analysis of Na in Opx. No systematic decrease in measured Na contents was observed using the higher currents and longer counting times, which excludes significant underestimation due to migration of this element under the electron beam. Analytical standards for pyroxenes and olivine were diopside (for Si and Ca), albite (for Na), orthoclase (for K) and pure oxides (for

Mg, Al, Cr, Fe, Mn and Ti). For garnet, pyrope was used as a standard for Mg and Si. The CAMECA-PAP program was used to convert X-ray counts into weight percent oxides. The analyses are reported in Table 2.

Mössbauer analysis

Pure Grt, Opx and Cpx grains were handpicked under a microscope from 0.5 to 2.0 mm size fractions of crushed and sieved rock material. Owing to the small size of some xenoliths and low modal proportions of Cpx, sufficient Cpx separates for Mössbauer analysis could be obtained only for nine of the investigated samples. The valence state of iron and its structural position in the minerals were determined using a SM-1201 Mössbauer spectrometer at the IPGG RAS (Saint-Petersburg, Russia) at room temperature in a constant acceleration mode over a velocity range of ±7 mm/s with a nominal 50 mCi ^{57}Co source in a Rh matrix. The spectrometer was calibrated relative to metallic iron at room temperature. The minerals were crushed in an agate capsule filled with acetone to avoid iron oxidation in contact with air, pressed in plastic discs and fixed on a special aluminum holder, ensuring an angle between gamma rays and absorber of 54.7°, to avoid asymmetry of the spectra due to preferred orientation of mineral grains. The density of the natural iron in the absorber was about 5 mg/cm^3.

The spectra were approximated by a sum of Lorentzian lines using the MOSSFIT© software. The relative amounts of Fe^{2+} and Fe^{3+} and their site positions in the crystal lattice were determined from integral doublet intensities and hyperfine parameters, assuming equal Mössbauer effect probabilities for Fe^{2+} and Fe^{3+} at different sites for Opx and different recoil-free fractions of Fe in octahedral and dodecahedral sites for Grt.

Constraints on the equality of halfwidths (HW) and integral intensities of the lines in each doublet component of quadrupole splitting (QS) were imposed during spectra fitting. The quality of experimental spectra was assessed by background intensity and the quality of fitting by chi-square distribution.

The fitting model for Grt included a single QS doublet for Fe^{2+} and Fe^{3+}. The relative peak widths and areas of the Fe^{2+} doublet, assigned to dodecahedral (distorted cube) site occupancy, were left unconstrained to account for spectra asymmetry (Amthauer et al. 1976). The doublet attributable to octahedrally coordinated Fe^{3+} was constrained to have components with equal widths and intensities. The Fe^{3+}/Fe_{tot} values obtained were corrected for different recoil-free fractions (Woodland and Ross 1994).

The fitting model for Opx and Cpx included two QS doublets for Fe^{2+} and one for Fe^{3+}. Although previous studies (e.g. Luth and Canil 1993; Canil and O'Neill 1996), used three QS doublets for Fe^{2+} in Opx in the fitting procedure, this approach led to unreasonably small HW. Addition of the extra doublet is not statistically justified when the lines overlap by more than their HW, where the errors of hyperfine parameters increase dramatically (Dollase, 1975). We also note that adding the extra doublet for Fe^{2+} did not alter $Fe^{3+/}Fe_{tot}$ ratios. Therefore, to reach best fitting results, exclude peak overlap and minimize errors, only two QS doublets for Fe^{2+} were used to fit Opx spectra.

The hyperfine parameters and calculated proportions of Fe^{2+} and Fe^{3+} at different sites, calculated from HW and integral intensities of lines in QS doublets, are reported in Tables 3 to 5. The hyperfine parameters of Fe^{3+} doublets in Opx are consistent with octahedral coordination (Annersten et al., 1978). No additional lines were observed in any of the spectra, which confirms the absence of other mineral phases, including possible exsolutions. The absolute errors on the Fe^{3+}/Fe_{tot} ratios varied from 0.003 to

0.017 for Opx, from 0.009 to 0.024 for Grt, and from 0.01 to 0.06 for Cpx. Two examples of spectra pairs showing different partitioning of Fe^{3+} between Opx and Grt are shown in Figure 1.

Mössbauer spectra of Opx, Cpx and Grt from mantle xenoliths that had been obtained by conventional Mössbauer spectroscopy by Canil and O'Neill (1996) were reprocessed for this study using the same software and fitting approach used for our samples to ensure robust comparison of the new and old data. Seven sets of spectra could be retrieved from the original Canil and O'Neill (1996) files. We obtained similar results to Canil and O'Neill (1996) using their fitting approach; however, for several Opx spectra we observed that the fitting residuals were larger than the baseline scatter and indicated unequal areas of the main doublet components. This asymmetry is likely caused by a slight preferred orientation of crystallites arising from the nature of the sample mount; therefore the Opx spectra were re-fitted allowing the two Fe^{2+} doublets to have components with equal HW but unequal intensity according to the fitting approach of McCammon et al. (2000). One of the spectra (sample FRB1350) showed a contribution from olivine, which was estimated to be roughly 13% of the total area based on the intensity of the high QS impurity. Accordingly, an empirical correction was made to the Fe^{3+}/Fe_{tot} ratio in Opx based on the well established observation that olivine contains no Fe^{3+}. For the garnets, the same fitting model used for our samples produced Fe^{3+}/Fe_{tot} values within 0.01 of the data reported in Canil and O'Neill (1996), provided the latter were corrected for different recoil-free fractions. Most of our refitted Fe^{3+}/Fe_{tot} data for the clinopyroxenes were within 0.02 of those reported in Canil and O'Neill (1996), with only two samples at 0.03–0.04 of the originally reported values. The results of the refitting are reported in Tables 3 to 5. We emphasize that the change in Fe^{3+}/Fe_{tot}

values from our reprocessing of the Canil and O'Neill (1996) data compared to their original values is minor and does not alter the general conclusions presented in their paper.

Thermobarometry

The pressures and temperatures of equilibration of the studied xenoliths and of the reprocessed Canil and O'Neill (1996) data (Table 1) were calculated using a combination of the Taylor (1998) two-pyroxene thermometer and Nickel and Green (1985) Opx–Grt barometer recommended by Nimis and Grütter (2010). Given the presence of a few sodium-rich Opx in our data set, we adopted the modified version of the Nickel and Green (1985) barometer proposed by Carswell (1991). This modification was neither expressly favored nor disfavored by Nimis and Grütter (2010), who showed that both versions of the barometer are consistent with constraints imposed by natural xenoliths and experiments in peridotitic systems. Carswell's (1991) version only diverges from the original Nickel and Green (1985) for Opx with $Na > Cr + Fe^{3+} + Ti$, for which it yields somewhat higher pressures (up to 1.2 GPa higher in our data set; Table 1) and is claimed to be more robust. Owing to the large relative uncertainties in the determination of the small Fe^{3+} contents in Opx, Fe^{3+} was neglected in the application of Carswell's (1991) correction.

Only two samples from Udachnaya (U267 and 87/70) showed discrepancies between Opx–Grt (Nimis and Grütter 2010) and two-pyroxene (Taylor 1998) temperatures slightly larger than the assumed safety threshold of ±70 °C proposed by Nimis and Grütter (2010), i.e., +96 °C and –77 °C, respectively. Neither of these two samples,

however, showed anomalous behavior in terms of Opx/Grt Fe^{3+} distribution compared with the other samples.

Three of the samples from the Canil and O'Neill (1996) set for which the Mössbauer spectra were refitted, i.e., BD1140, BD1150 and BD1354, show less than optimal agreement between internally-consistent clinopyroxene-based (Taylor 1998 or Nimis and Taylor 2000) and Opx-based thermometers (Brey and Köhler 1990, with correction in Nimis and Grütter 2010) (ΔT = 100–165 °C). *P–T* estimates for these samples should thus be used with caution. Therefore, these three samples will be used for general comparative purposes, but not for quantitative evaluation of Fe^{3+} systematics.

Results

The samples studied in this work cover a wide range of estimated *P–T* conditions (2.1–6.6 GPa, 690–1,412 °C) and geothermal gradients, and are thus representative for Earth's upper mantle in both on-craton and off-craton continental settings (Fig. 2). Garnet has Fe^{3+}/Fe_{tot} ratios of 0.03–0.13 and Fe_2O_3 contents of 0.24–1.00 wt%. Orthopyroxene has, on average, lower Fe^{3+}/Fe_{tot} ratios (0.01–0.09) and Fe_2O_3 contents (0.05–0.63 wt%). In the low-pressure, high-temperature Dariganga suite, however, Opx is systematically richer in Fe_2O_3 than the coexisting Grt (Table 2). Such systematic Fe^{3+}-enrichment appears to be unrelated to the abundance of other phases competing for Fe^{3+}, since the modal ranges of Cpx (6–13 vol%) and Grt (3.5–11 vol%) in Dariganga xenoliths overlap those in the other investigated samples (Cpx = 1.4–16 vol%; Grt = 2.1–13 vol%), and spinel only occurs in minor amounts (< 0.5 vol%) in one Dariganga and one Udachnaya

sample (Table 1). The main reason for the enhanced partitioning of Fe^{3+} in Opx must therefore be found in the specific *P–T* conditions recorded by the off-craton Dariganga xenoliths and, possibly, in specific compositional controls.

The higher Fe^{3+} contents in Dariganga Opx are coupled with higher $^{[4]}Al$ contents (Fig. 4a). The latter essentially reflects the low-*P* and relatively high-*T* conditions of equilibration of these samples, which are typical of the garnet-facies off-craton lithospheric mantle (Fig. 2). The association of high Fe^{3+} and high $^{[4]}Al$ suggests a major role of Tschermaks-type substitution in the incorporation of Fe^{3+} in Opx. In addition, the three most Fe^{3+}-rich samples in the low-$^{[4]}Al$ Opx group are those with the highest Na content, and a correlation of Fe^{3+} with Na is also shown by all of the Dariganga samples except for one, which contains spinel (Fig. 4b). This indicates that an additional minor aegirine component $NaFe^{3+}Si_2O_6$ may also have contributed to the incorporation of Fe^{3+} in Opx.

The Fe^{3+} Opx/Grt partition coefficient ($D_{Fe^{3+}}^{Opx/Grt} = \frac{\left(Fe^{3+}\right)^{Opx}}{\left(Fe^{3+}\right)^{Grt}}$, at. per 4-cation formula unit) shows no obvious relationship with temperature and a roughly negative correlation with pressure (Fig. 3a,b). Detailed examination of the relationships between $\ln D_{Fe^{3+}}^{Opx/Grt}$ and *P* showed that the scatter in Figure 3b was at least in part correlated with changes in the Na content of Opx. This is illustrated by a plot of the residuals of a $\ln D_{Fe^{3+}}^{Opx/Grt}$ vs. *P* linear regression, which show a positive correlation with the Na content in Opx (Fig. 3c). Such a correlation is consistent with the inferred contribution of aegirine component to Fe^{3+} incorporation and suggests an additional compositional control on the partitioning of Fe^{3+} between Opx and Grt. The original data of Canil and

O'Neill (1996) are systematically shifted to higher $D_{Fe^{3+}}^{Opx/Grt}$, but the refitted data are in good agreement with our data if the effect of Na and the uncertainties in *P*, $D_{Fe^{3+}}^{Opx/Grt}$ and Na content are taken into account (Fig. 3c).

The partitioning behavior observed in our Opx–Grt pairs is in contrast with existing reports for natural mantle and experimental Cpx–Grt pairs: these show enhanced partitioning of Fe^{3+} to Grt with increasing temperature (Canil and O'Neill 1996; Woodland 2009; Purwin et al. 2013), a tendency which is confirmed also by our Cpx–Grt pairs (Fig. 5a). A correlation between Fe^{3+} and Na in Cpx is also apparent in our data (Table 2), in line with previous observations in garnet peridotites (Woodland 2009; Malaspina et al. 2012). Owing to the complex combination of *P*–*T* and compositional effects, the distribution of Fe^{3+} between the pyroxenes varies significantly among different samples ($D_{Fe^{3+}}^{Opx/Cpx}$ = 0.1–0.8; Fig. 5b). In particular, the high $D_{Fe^{3+}}^{Opx/Cpx}$ in Dariganga xenoliths (0.5–0.7) is probably due mostly to a combination of relatively high *T*, low *P* conditions and moderate Na^{Cpx} contents. Quantitative evaluation of Opx/Cpx Fe^{3+} partitioning systematics is beyond the scope of the present work. We only emphasize that estimates of Opx Fe^{3+} contents from Fe^{3+} measured in Cpx, based on linear regression of data extracted from limited sets of samples from on-craton mantle settings (cf. Canil and O'Neill 1996), are probably unreliable when applied to Opx–Cpx pairs from different mantle environments.

Discussion

Because the thermodynamic properties of Fe^{3+}-bearing Opx end-members are unknown, a rigorous thermodynamic treatment of the equilibria involved in the Fe^{3+} partitioning between Opx and Grt is not possible. However, the topology of the possible relevant reactions and a few approximations allow us to make some qualitative predictions, which may explain the observed partitioning systematics.

Assuming Fe^{3+} enters into Opx in octahedral coordination, in line with our Mössbauer data, the equilibrium controlling Fe^{3+} partitioning at constant f_{O_2} can be expressed by an Fe^{3+}–Al exchange reaction of the type

$$\underset{\text{Grt}}{\tfrac{1}{2}M_3Fe^{3+}{}_2Si_3O_{12}} + \underset{\text{Opx}}{MgAl_2SiO_6} \rightarrow \underset{\text{Opx}}{MgFe^{3+}AlSiO_6} + \underset{\text{Grt}}{\tfrac{1}{2}M_3Al_2Si_3O_{12}}, \qquad (1)$$

where M represents a divalent cation (essentially, Mg, Fe^{2+} or Ca). At equilibrium,

$$-\frac{\Delta G^\circ}{RT} = \ln K^{\text{Grt–Opx}}_{Fe^{3+}-Al} = \ln\left(K_D \cdot K_\gamma\right) = \ln \frac{\left(Fe^{3+}\right)^{Opx}}{\left(Fe^{3+}\right)^{Grt}} - \ln \frac{\left(Al_{M1}\right)^{Opx}}{\left(Al\right)^{Grt}} + \ln K_\gamma, \qquad (2)$$

where elements are atomic fractions in octahedral sites and $\ln K_\gamma$ includes all non-ideal terms. Since reactants and products in reaction (1) are the same and the coordination number of the exchanged cations does not change in the reaction, the volume change of the reaction should be small. Large extrapolation of Domeneghetti et al.'s (1995) data for Pbca orthopyroxenes allows us to predict a molar volume of ~6.1 J/bar for the $MgFe^{3+}AlSiO_6$ end-member. As expected, the calculated ΔV° of reaction (1) is small (ca. –0.1 J/bar), hence the P dependency of the reaction should also be small. Since the Al

term in Equation (2) typically decreases with pressure in garnet peridotites, owing to the net-transfer reaction

$$MgAl_2SiO_6 + Mg_2Si_2O_6 \rightarrow Mg_3Al_2Si_3O_{12}, \quad (3)$$

Opx Opx Grt

the sum of the other right-hand terms in Equation (2) should also do so in order to maintain the P dependency of $\ln K^{\mathrm{Grt-Opx}}_{\mathrm{Fe^{3+}-Al}}$ small. If the $\ln K_\gamma$ term is sufficiently small or does not vary significantly with P, then the $\frac{\left(\mathrm{Fe^{3+}}\right)^{\mathrm{Opx}}}{\left(\mathrm{Fe^{3+}}\right)^{\mathrm{Grt}}}$ ratio (i.e., $D^{\mathrm{Opx/Grt}}_{\mathrm{Fe^{3+}}}$), should decrease with increasing pressure.

An alternative equilibrium, again with Fe^{3+} in octahedral coordination, is

$$M\mathrm{Fe^{3+}AlSiO_6} + M_2Si_2O_6 \rightarrow \tfrac{1}{2}M_3\mathrm{Fe^{3+}{}_2Si_3O_{12}} + \tfrac{1}{2}M_3Al_2Si_3O_{12}. \quad (4)$$

Opx Opx Grt Grt

This net-transfer reaction involves an increase of mean coordination number for both divalent and trivalent cations and is therefore expected to be favored by pressure. In fact, a similar equilibrium, with Cr in lieu of Fe^{3+}, was experimentally calibrated as a geobarometer by Nickel (1989).

If Fe^{3+} is assumed to enter Opx to a minor extent also in tetrahedral coordination (cf. Annersten et al. 1978), then the following net-transfer reaction may become relevant:

$$M\mathrm{Fe^{3+}{}_2SiO_6} + M_2Si_2O_6 \rightarrow M_3\mathrm{Fe^{3+}{}_2Si_3O_{12}}. \quad (5)$$

Opx Opx Grt

The topology of this reaction is similar to that of equilibrium (3) (with Al instead of Fe^{3+}), on which the Opx–Grt barometer is based (e.g., Nickel and Green 1985). Therefore, regardless of the mechanisms of incorporation of Fe^{3+} in Opx, the $D_{Fe^{3+}}^{Opx/Grt}$ partition coefficient can be predicted to be negatively correlated with pressure, which is in line with our results (Fig. 3).

The positive correlation of the residuals of the $\ln D_{Fe^{3+}}^{Opx/Grt}$ vs. P regression with the Na content in Opx (Fig. 3c) suggests that Na also favors incorporation of Fe^{3+} in Opx, probably as an aegirine component. In our data set, no compositional variable other than the Na content was found to have a significant relationship with these residuals. Weighted regression of our data plus the refitted Canil and O'Neill's (1996) data yielded the following expression for $D_{Fe^{3+}}^{Opx/Grt}$ as a function of P and Na^{Opx}:

$$\ln D_{Fe^{3+}}^{Opx/Grt} = \ln \frac{\left(Fe^{3+}\right)^{Opx}}{\left(Fe^{3+}\right)^{Grt}} = -0.0551(47)\cdot P\,(GPa) + 181(23)\cdot Na^{Opx} - 0.12(23),$$

$$(R^2 = 0.86), \qquad (6)$$

with atoms per 4-cation formula units for both Opx and Grt. The good agreement between measured and calculated $\ln D_{Fe^{3+}}^{Opx/Grt}$ (Fig. 6) suggests that most of the observed $D_{Fe^{3+}}^{Opx/Grt}$ variability can effectively be explained by the influence of P and Na^{Opx} on Opx/Grt Fe^{3+} partitioning. Since the partitioning of Na in Opx is favored by T in Cpx-bearing garnet peridotites (cf. Brey and Köhler 1990), the sodium terms in Equation (6)

may also incorporate some minor temperature effect. Attempts to consider explicitly T in the regressions were, however, unsuccessful.

The practical utility of Equation (6) as a geobarometer is hindered by the relatively small sensitivity of $\ln D_{Fe^{3+}}^{Opx/Grt}$ to P and by difficult accurate measurement of Fe^{3+} concentrations in both Opx and Grt and of Na_2O in sodium-poor Opx. More interestingly, the equations can be used to estimate Fe^{3+} contents in orthopyroxenes from mantle peridotites in which only garnets have been analyzed for Fe^{3+}. The Fe^{3+} systematics expressed by Equation (6) may thus be of help in calculations of Fe_2O_3 budgets and fluxes during geochemical processes involving mantle rocks. A detailed investigation of these issues is beyond the scope of the present work. We only note that, given its relatively large modal proportion in Grt peridotites and significant affinity for Fe^{3+}, especially at moderate pressure, Opx may represent one of the most important Fe^{3+} carriers in Earth's lithospheric mantle.

Implications for mantle thermobarometry

Opx–Grt Fe–Mg exchange thermometry is based on the equilibrium

$$MgSiO_3 + \tfrac{1}{3}Fe_3Al_2Si_3O_{12} \rightarrow FeSiO_3 + \tfrac{1}{3}Mg_3Al_2Si_3O_{12} \qquad (7)$$

Opx Grt Opx Grt

and depends on

$$\ln K_{D\,\mathrm{Fe^{2+}-Mg}}^{\mathrm{Grt-Opx}} = \ln \frac{\left(\mathrm{Fe^{2+}}\right)^{\mathrm{Grt}}}{\left(\mathrm{Fe^{2+}}\right)^{\mathrm{Opx}}} + \ln \frac{\left(\mathrm{Mg}\right)^{\mathrm{Opx}}}{\left(\mathrm{Mg}\right)^{\mathrm{Grt}}}. \quad (8)$$

In common practice, total Fe is treated as Fe^{2+}, therefore variations in ferric iron contents may affect temperature estimates. Following Nimis and Grütter (2010), the difference between the lnK_Ds calculated using total Fe and Fe^{2+} is given by

$$\ln K_{D\,\mathrm{Fe_{tot}-Mg}}^{\mathrm{Grt-Opx}} - \ln K_{D\,\mathrm{Fe^{2+}-Mg}}^{\mathrm{Grt-Opx}} = \ln \frac{\left(\mathrm{Fe_{tot}}\right)^{\mathrm{Grt}}}{\left(\mathrm{Fe_{tot}}\right)^{\mathrm{Opx}}} - \ln \frac{\left(\mathrm{Fe^{2+}}\right)^{\mathrm{Grt}}}{\left(\mathrm{Fe^{2+}}\right)^{\mathrm{Opx}}} = \ln \frac{\left(\mathrm{Fe^{2+}/Fe_{tot}}\right)^{\mathrm{Opx}}}{\left(\mathrm{Fe^{2+}/Fe_{tot}}\right)^{\mathrm{Grt}}} =$$

$$= \ln \frac{1-\left(\mathrm{Fe^{3+}/Fe_{tot}}\right)^{\mathrm{Opx}}}{1-\left(\mathrm{Fe^{3+}/Fe_{tot}}\right)^{\mathrm{Grt}}}. \quad (9)$$

The difference is null only if the $\frac{1-\left(\mathrm{Fe^{3+}/Fe_{tot}}\right)^{\mathrm{Opx}}}{1-\left(\mathrm{Fe^{3+}/Fe_{tot}}\right)^{\mathrm{Grt}}}$ ratio (hereafter, 'the iron ratio') is equal to unity, i.e., if Opx and Grt have the same Fe^{3+}/Fe_{tot} ratio. If this condition is not satisfied, then temperature estimates may be affected by changes in redox conditions, which will affect the Fe^{3+}/Fe_{tot} ratios in both minerals. Therefore, temperature estimates will only be accurate if Fe^{3+} partitioning and redox conditions in the mantle are comparable to those in the samples used to calibrate the thermometer or if the contributions of ferric iron in the two minerals compensate each other. The latter condition seems to hold for the Cpx–Grt thermometer, at least in sodium-free systems (Purwin et al. 2013). Based on experimental data at 5 GPa, Matjuschkin et al. (2014) suggested that this condition does not apply instead to the Opx–Grt thermometer, owing to strong preferential partitioning of Fe^{3+} into Grt, but they did not explore the role of pressure. Nimis and Grütter (2010) recalibrated the Opx–Grt thermometer empirically, using well-equilibrated mantle xenoliths as calibrants. They found that a correction for

pressure was needed, which was larger than expected from thermodynamic treatment of the Fe^{2+}–Mg exchange equilibrium, and suggested that this could be due to a systematic increase of the 'iron ratio' with depth. Our results support this hypothesis (Fig. 7).

Using our observed Fe^{3+} partitioning systematics, we can now explore the effect of changing redox conditions on Opx–Grt thermometry on a quantitative basis. We have estimated potential variations induced on Opx–Grt temperature estimates (Nimis and Grütter 2010; hereafter TNG10) by fO_2 changes within the typical upper mantle range (Fig. 8) for a set of xenoliths recording 'average' redox conditions for their respective depths of provenance (see Appendix for details of the calculations). The results (Table 6) show that conditions more *oxidized* than average, within the typical fO_2 range of upper mantle peridotites, will produce negligible (at low *P*) to significant (at high *P*) *T* *underestimation* (over 100 °C), whereas conditions more *reduced* than average will always produce negligible *T* overestimation (< 40 °C).

Nimis and Grütter (2010) suggested that the commonly observed discrepancies between temperature estimates for mantle xenoliths using the Opx–Grt thermometer (TNG10) and the more redox-robust two-pyroxene thermometer of Taylor (1998; hereafter, TTA98), *using the same input P*, could be due either to redox effects (i.e., highly oxidized or highly reduced conditions) or to kinetic decoupling of the fast Fe–Mg and slow Ca–Mg equilibria due to transient heating. Our results now allow us to refine this premise. Figure 9 shows TNG10 – TTA98 discrepancies for a few sets of xenoliths and the maximum potential bias due to redox effects, as derived from data in Table 6. It appears that large *positive* TNG10 – TTA98 discrepancies, such as those shown by some Jagersfontein xenoliths (Fig. 9a), *cannot* be ascribed to redox variations and are most likely accounted for by short-term thermal perturbations at depth and consequent

disequilibrium. Large *negative* TNG10 – TTA98 discrepancies, such as those shown by some Jagersfontein, Slave or Nikos xenoliths (Fig. 9a–c) might in part be explained by a high fO_2, although disequilibrium or inconsistencies of the TNG10 thermometer for specific *P*–*T*–*X* conditions cannot be excluded.

If *P* is not kept fixed and both *T* and *P* are calculated by iteration according to common practice, the bias on temperature estimates can be considerably amplified. Even so, deviations due to strongly *reduced* conditions remain small in all cases (< 65 °C) and both positive and negative in sign (Table 6). This is because the increase of Al that is assumed to compensate for the decrease of Fe^{3+} in Opx (see Appendix) determines a decrease in the *P* calculated with the Opx–Grt barometer, which in turn tends to counteract the effect of decreasing total Fe on *T* estimates, owing to the positive dependency of the Opx–Grt thermometer on *P*. The calculated pressures still remain within only 0.3 GPa of those calculated with the original mineral compositions. Owing to the low Al in Opx coexisting with Grt, the Al-dependent *P* estimates may instead be extremely sensitive to the Al → Fe^{3+} substitution imposed by strongly *oxidized* conditions. In this case, the corresponding deviations on both *P* and *T* estimates become erratic, from strongly negative to strongly positive (Table 6), depending on even modest differences in the original Al and Na contents in Opx.

The above exercises contain a significant degree of uncertainty, which derives from uncertainties in the oxybarometer of Stagno et al. (2013), which is used to readjust the Fe^{3+}/Fe_{tot} in the Grt, in the calibration of $\left(Fe^{3+}\right)^{Opx} / \left(Fe^{3+}\right)^{Grt}$ dependency on *P* and Na^{Opx}, in the determination of Na_2O^{Opx} in the test samples, and in the mechanisms of incorporation of Fe^{3+} in Opx and its effects on the activity of Al-components (see

Appendix). Nonetheless, the results cast doubts on the reliability of many existing thermobarometric estimates for Cpx-free garnet harzburgites and Grt–Opx inclusions in diamonds, for which no independent, sufficiently accurate control on *T* and *P* estimates is generally possible (Nimis and Grütter 2010). It is noteworthy that any inconsistency in published *T* estimates for Cpx-free xenoliths based on Opx–Grt thermobarometry will be difficult to recognize, because the *T*–dependency of the Opx–Grt barometer will force the *P*–*T* points to move roughly along the same conductive geotherm on which the 'good' *P*–*T* points will fall (Brey and Köhler 1990).

Conclusions

The partitioning of Fe^{3+} between orthopyroxene and garnet in our set of mantle xenoliths shows no obvious relationship with temperature, but appears to vary with pressure and the Na_2O content of the orthopyroxene. This result is unlike previous observations for clinopyroxene–garnet pairs (cf. Woodland 2009; Purwin et al. 2013). As a consequence, the proportion of Fe^{3+} over total Fe in garnet-buffered mantle orthopyroxene is not uniformly low, as commonly assumed, but varies from 1% (in some high-*P* and low-Na orthopyroxenes) to at least 9% (in some low-*P*, relatively high-Na orthopyroxenes equilibrated with garnet). Some low-*P*, high-Na (high-*T*) mantle orthopyroxenes contain more Fe_2O_3 than coexisting garnets.

In common practice, redox conditions for garnet peridotites are estimated assuming that Fe^{3+} in Opx is negligible, so that fO_2 and activity of ferrosilite in Opx can simply be calculated using total Fe concentrations (Gudmundsson and Wood 1995; Stagno et al.

2013). Recalculating ferrsosilite activities in our samples using only Fe^{2+} instead of Fe_{tot}, produces a decrease in the calculated fO_2 of only 0.02 log units. Therefore, although higher than commonly assumed, the observed Fe^{3+}/Fe_{tot} ratios of up to 9% in Opx should not affect fO_2 estimates based on currently available oxybarometers.

The Fe^{3+} systematics observed in the studied xenoliths instead imply that the Opx–Grt Fe–Mg exchange thermometer is not robust against redox changes if total Fe is treated as Fe^{2+}. In particular, variations in Fe^{3+} partitioning with pressure in mantle peridotites may account for some systematic discrepancies observed between experimentally calibrated Opx–Grt and two-pyroxene thermometers (cf. Nimis and Grütter 2010). An approximate evaluation of errors on Opx–Grt temperatures due to redox effects predicts negligible deviations of *P*–*T* estimates for strongly reduced conditions, but potentially large deviations for strongly oxidized conditions, especially at very high pressure and when both *P* and *T* are calculated by iteration. Therefore, comparisons between *P*–*T* estimates derived using Opx–Grt and two-pyroxene thermometers, a common necessity when studying, for instance, both clinopyroxene-bearing and clinopyroxene-free peridotites, may be problematic if redox conditions are unknown. An experimental verification of Fe^{3+} partitioning systematics, e.g., by high-resolution Mössbauer analysis of Opx–Grt pairs re-equilibrated under controlled *P*–*T*–fO_2 and with varying Na_2O contents, would be desirable to derive a more robust evaluation and, hopefully, recalibration of Opx–Grt thermometers for mantle peridotites.

Acknowledgments We are grateful to Dante Canil for providing access to his original dataset. Sula Milani is thanked for her help in retrieving the old Mössbauer files. Formal reviews by Bob Luth and two anonymous referees helped us to improve the paper. PN

acknowledges financial support by MIUR ex60%. DAI thanks Igor Ashchepkov for providing some of the xenoliths used in this study and acknowledges financial support from the French CNRS, including PNP-INSU and PICS grants, and from the Australian Research Council including Research fellowship and grants in 1994-1998.

Appendix

Estimation of maximum bias on Opx–Grt temperature estimates due to changing redox conditions

Figure 8 shows a compilation of existing fO_2 data for mantle xenoliths worldwide, recalculated using input *P*–*T* values obtained with the thermobarometer combinations recommended by Nimis and Grütter (2010). This choice significantly reduced the scatter of points (especially for Diavik) compared to earlier published versions of this plot (e.g., Stagno et al. 2013). Correction of Canil and O'Neill's (1996) Mössbauer data for different recoil-free fractions in Grt (Table 4) produced a slight decrease in calculated fO_2 of about 0.6 Δlog units. The plot shows the well-known overall decrease of FMQ-normalized oxygen fugacity with increasing mantle depth and a range for fO_2 at each depth.

From this compilation, we selected five xenoliths coming from different depths and recording 'average' redox conditions for their particular depths of provenance (Table 6; Fig. 8). We calculated the Opx–Grt temperatures for these xenoliths with the thermometer version of Nimis and Grütter (2010) (hereafter TNG10) at *P* given by the thermobarometers combination recommended by the same authors, using total Fe. The TNG10 thermometer was calibrated against a large set of mantle xenoliths from localities worldwide and should therefore be robust when applied to mantle rocks characterized by 'average' redox conditions. All selected xenoliths showed very good agreement ($\Delta T < 60$ °C) between thermometric estimates using the internally consistent thermometers recommended by Nimis and Grütter (2010). This indicates good

equilibrium and also confirms that redox conditions in the xenoliths were indeed 'average' and compatible with the TNG10 thermometer calibration (cf. Nimis and Grütter 2010). Therefore the calculated *P*–*T* conditions should be reliable.

We then allowed fO_2 for each of the selected xenoliths to vary to the maximum and minimum values expected for the mantle at the corresponding depths, as indicated by our compilation in Figure 8. We estimated the Fe^{3+}/Fe_{tot} ratios in the garnets at these maximum and minimum redox conditions by reversing the oxybarometer of Stagno et al. (2013), and those in the coexisting orthopyroxenes by using the Fe^{3+} partitioning systematics obtained in our work (cf. Equation 6). The mineral compositions were modified using the new Fe^{3+}/Fe_{tot} ratios while keeping $K_{D_{Fe^{2+}-Mg}}^{Grt-Opx}$ unvaried—the latter depends essentially on *T*, therefore keeping it fixed corresponds to keeping *T* fixed. An increase (or decrease) in the Fe^{3+}/Fe_{tot} ratio thus determined a net increase (or decrease) in the total Fe content (actually Fe^{3+}), which was compensated by varying the $Al^{3+} + Cr^{3+}$ contents by the same magnitude at constant Al/Cr ratio. Since the solid solution model for garnet which is used in the oxybarometer of Stagno et al. (2013) is sensitive to the Al and Cr contents, the Fe^{3+}/Fe_{tot} ratios had to be readjusted by iteration, although the effect of this correction was found to be minimal.

We then recalculated the TNG10 temperatures using the modified total Fe contents in both orthopyroxenes and garnets, either keeping *P* fixed or recalculating both *P* and *T* iteratively. The *P*–*T* estimates obtained for the selected xenoliths using the original mineral compositions and the compositions modified for their respective maximum and minimum redox conditions are reported in Table 6. We emphasize that the aim of this exercise was to assess 'relative' variations on final *P*–*T* estimates, and that possible

small interlab discrepancies in Fe^{3+}/Fe_{tot} ratios for Grt extracted from the literature and from this work do not significantly alter our results.

References

Annersten H, Olesch M, Seifert FA (1978) Ferric iron in orthopyroxene: a Mössbauer spectroscopic study. Lithos 11:301–310

Ballhaus C (1995) Is the upper mantle metal-saturated? Earth Planet Sci Lett 132:75–86

Boyd FR, Mertzman SA (1987) Composition and structure of the Kaapvaal lithosphere, southern Africa. In: Mysen BO (ed.) Magmatic Processes: Physiochemical Principles. Geochem Soc Spec Publ 1:13-24

Brey GP, Köhler T (1990) Geothermobarometry in four-phase lherzolites II. New thermobarometers, and practical assessment of existing thermobarometers. J Petrol 31:1353–1378

Canil D, O'Neill HStC (1996) Distribution of ferric iron in some upper-mantle assemblages. J Petrol 37:609–635

Caro G (2000) Petrography of the Kennedy Lake orangeite and its mantle xenoliths. Unpubl MSc thesis, University of British Columbia, 100 p

Carswell DA (1991) The garnet-orthopyroxene Al barometer: problematic application to natural garnet lherzolite assemblages. Mineral Mag 55:19–31

Cox KG, Smith MR, Beswetherick S (1987) Textural studies of garnet lherzolites: evidence of exsolution origin from high-temperature harzburgites. In: Nixon PH (ed.) Mantle Xenoliths. John Wiley & Sons, pp 537–550

Creighton S, Stachel T, Matveev S, Höfer HE, McCammon C, Luth RW (2009) Oxidation of the Kaapvaal lithospheric mantle driven by metasomatism. Contrib Mineral Petrol 157:491–504

Creighton S, Stachel T, Eichenberg D, Luth RW (2010) Oxidation state of the lithospheric mantle beneath Diavik diamond mine, central Slave craton, NWT, Canada. Contrib Mineral Petrol 159:645–657

Dollase WA (1975) Statistical limitations of Mössbauer spectral fitting. Am Miner 60: 257-264

Domeneghetti MC, Molin GM, Tazzoli V (1995) A crystal-chemical model for PBCA orthopyroxene. Am Mineral 80:253–267

Doucet LS, Ionov DA, Golovin AV (2013) The origin of coarse garnet peridotites in cratonic lithosphere: new data on xenoliths from the Udachnaya kimberlite, central Siberia. Contrib Mineral Petrol 165:1225–1242

Doucet LS, Peslier AH, Ionov DA, Brandon AD, Golovin AV, Goncharov AG, Ashchepkov IV (2014) High water contents in the Siberian cratonic mantle linked to metasomatism: an FTIR study of Udachnaya peridotite xenoliths. Geochim Cosmochim Acta 137:159–187

Frost DJ, McCammon CA (2008) The redox state of Earth's mantle. Annu Rev Earth Planet Sci 36:389–420

Goncharov AG, Ionov DA (2012) Redox state of deep off-craton lithospheric mantle: new data from garnet and spinel peridotites from Vitim, southern Siberia. Contrib Mineral Petrol 164:731–745

Goncharov AG, Ionov DA, Doucet LS, Pokhilenko LN (2012) Thermal state, oxygen fugacity and C–O–H fluid speciation in cratonic lithospheric mantle: New data on peridotite xenoliths from the Udachnaya kimberlite, Siberia. Earth Planet Sci Lett 357-358:99–110

Gregoire M, Bell DR, le Roux AP (2003) Garnet lherzolites from the Kaapvaal craton (South Africa): Trace element evidence for a metasomatic history. J Petrol 44:629–657

Gudmundsson G, Wood BJ (1995) Experimental tests of garnet peridotite oxygen barometry. Contrib Mineral Petrol 119:56–67

Harley SL (1984) An experimental study of the partitioning of Fe and Mg between garnet and orthopyroxene. Contrib Mineral Petrol 86:359–373

Hops JJ, Gurney JJ, Harte B, Winterburn P (1989) Megacrysts and high temperature nodules from the Jagersfontein kimberlite pipe. In: Ross J (ed) Kimberlites and related rocks, vol 2, Their mantle/crust setting, diamonds and diamond exploration. Geol Soc Aus Spec Publ, vol 14, pp 759–770

Ionov DA (2002) Mantle structure and rifting processes in the Baikal-Mongolia region: geophysical data and evidence from xenoliths in volcanic rocks. Tectonophysics 351:41–60

Ionov DA, Griffin WL, O'Reilly SY (1999) Off-cratonic garnet and spinel peridotite xenoliths from Dsun-Bussular, SE Mongolia. In: Gurney JJ, Gurney JL, Pascoe MD, Richardson SH (eds) Proc 7th Int. Kimb Conf, vol 1. RedRoof Design Cape Town, pp 383–390

Ionov DA, Doucet LS, Ashchepkov IV (2010) Composition of the lithospheric mantle in the Siberian craton: New constraints from fresh peridotites in the Udachnaya-East kimberlite. J Petrol 51:2177–2210

Kopylova MG, Caro G (2004) Mantle xenoliths from the southeastern Slave craton: evidence for chemical zonation in a thick, cold lithosphere. J Petrol 45:1045–1067

Kopylova MG, Russel JK, Cookenboo H (1999a) Petrology of peridotite and pyroxenite xenoliths from the Jericho kimberlite: Implications for the thermal state of the mantle beneath the Slave craton, Northern Canada. J Petrol 40:79–104

Kopylova MG, Russel JK, Cookenboo H (1999b) Mapping the lithosphere below the north central Slave craton. In: Gurney JJ, Gurney JL, Pascoe MD, Richardson SH (eds), J. B. Dawson Volume, Proc 7th Int Kimb Conf, Red Roof Design Cape Town, pp 468–479

Lazarov M, Woodland AB, Brey GP (2009) Thermal state and redox conditions of the Kaapvaal mantle: A study of xenoliths from the Finsch mine, South Africa. Lithos 112S:913–923

Luth RW, Canil D (1993) Ferric iron in mantle-derived pyroxenes and a new oxybarometer for the mantle. Contrib Mineral Petrol 113:236–248

Luth RW, Virgo D, Boyd FR, Wood BJ (1990) Ferric iron in mantle-derived garnets. Implications for thermobarometry and for the oxidation state of the mantle. Contrib Mineral Petrol 104:56–72

Malaspina N, Langenhorst F, Fumagalli P, Tumiati S, Poli S (2012) Fe^{3+} distribution between garnet and pyroxenes in mantle wedge carbonate-bearing garnet peridotites (Sulu, China) and implications for their oxidation state. Lithos 146-147:11–17

Matjuschkin V, Brey GP, Höfer HE, Woodland AB (2014) The influence of Fe^{3+} on garnet–orthopyroxene and garnet–olivine geothermometers. Contrib Mineral Petrol 167:1–10

McCammon C, Kopylova MG (2004) A redox profile of the Slave mantle and oxygen fugacity control in the cratonic mantle. Contrib Mineral Petrol 148:55–68

McCammon CA, Tennant WC, Miletich RM (2000) A new method for single crystal measurements: Application to studies of mineral inclusions in diamonds. Hyper Inter 126: 241–245

McCammon CA, Griffin WL, Shee SR, O'Neill HStC (2001) Oxidation during metasomatism in ultramafic xenoliths from the Wesselton kimberlite, South Africa: implications for the survival of diamond. Contrib Mineral Petrol 141:287–296

Nickel KG (1989) Garnet-pyroxene equilibria in the system SMACCR (SiO_2-MgO-Al_2O_3-CaO-Cr_2O_3): the Cr-geobarometer. In Ross J (ed) Kimberlites and related rocks, vol 2, Their mantle/crust setting, diamonds and diamond exploration. Proc 4th Int Kimb Conf, Geol Soc Aus Spec Publ, vol 14, pp 901–912

Nickel KG, Green DH (1985) Empirical geothermobarometry for garnet peridotites and implications for the nature of the lithosphere, kimberlites and diamonds. Earth Planet Sci Lett 73:158–170

Nimis P, Grütter H (2010) Internally consistent geothermometers for garnet peridotites and pyroxenites. Contrib Mineral Petrol 159:411–427

Nimis P, Taylor WR (2000) Single-clinopyroxene thermobarometry for garnet peridotites. Part I. Calibration and testing of a Cr-in-Cpx barometer and an enstatite-in-Cpx thermometer. Contrib Mineral Petrol 139:541–554

O'Neill HStC, Wall VJ (1987) The olivine-orthopyroxene-spinel oxygen geobarometer, the nickel precipitation curve, and the oxygen fugacity of the earth's upper mantle. J Petrol 28:1169–1191

Pearson DG, Boyd FR, Haggerty SE, Pasteris JD, Field SW, Nixon PH, Pokhilenko NP (1994) The characterisation and origin of graphite in cratonic lithospheric mantle: a petrological carbon isotope and Raman spectroscopic study. Contrib Mineral Petrol 115:449–466

Pollack HN, Chapman DS (1977) On the regional variations of heat flow, geotherms and lithospheric thickness. Tectonophysics 38:279–296

Purwin H, Lauterbach S, Brey GP, Woodland AB, Kleebe H-J (2013) An experimental study of the Fe oxidation states in garnet and clinopyroxene as a function of temperature in the system CaO–FeO–Fe_2O_3–MgO–Al_2O_3–SiO_2: implications for garnet–clinopyroxene geothermometry. Contrib Mineral Petrol 165:623–639

Saltzer RL, Chatterjee N, Grove TL (2001) The spatial distribution of garnets and pyroxenes in mantle peridotites: Pressure-temperature history of peridotites from the Kaapvaal craton. J Petrol 42:2215–2229

Schmidberger SS, Francis D (1999) Nature of mantle roots beneath the North American craton: mantle xenolith evidence from Somerset Island kimberlites. Lithos 48:195–216

Shirey SB, Cartigny P, Frost DJ, Keshav S, Nestola F, Nimis P, Pearson DG, Sobolev NV, Walter MJ (2013) Diamonds and the Geology of Mantle Carbon. Rev Mineral Geochem 75:355–421

Smith D (1999) Temperatures and pressures of mineral equilibration in peridotite xenoliths: Review, discussion, and implications. In: Fei Y, Bertka CM, Mysen BO (eds) Mantle Petrology: Field Observations and high pressure experimentation: A tribute to Francis R. (Joe) Boyd. Geochem Soc Spec Publ, vol 6, pp 171–188

Stagno V, Ojwang DO, McCammon CA, Frost DJ (2013) The oxidation state of the mantle and the extraction of carbon from Earth's interior. Nature 493:84–88

Taylor WR (1998) An experimental test of some geothermometer and geobarometer formulations for upper mantle peridotites with application to the thermobarometry of fertile lherzolite and garnet websterite. Neues Jb Miner Abh 172:381–408

Woodland AB (2009) Ferric iron contents of clinopyroxene from cratonic mantle and partitioning behaviour with garnet. Lithos 112S:1143–1149

Woodland AB, Koch M (2003) Variation in oxygen fugacity with depth in the upper mantle beneath the Kaapvaal craton, Southern Africa. Earth Planet Sci Lett 214:295–310

Woodland AB, Peltonen P (1999) Ferric iron contents of garnet and clinopyroxene and estimated oxygen fugacities of peridotite xenoliths from the Eastern Finland Kimberlite Province. In JJ Gurney, JL Gurney, MD Pascoe, SH Richardson (eds) Proc 7th Int Kimb Conf, pp 904–911. Red Roof Design Cape Town South Africa

Woodland AB, Ross CR (1994) A crystallographic and Mössbauer spectroscopy study of $Fe_3Al_2Si_3O_{12}$-$Fe_3^{2+}Fe_2^{3+}Si_3O_{12}$ (almandine-skiagite) and $Ca_3Fe_2^{3+}Si_3O_{12}$-$Fe_3^{2+}Fe_2^{3+}Si_3O_{12}$ (andradite-skiagite) garnet solid solutions. Phys Chem Minerals 21:117–132

Yaxley GM, Berry AJ, Kamenetsky VS, Woodland AB, Golovin AV (2012) An oxygen fugacity profile through the Siberian Craton — Fe K-edge XANES determinations of $Fe^{3+}/\sum Fe$ in garnets in peridotite xenoliths from the Udachnaya East kimberlite. Lithos 140–141:142–151

Figure Captions

Fig. 1 Mössbauer spectra for orthopyroxene and garnet in two xenoliths showing different partitioning of Fe^{3+}.

Fig. 2 *P–T* estimates for mantle xenoliths studied in this work. Reference geotherms after Pollack and Chapman (1977). CO'N96 *P–T* values recalculated using compositional data in Canil and O'Neill (1996) and references therein. The fields of typical on-craton and off-craton garnet peridotites are shown for comparison.

Fig. 3 Opx–Grt Fe^{3+} partitioning systematics in mantle xenoliths. Error bars for $\ln D Fe^{3+}$ and Na_2O are at 1σ. Uncertainties on Na_2O were not reported for the literature samples and were calculated as $0.026 – 0.08 \cdot Na_2O$ (wt%), based on systematic relationships in our analyses using routine analytical conditions. Error bars for *P* and *T* were fixed to 0.4 GPa, 50 °C, and raised to 0.5 GPa, 70 °C for samples equilibrated at $T < 800$ °C and for some samples showing poor agreement between internally consistent thermometers (cf. Nimis and Grütter 2010). Dashed lines indicate unweighted linear regressions through the data.

Fig. 4 Fe^{3+} contents vs. tetrahedral Al (**a**) and Na contents (**b**) in the investigated Opx. The low-$^{[4]}$Al group corresponds to the on-craton xenoliths, the high-$^{[4]}$Al group consists of the off-craton Dariganga xenoliths. The dashed line in **b** separates the two groups. Spinel-bearing sample BY-18 falls off the trend shown by the other Dariganga samples.

Fig. 5 a Variation of Grt/Cpx $\ln D Fe^{3+}$ with reciprocal *T* in the investigated xenoliths. Shaded field: data for garnet peridotites after Woodland and Peltonen (1999), Woodland (2009), Lazarov et al. (2009), plus additional data from Canil and O'Neill (1996). As already pointed out by Canil and O'Neill (1996), the spinel-bearing, very low-*T* sample FRB1350 falls off the main trend. **b** Fe^{3+} distribution between Opx and Cpx.

Fig. 6 Calculated (Equation 6) vs. measured Fe^{3+} partitioning between Opx and Grt. Data for Canil and O'Neill's (1996) samples that showed poor agreement between independent thermometric estimates were not considered in the regression. Error bars are at 1σ. Same symbols as in Fig. 2.

Fig. 7 Variation in the Grt–Opx 'iron ratio' with *P* in mantle xenoliths. The relationship with *P* mimics that shown by $D Fe^{3+}$ (cf. Fig. 3b). Same symbols as in Fig. 2.

Fig. 8 Estimated fO_2 normalized to the FMQ buffer (Stagno et al. 2013) for garnet peridotite xenoliths worldwide. The EMOG/D curve corresponds to the enstatite–magnesite–graphite/diamond buffer along a cratonic geotherm (Stagno et al. 2013). The Fe–Ni precipitation curve after O'Neill and Wall (1987). Shaded field approximately indicates the diamond stability field. Dashed lines indicate the apparent typical fO_2 range at various mantle depths. Arrows connect five selected well-equilibrated samples recording 'average' fO_2 for their respective depth to corresponding maximum and minimum fO_2 values. Sources of compositional data: Siberia – Yaxley et al. (2012), Goncharov et al. (2012); Kaapvaal – Luth et al. (1990), Lazarov et al. (2009), Creighton et al. (2009), Canil and O'Neill (1996, as revisited in this work); N and SE Slave – McCammon and Kopylova (2004); Diavik – Creighton et al. (2010); Mongolia – this work. Seventeen data showing poor agreement (>100 °C) between independent, internally consistent pyroxene thermometers (cf. Nimis and Grütter 2010) were excluded.

Fig. 9 Differences between temperatures calculated with the Opx–Grt thermometer (Nimis and Grütter 2010; TNG10) and the two-pyroxene thermometer (Taylor 1998; TTA98) for mantle xenoliths from different localities. All xenoliths show good equilibrium between pyroxenes based on criteria in Nimis and Grütter (2010). Shaded fields indicate the declared uncertainty (2 standard errors of estimate, ±70 °C) of the TNG10 thermometer. Dashed lines indicate the maximum predicted bias on TNG10 for strongly reducing and, respectively, strongly oxidized conditions. Several xenoliths from Jagersfontein show positive deviations well beyond estimated uncertainties, suggesting disequilibrium due to transient heating. Xenolith data from Nimis and Grütter's (2010) compilation, specifically: Jagersfontein – Boyd (pers. comm. to H. Grütter), Cox et al. (1987), Boyd and Mertzman (1987), Hops et al. (1989), Mofokeng (1998), Smith (1999), Saltzer et al. (2001), Grégoire et al. (2003); Slave – Kopylova et al. (1999a,b), Caro (2000), McCammon and Kopylova (2004), Kopylova and Caro (2004); Nikos – Schmidberger and Francis (1999).

Figure 1
Click here to download high resolution image

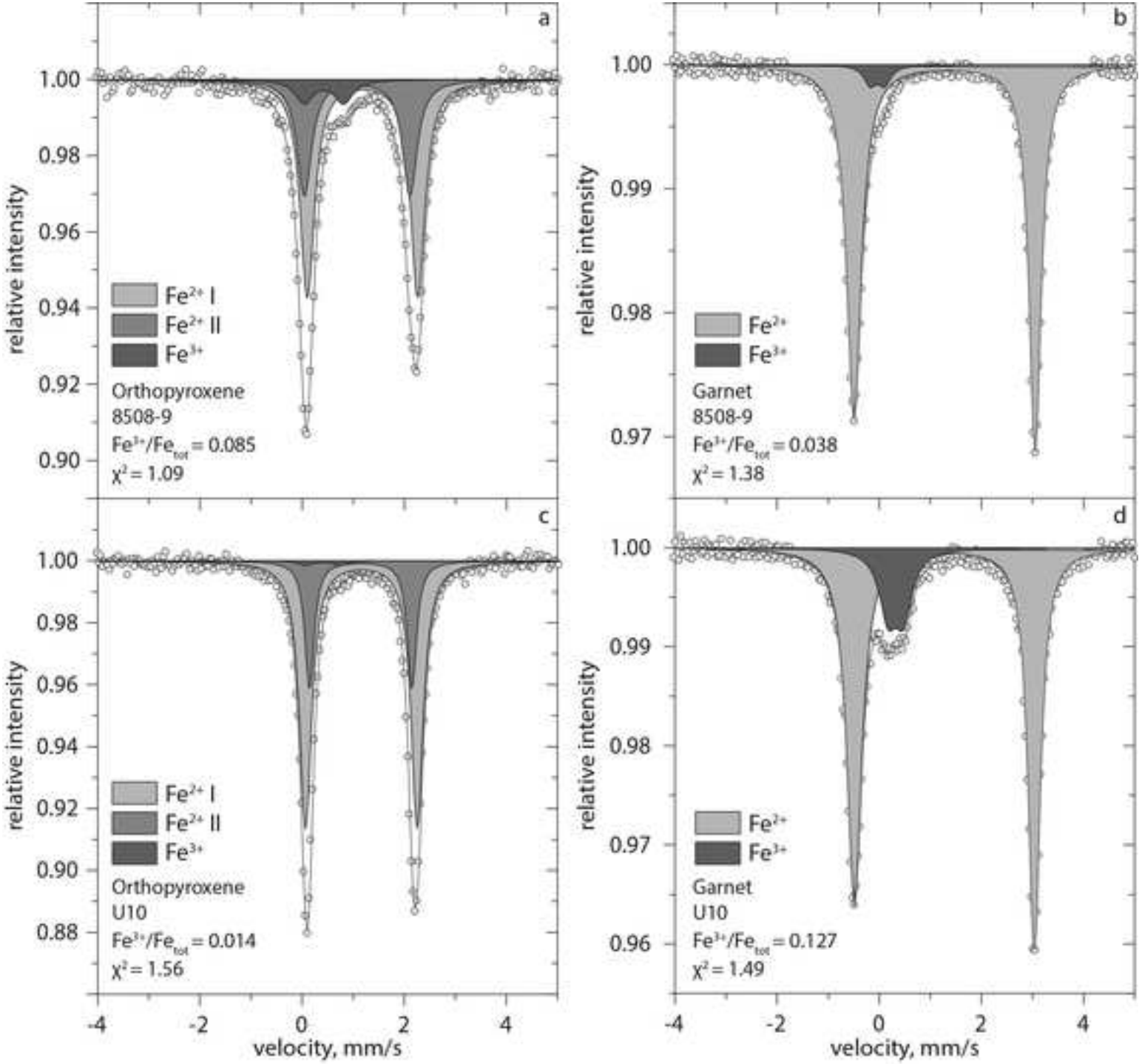

Figure 2
Click here to download high resolution image

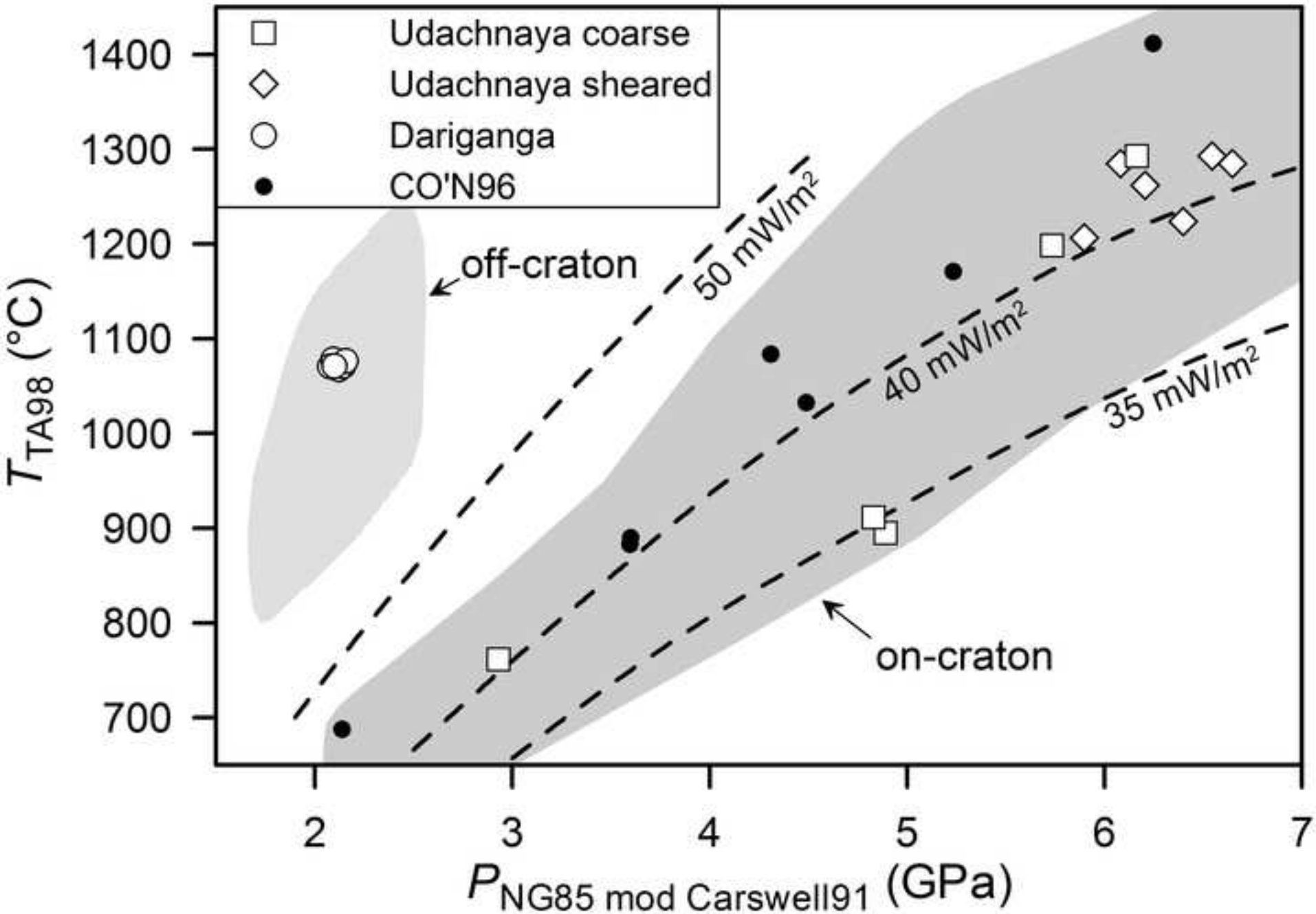

Figure 3
Click here to download high resolution image

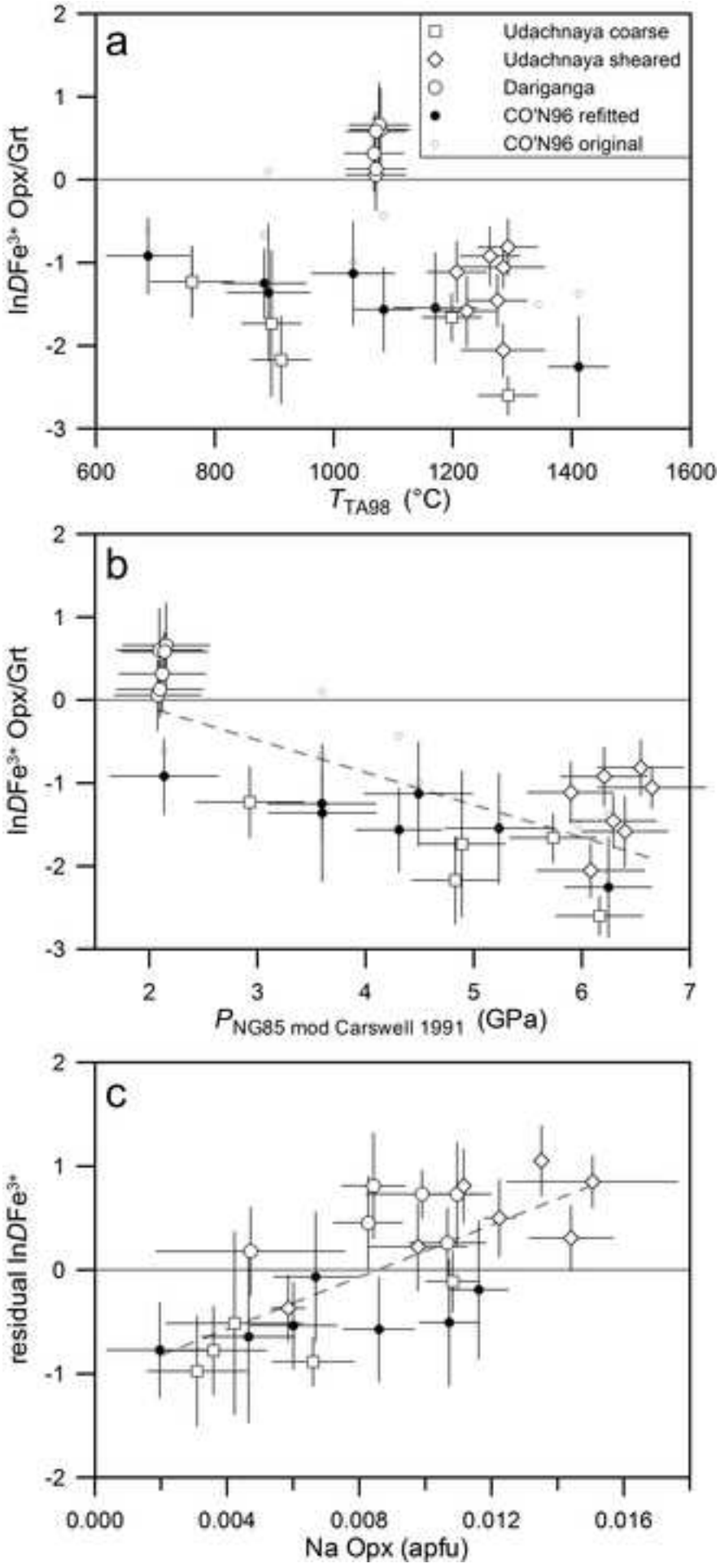

Figure 4
Click here to download high resolution image

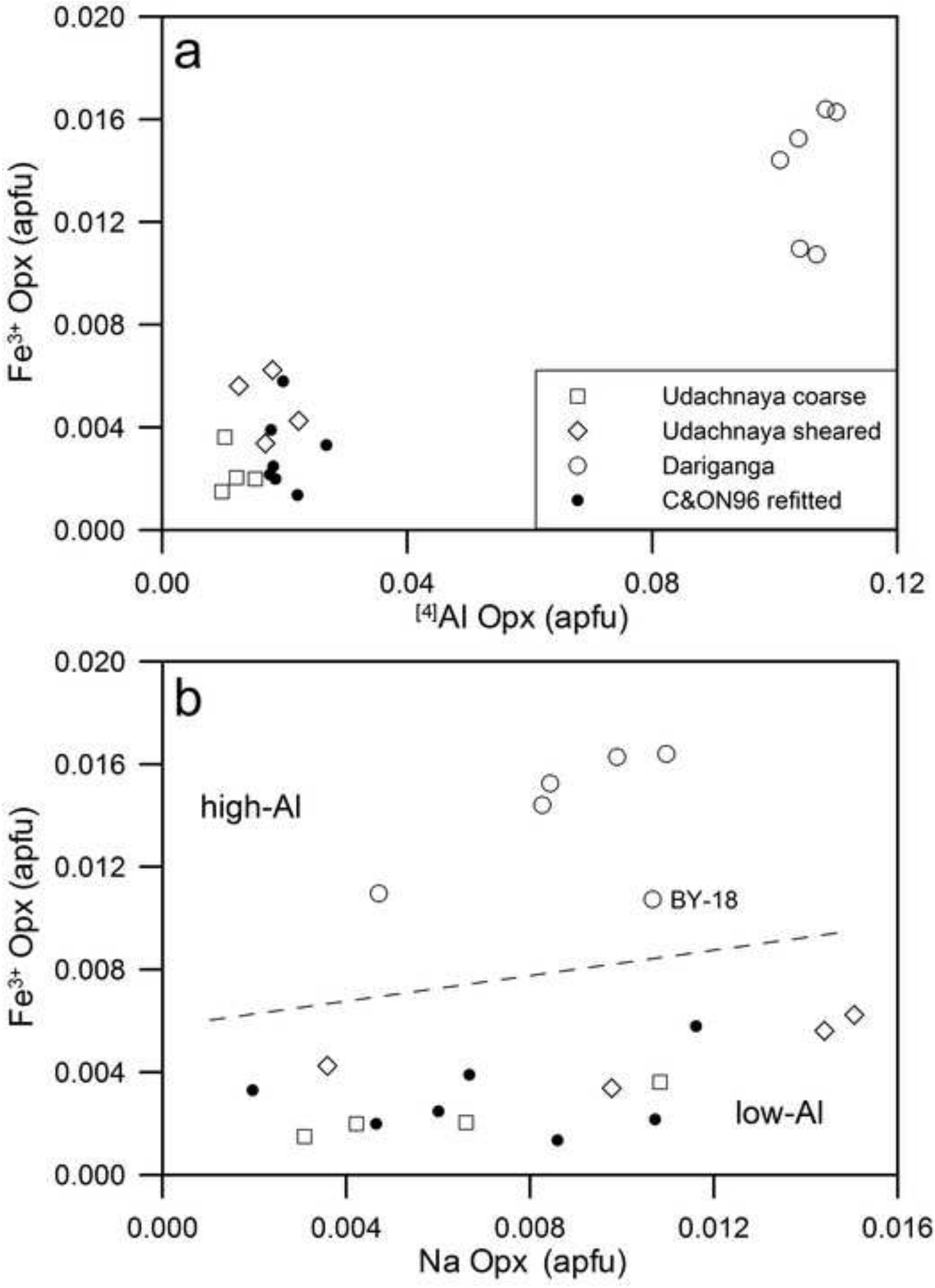

Figure 5
Click here to download high resolution image

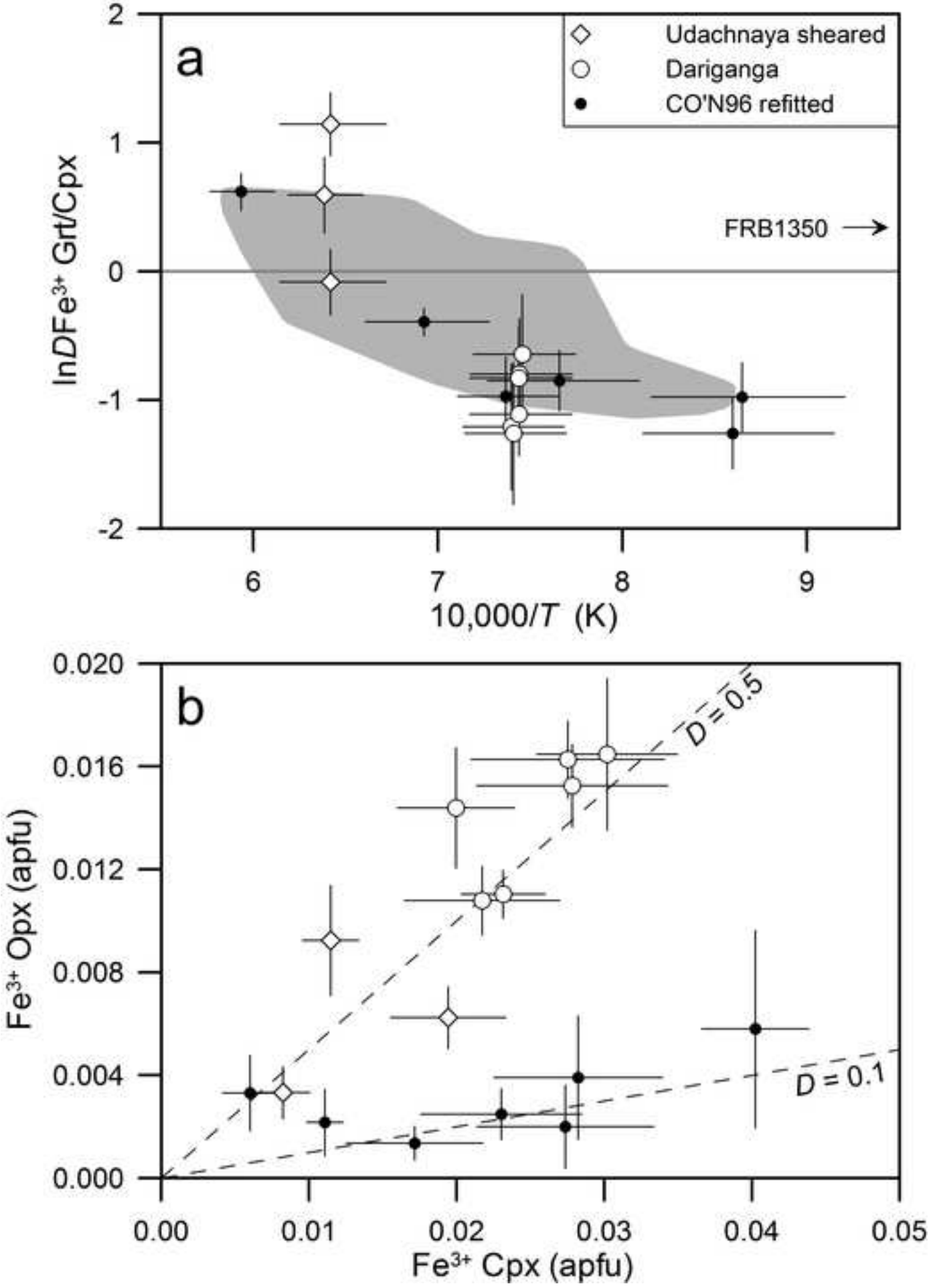

Figure 6
Click here to download high resolution image

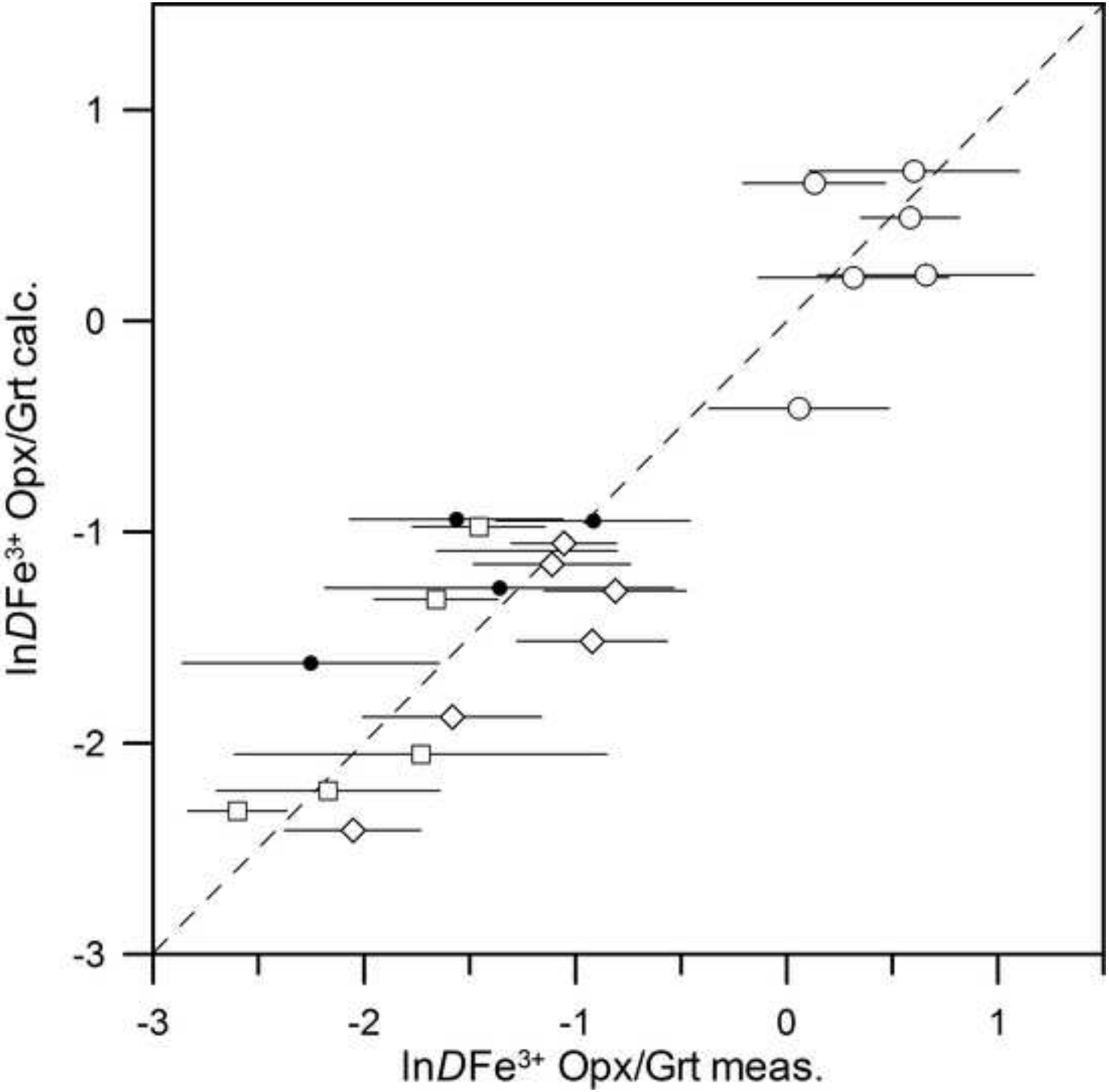

Figure 7
Click here to download high resolution image

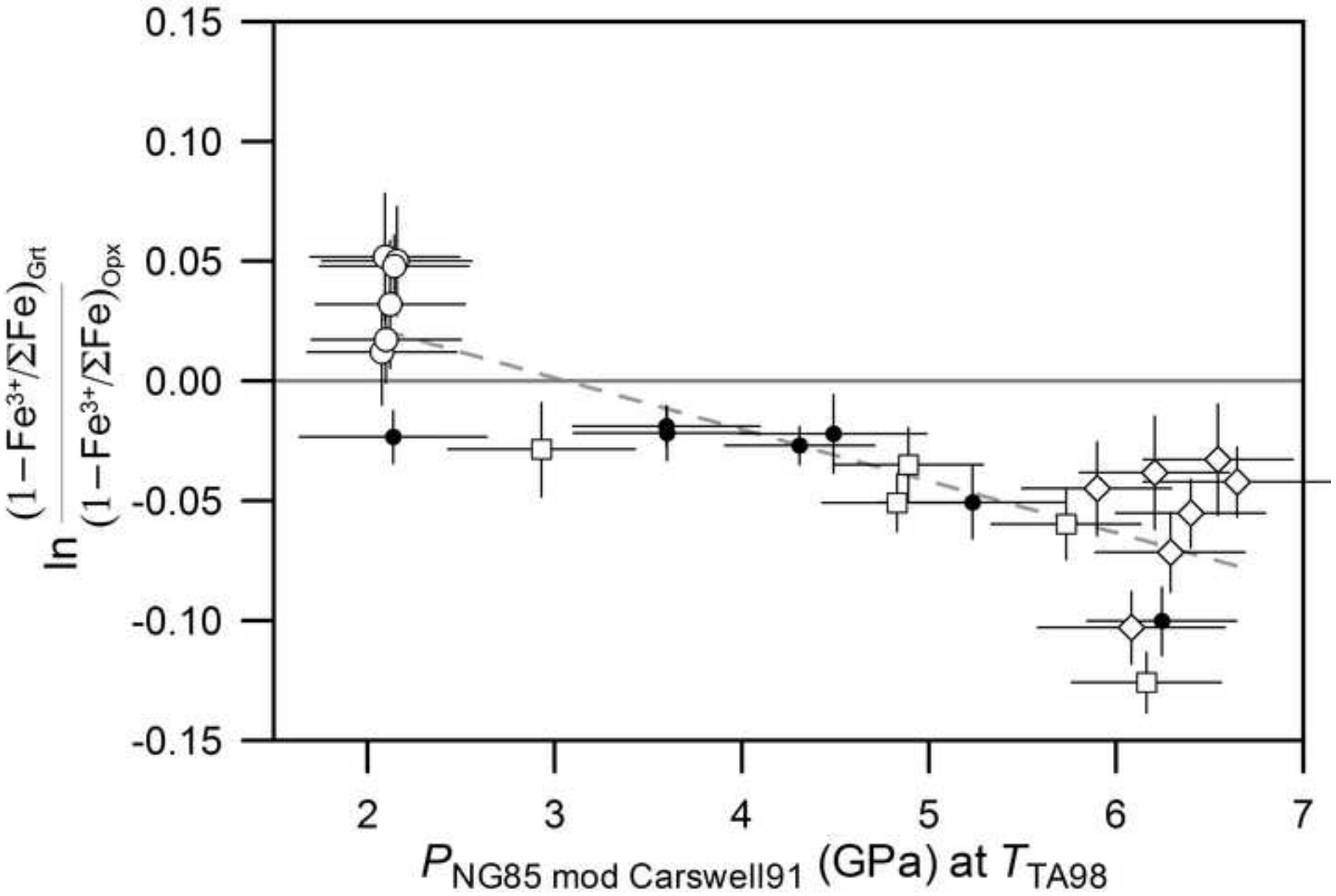

Figure 8
Click here to download high resolution image

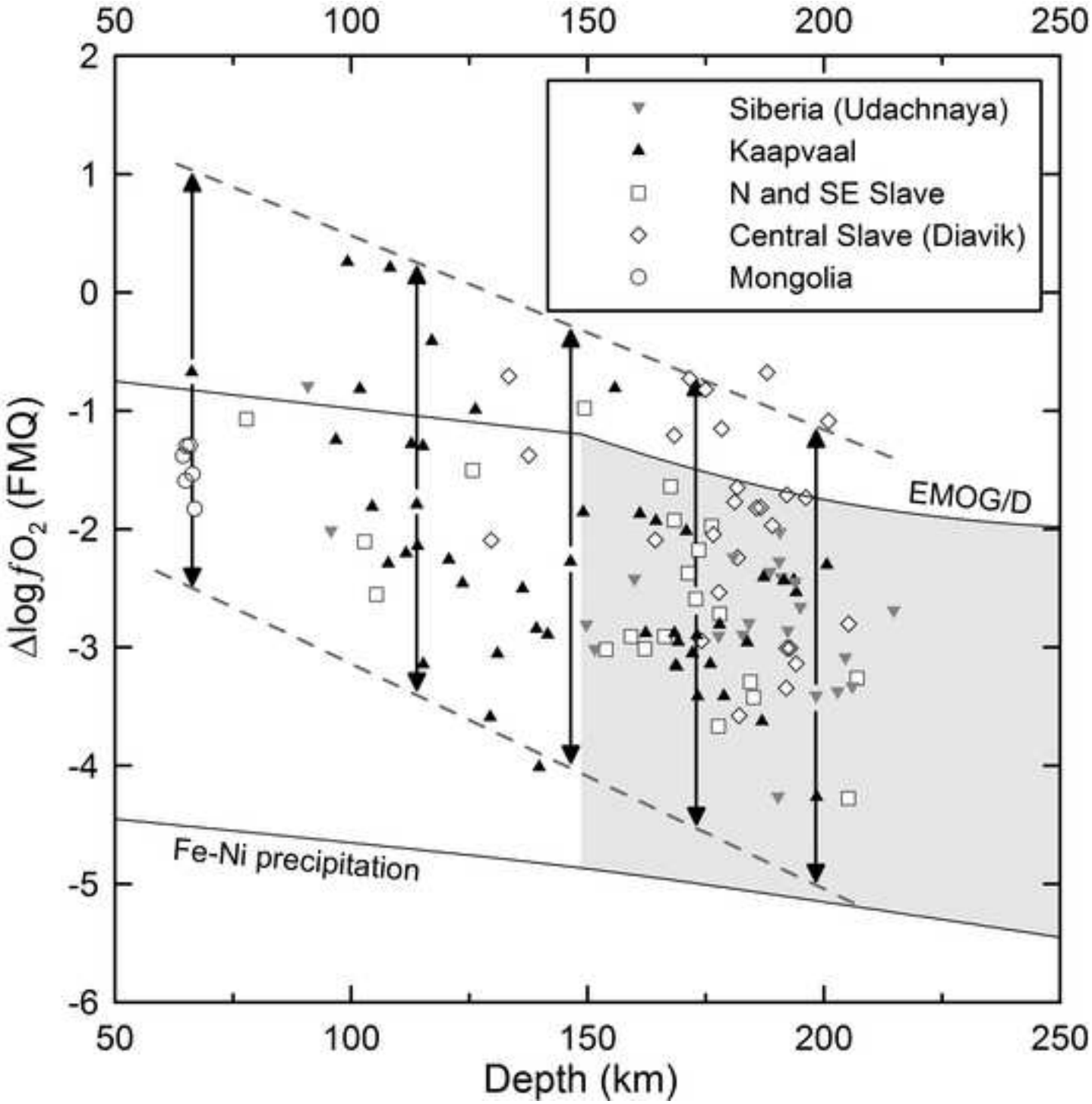

Figure 9
Click here to download high resolution image

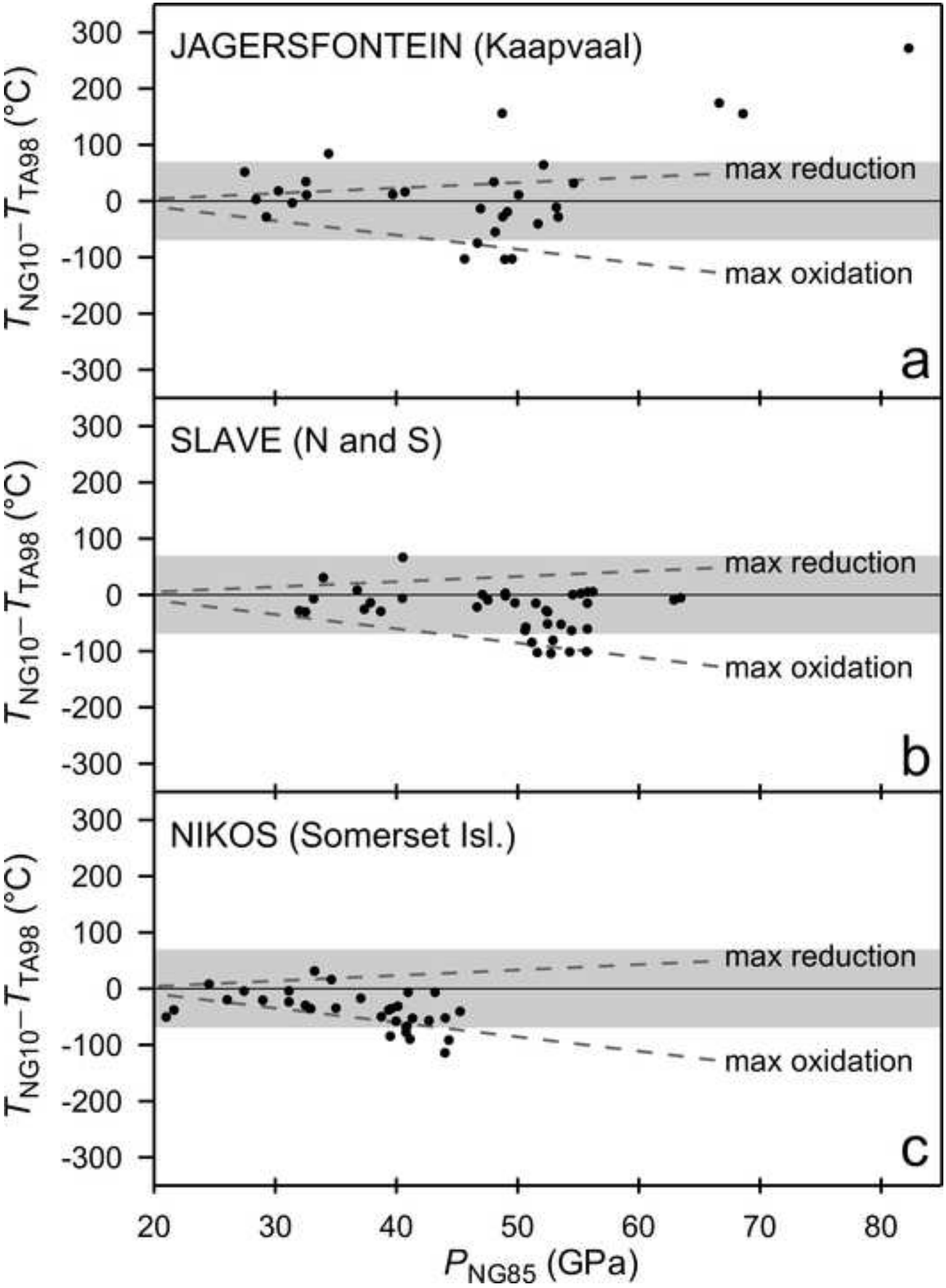

Table 1
Click here to download Table: Table1.doc

Table 1. Modal compositions, selected chemical data and thermobarometric estimates for the investigated xenoliths.

Sample	Rock type	Modal composition, wt%					Mg#	Al_2O_3	Thermobarometry						
		Ol	Opx	Cpx	Grt	Spl	WR	WR	*P* (GPa) NG85 at TTA98	*T* (°C) TA98 at PNG85	*T* (°C) NT00 at PNG85	*T* (°C) Ca-in-Opx at PNG85	*T* (°C) NG10 at PNG85	*P* (GPa) Ca91 at TTA98	*T* (°C) TA98 at PCa91
Udachnaya coarse and "transitional"															
U29	Lherzolite	69	20	5.6	2.1	0.0	0.921	1.13	4.83	911	892	950	949	4.83	911
U64	Harzburgite	77	17	3.8	2.5	0.0	0.910	0.50	5.62	1194	1183	1149	1129	5.73	1198
U283	Harzburgite	85	10	1.4	3.7	0.2	0.920	0.91	2.93	762	747	827	763	2.93	762
U501	Harzburgite	82	6.6	4.3	6.7	0.0	0.913	1.43	4.89	895	872	913	945	4.89	895
U10 (transit.)	Harzburgite	81	12	4.0	2.5	0.0	0.914	0.49	6.16	1293	1281	1288	1265	6.16	1293
Udachnaya sheared															
U70	Lherzolite	79	9.5	6.0	5.5	0.0	0.904	1.21	5.14	1233	1234	1219	1188	6.29	1275
U183	Harzburgite	81	14	1.9	3.8	0.0	0.919	0.77	6.40	1224	1205	1218	1237	6.40	1224
U267	Lherzolite	53	22	12	13	0.0	0.896	3.17	5.88	1257	1242	1265	1353	6.65	1285
Y-10	Lherzolite	71	16	6.0	7.0	0.0	0.905	1.59	5.87	1206	1192	1202	1262	5.90	1207
Y-19	Wehrlite	80	1.0	16	3.7	0.0	0.905	1.50	5.85	1249	1242	1239	1210	6.21	1262
87/70	Harzburgite	–	–	–	–	–	–	–	6.08	1285	1281	1268	1208	6.08	1285
87/97	Lherzolite	–	–	–	–	–	–	–	5.70	1262	1255	1249	1271	6.54	1293
Dariganga (coarse)															
8508-6	Lherzolite	66	20	6.0	8.0	0.0	0.895	3.05	2.08	1071	1051	1077	1081	2.08	1071
8508-9	Lherzolite	57	27	13	3.5	0.0	0.897	2.67	2.16	1076	1054	1104	1108	2.16	1076
BY-18	Lherzolite	57	19	13	11	0.3	0.903	3.94	2.10	1071	1048	1116	1102	2.10	1071
BY-19	Lherzolite	59	21	10	9.3	0.0	0.894	3.71	2.14	1071	1049	1107	1123	2.14	1071
BY-27	Lherzolite	56	26	12	6.5	0.0	0.892	3.41	2.09	1078	1057	1112	1070	2.09	1078
BY-33	Lherzolite	54	27	9.7	8.9	0.0	0.896	3.79	2.12	1068	1047	1093	1096	2.12	1068

Modal abundances obtained by least-squares method from whole-rock and mineral analyses (data for Udachnaya after Ionov et al. 2010 and Goncharov et al. 2012; data for samples 87/70 and 87/97 not available due to small xenolith size). Ol – olivine, Opx – orthopyroxene, Cpx – clinopyroxene, Grt – garnet, Spl – spinel, WR – whole rock. Thermobarometer labels: PNG85 – Nickel and Green (1985); PCa91 – Nickel and Green (1985), with correction in Carswell (1991); TTA98 – Taylor (1998); TNT00 – Nimis and Taylor (2000); TCa-in-Opx – Brey and Köhler (1990), with correction in Nimis and Grütter (2010); TNG10 – Nimis and Grütter (2010).

Table 2
Click here to download Table: Table2.doc

Table 2. Electron microprobe analyses (wt%) of minerals and *P–T* estimates.

Sample	Mineral	SiO_2	TiO_2	Al_2O_3	Cr_2O_3	FeOtot	FeO	Fe_2O_3	MnO	NiO	MgO	CaO	Na_2O	K_2O	Tot
Udachnaya coarse and transitional															
U29	ol	41.56	<0.10	<0.06	<0.12	7.59			0.10	0.37	50.53	<0.07	<0.05	<0.05	100.11
	opx	58.63	<0.10	0.37	0.22	4.37	4.31	0.06	0.10	0.10	35.95	0.35	0.05	<0.05	100.13
	cpx	54.47	<0.10	1.78	2.10	2.10			0.09	<0.06	16.20	20.71	1.73	<0.05	99.18
	grt	41.49	<0.10	19.17	6.57	7.37	6.94	0.48	0.46	<0.06	18.95	6.49	<0.05	<0.05	100.50
U64	ol	41.06	<0.10	<0.06	<0.12	8.87			0.11	0.31	49.50	<0.07	<0.05	<0.05	99.91
	opx	58.29	<0.10	0.43	0.38	5.14	5.02	0.14	0.13	0.13	34.84	0.65	0.16	<0.05	100.16
	cpx	55.12	0.18	1.43	2.47	2.96			0.11	0.06	17.66	17.97	1.90	0.05	99.90
	grt	40.74	0.13	14.86	11.27	7.63	7.01	0.69	0.40	<0.06	18.75	6.30	0.06	<0.05	100.14
U283	ol	41.40	<0.10	<0.06	<0.12	7.82			0.10	0.36	50.27	<0.07	<0.05	<0.05	99.91
	opx	58.33	<0.10	0.87	0.33	4.86	4.71	0.17	0.12	0.08	35.59	0.31	0.05	<0.05	100.55
	cpx	55.12	<0.10	2.09	1.84	1.37			0.09	<0.06	16.19	21.67	1.67	<0.05	100.05
	grt	41.27	<0.10	20.28	5.16	8.36	7.88	0.54	0.58	<0.06	18.84	6.30	<0.05	<0.05	100.79
	spl	0.00	<0.10	15.52	55.17	16.74	0.39	0.02	11.72	<0.06	0.00	0.00	99.63		
U501	ol	41.46	<0.10	<0.06	<0.12	8.16			0.09	0.34	50.27	<0.07	<0.05	<0.05	100.33
	opx	58.60	0.10	0.48	0.30	5.00	4.93	0.08	0.10	0.06	35.63	0.29	0.06	<0.05	100.62
	cpx	55.16	0.18	2.21	2.52	2.03			0.09	<0.06	15.65	20.11	2.23	<0.05	100.17
	grt	41.71	0.26	19.47	5.45	8.54	8.17	0.42	0.50	<0.06	19.34	5.47	0.06	<0.05	100.79
U10	ol	41.18	<0.10	<0.06	<0.12	8.68			0.12	0.35	49.62	<0.07	<0.05	<0.05	100.15
(transit.)	opx	58.14	<0.10	0.49	0.34	5.08	5.00	0.08	0.10	0.10	34.78	1.00	0.10	<0.05	100.12
	cpx	55.16	<0.10	0.80	1.05	2.78			0.12	0.07	19.26	19.24	0.74	0.09	99.32
	grt	41.12	0.45	15.55	9.54	7.06	6.16	1.00	0.30	<0.06	19.11	6.73	<0.05	<0.05	99.86
Udachnaya sheared															
U70	ol	41.34	<0.10	<0.06	<0.12	9.52			0.09	0.38	48.88	<0.07	<0.05	<0.05	100.33
	opx	58.33	<0.10	0.65	0.27	5.67	5.47	0.22	0.12	n.a.	34.03	0.92	0.22	n.a.	100.21
	cpx	55.48	0.14	1.71	1.25	3.56			0.11	n.a.	18.45	17.67	1.65	<0.05	100.02
	grt	42.31	0.49	19.00	5.00	8.00	7.19	0.90	0.31	n.a.	20.69	4.88	0.06	n.a.	100.75
U183	ol	41.16	<0.10	<0.06	<0.12	8.21			0.14	0.38	49.80	<0.07	<0.05	<0.05	99.9
	opx	57.96	0.18	0.53	0.34	4.79	4.67	0.13	0.10	0.08	35.04	0.74	0.15	<0.05	99.92
	cpx	54.90	0.33	1.33	1.52	2.82			0.11	0.06	18.04	18.63	1.53	<0.05	99.29
	grt	41.05	0.27	16.47	9.22	7.04	6.49	0.60	0.34	<0.06	19.28	6.56	<0.05	<0.05	100.22
U267	ol	41.10	<0.10	<0.06	<0.12	9.94			0.12	0.32	48.75	<0.07	<0.05	<0.05	100.51
	opx	57.90	0.22	0.69	0.21	5.97	5.75	0.24	0.13	0.13	33.91	0.96	0.23	<0.05	100.34
	cpx	55.23	0.33	1.85	0.69	3.68	3.03	0.72	0.10	0.07	18.53	17.83	1.54	0.06	99.91
	grt	42.49	0.43	21.03	2.63	7.97	7.36	0.67	0.24	<0.06	21.43	4.37	<0.05	<0.05	100.59
Y-10	ol	40.65	n.a.	n.a.	n.a.	9.1			0.10	0.51	49.87	n.a.	n.a.	n.a.	100.23
	opx	58.40	0.21	0.60	0.25	5.44	5.23	0.23	0.13	n.a.	34.84	0.77	0.19	n.a.	100.83
	cpx	55.44	0.31	1.37	1.15	3.02			0.10	n.a.	18.43	19.14	1.41	n.a.	100.37
	grt	41.73	0.37	18.94	5.64	7.54	6.93	0.68	0.37	0.01	20.32	5.42	0.04	n.a.	100.36
Y-19	ol	41.01	0.04	0.01	n.a.	8.74			0.11	0.40	50.72	0.04	0.01	n.a.	101.08
	opx	57.31	0.11	0.60	0.25	5.31	5.04	0.30	0.12	n.a.	35.89	0.88	0.17	n.a.	100.64

	cpx	54.86	0.18	1.53	1.05	3.20			0.11	n.a.	19.10	18.31	1.40	n.a.	99.75
	grt	41.99	0.19	19.77	4.94	7.48	6.83	0.72	0.32	n.a.	20.42	4.94	0.03	n.a.	100.07
87-70	ol	41.10	0.02	0.00	n.a.	8.37			0.11	0.40	51.12	0.05	0.00	n.a.	101.17
	opx	57.87	0.02	0.53	0.27	4.95	4.83	0.13	0.14	n.a.	35.47	0.94	0.09	n.a.	100.28
	cpx	55.04	0.01	0.89	0.81	2.95	2.67	0.31	0.11	n.a.	20.12	19.39	0.76	n.a.	100.08
	grt	41.46	0.05	17.44	7.93	7.19	6.33	0.95	0.32	n.a.	19.50	6.30	0.01	n.a.	100.19
87-97	ol	40.42	0.04	0.02	n.a.	11.40			0.11	0.36	49.00	0.04	0.02	n.a.	101.40
	opx	57.16	0.18	0.66	0.17	6.79	6.46	0.36	0.12	n.a.	34.13	0.93	0.20	n.a.	100.34
	cpx	54.55	0.32	1.85	0.71	4.45	4.07	0.42	0.13	n.a.	18.88	17.15	1.62	n.a.	99.66
	grt	41.75	0.45	20.19	4.21	8.90	8.20	0.77	0.32	n.a.	19.60	4.99	0.06	n.a.	100.47
Dariganga coarse															
8508-6	ol	40.30	n.a.	n.a.	n.a.	10.09			0.21	0.42	48.76	n.a.	n.a.	n.a.	99.77
	opx	54.34	<0.10	4.44	0.74	6.40	6.02	0.42	0.11	n.a.	32.50	0.97	0.07	n.a.	99.58
	cpx	52.36	0.20	5.60	1.38	3.36	2.59	0.85	0.00	n.a.	16.13	19.54	1.39	n.a.	99.94
	grt	41.74	0.12	22.78	1.60	7.32	6.97	0.39	0.25	n.a.	20.71	5.35	n.a.	n.a.	99.87
8508-9	ol	40.62	<0.10	0.08	0.02	9.71			0.12	0.38	49.20	0.09	<0.05	<0.05	100.23
	opx	54.55	0.11	4.35	0.65	6.20	5.67	0.59	0.12	0.11	32.59	1.05	0.13	<0.05	99.88
	cpx	51.91	0.30	5.32	1.05	3.33	2.41	1.02	0.09	<0.06	16.48	19.34	1.38	<0.05	99.27
	grt	42.04	0.12	22.70	1.28	7.00	6.74	0.30	0.28	<0.06	20.77	5.42	<0.05	<0.05	99.65
BY-18	ol	40.87	<0.10	0.04	0.00	9.09			0.13	0.41	50.00	0.08	<0.05	<0.05	100.64
	opx	54.75	0.16	4.61	0.71	5.85	5.47	0.42	0.11	0.14	32.97	1.12	0.16	<0.05	100.58
	cpx	51.93	0.49	5.94	1.27	3.25	2.53	0.80	0.05	<0.06	16.46	19.16	1.57	<0.05	100.15
	grt	42.17	0.20	22.59	1.67	6.72	6.40	0.36	0.30	<0.06	21.53	5.30	<0.05	<0.05	100.53
	spl	0.11	0.40	43.73	21.76	13.05			<0.06	0.32	18.92	0.01	<0.05	<0.05	98.30
BY-19	ol	40.66	<0.10	<0.06	<0.12	10.01			0.13	0.39	49.36	0.08	<0.05	<0.05	100.70
	opx	54.80	0.23	4.54	0.67	6.53	5.96	0.63	0.10	0.10	32.68	1.07	0.15	<0.05	100.88
	cpx	51.93	0.68	5.94	1.25	3.49	2.58	1.01	0.06	0.06	16.08	18.95	1.59	<0.05	100.04
	grt	42.11	0.25	22.61	1.43	7.34	7.04	0.34	0.31	<0.06	21.18	5.32	<0.05	<0.05	100.63
BY-27	ol	40.57	<0.10	<0.06	<0.12	10.11			0.20	0.31	49.62	0.09	<0.05	<0.05	101.03
	opx	54.70	0.18	4.63	0.53	6.41	5.84	0.63	0.16	0.09	32.64	1.10	0.16	<0.05	100.62
	cpx	52.18	0.51	6.08	0.91	3.54	2.54	1.12	0.08	0.07	16.37	18.78	1.69	<0.05	100.20
	grt	42.17	0.22	22.79	1.38	7.48	7.18	0.34	0.31	<0.06	20.99	5.29	<0.05	<0.05	100.71
BY-33	ol	40.80	<0.10	0.06	<0.12	9.75			0.15	0.31	49.29	0.07	<0.05	<0.05	100.44
	opx	55.03	0.09	4.32	0.62	6.29	5.78	0.56	0.13	0.09	33.08	1.03	0.12	<0.05	100.80
	cpx	52.25	0.27	5.40	1.24	3.12	2.45	0.73	0.09	0.06	16.45	19.57	1.39	<0.05	99.84
	grt	42.20	0.17	22.58	1.54	7.12	6.77	0.40	0.25	<0.06	21.05	5.45	<0.05	<0.05	100.43

n.a. – not analyzed.

Table 3

Table 3. Mössbauer hyperfine parameters (mm/s) and Fe^{2+} and Fe^{3+} percentages for orthopyroxenes

Sample	Fe^{2+} I				Fe^{2+} II				Fe^{3+}				$Fe^{3+}/\Sigma Fe$	err
	QS	IS	HW	%	QS	IS	HW	%	QS	IS	HW	%		
Udachnaya coarse														
U29	2.23	1.15	0.28	86.7	2.08	1.13	0.27	12.2	0.70	0.44	0.23	1.2	0.012	0.007
U64	2.24	1.16	0.27	29.1	2.10	1.15	0.29	68.4	0.79	0.45	0.31	2.5	0.025	0.006
U283	2.26	1.17	0.26	19.2	2.11	1.15	0.25	77.7	0.78	0.44	0.29	3.1	0.031	0.010
U501	2.31	1.16	0.29	16.2	2.10	1.16	0.27	82.5	0.80	0.50	0.26	1.4	0.014	0.012
Udachnaya sheared														
U10	2.19	1.16	0.29	72.5	2.01	1.15	0.29	26.1	0.77	0.46	0.29	1.4	0.014	0.003
U70	2.26	1.17	0.30	36.0	2.08	1.13	0.29	60.6	0.75	0.44	0.31	3.4	0.034	0.010
U183	2.23	1.13	0.29	13.0	2.11	1.15	0.28	84.5	0.69	0.45	0.30	2.5	0.025	0.010
U267	2.31	1.21	0.31	12.3	2.10	1.15	0.28	84.2	0.75	0.45	0.24	3.6	0.036	0.007
Y-10	2.18	1.16	0.40	36.3	2.08	1.14	0.26	59.8	0.81	0.49	0.30	3.9	0.039	0.013
Y-19	2.30	1.20	0.29	17.5	2.10	1.15	0.27	77.5	0.77	0.48	0.33	5.1	0.051	0.017
87-70	2.22	1.19	0.44	22.6	2.08	1.19	0.30	75.1	0.71	0.50	0.27	2.4	0.024	0.007
87-97	2.27	1.14	0.45	11.1	2.09	1.19	0.35	84.2	0.77	0.49	0.45	4.7	0.047	0.011
Dariganga coarse														
8508-6	2.19	1.16	0.40	76.2	1.99	1.10	0.34	17.9	0.65	0.51	0.25	5.9	0.059	0.005
8508-9	2.18	1.17	0.40	62.9	2.02	1.10	0.36	28.6	0.79	0.43	0.37	8.5	0.085	0.009
BY-18	2.24	1.22	0.41	19.3	2.12	1.12	0.40	74.3	0.74	0.43	0.30	6.4	0.064	0.009
BY-19	2.19	1.16	0.39	73.6	1.99	1.12	0.31	17.8	0.77	0.46	0.29	8.7	0.087	0.008
BY-27	2.20	1.16	0.39	69.3	1.98	1.12	0.31	21.8	0.79	0.42	0.28	8.9	0.089	0.016
BY-33	2.19	1.20	0.40	39.1	2.09	1.10	0.37	52.9	0.78	0.47	0.27	8.0	0.080	0.013
Canil and O'Neill (1996) refitted														
89-719	2.26	0.90	0.33	47.3	2.00	0.89	0.33	51.6	0.90	0.14	0.37	1.1	0.011	0.005
BD1150	2.27	0.87	0.33	61.1	2.03	0.84	0.24	36.5	1.07	0.02	0.39	2.4	0.024	0.015
BD1140	2.52	0.91	0.26	9.1	2.12	0.90	0.29	89.1	0.96	0.01	0.32	1.8	0.018	0.007
BD1201	2.35	0.88	0.28	12.3	2.03	0.86	0.28	86.6	0.97	0.12	0.35	1.2	0.012	0.009
BD1354	2.30	0.85	0.31	16.0	2.01	0.86	0.29	82.0	0.68	0.13	0.24	2.0	0.020	0.014
PHN5276	2.53	0.85	0.38	5.6	2.10	0.89	0.30	89.9	0.71	0.22	0.25	1.5	0.015	0.009
FRB1350	2.91	0.89	0.36	12.8	2.12	0.90	0.32	85.2	0.69	0.18	0.25	2.0	0.020	0.009

Table 4

Table 4. Mössbauer hyperfine parameters (mm/s) and Fe^{2+} and Fe^{3+} percentages for garnets

Sample	Fe^{2+} asymm					Fe^{3+}				$Fe^{3+}/\Sigma Fe$	$Fe^{3+}/\Sigma Fe$ corrected*	err
	QS	IS	HW1	HW2	%	QS	IS	HW	%			
Udachnaya coarse												
U29	3.56	1.28	0.36	0.30	91.9	0.42	0.16	0.59	8.1	0.081	0.059	0.010
U64	3.55	1.28	0.37	0.29	88.8	0.29	0.34	0.34	11.2	0.112	0.081	0.013
U283	3.56	1.28	0.35	0.27	92.0	0.49	0.17	0.24	8.0	0.080	0.058	0.016
U501	3.55	1.29	0.35	0.28	94.2	0.31	0.17	0.55	5.8	0.058	0.044	0.009
Udachnaya sheared												
U10	3.55	1.28	0.36	0.29	83.0	0.30	0.32	0.40	17.1	0.171	0.127	0.013
U70	3.55	1.28	0.36	0.30	86.4	0.29	0.33	0.35	13.6	0.136	0.101	0.013
U183	3.55	1.29	0.37	0.29	89.5	0.33	0.34	0.30	10.5	0.105	0.077	0.009
U267	3.55	1.29	0.36	0.30	89.6	0.27	0.34	0.35	10.4	0.104	0.076	0.012
Y-10	3.55	1.29	0.36	0.29	89.3	0.28	0.35	0.37	10.8	0.108	0.081	0.014
Y-19	3.55	1.29	0.37	0.30	88.3	0.25	0.33	0.34	11.7	0.117	0.087	0.016
87/70	3.55	1.28	0.37	0.32	84.0	0.30	0.37	0.42	16.0	0.160	0.119	0.013
87/97	3.56	1.29	0.38	0.30	89.5	0.32	0.38	0.31	10.5	0.105	0.078	0.019
Dariganga coarse												
8508-6	3.56	1.29	0.36	0.31	93.8	0.28	0.13	0.30	6.2	0.062	0.048	0.022
8508-9	3.55	1.29	0.36	0.29	95.2	0.27	0.10	0.29	4.9	0.049	0.038	0.020
BY-18	3.55	1.29	0.39	0.31	94.1	0.27	0.20	0.36	5.9	0.059	0.048	0.017
BY-19	3.55	1.29	0.37	0.29	94.9	0.31	0.12	0.31	5.1	0.051	0.042	0.011
BY-27	3.55	1.28	0.36	0.30	94.9	0.30	0.33	0.27	5.1	0.051	0.041	0.021
BY-33	3.55	1.29	0.38	0.31	93.9	0.36	0.25	0.55	6.1	0.061	0.050	0.024
Canil and O'Neill (1996) refitted												
89-719	3.58	1.30	0.36	0.30	89.6	0.32	0.15	0.50	5.2	0.052	0.037	0.006
BD1150	3.57	1.29	0.33	0.28	93.7	0.36	0.29	0.47	6.3	0.063	0.045	0.005
BD1140	3.57	1.29	0.34	0.28	95.0	0.28	0.29	0.50	5.0	0.050	0.036	0.004
BD1201	3.58	1.30	0.33	0.27	95.4	0.26	0.33	0.37	4.6	0.046	0.033	0.006
BD1354	3.58	1.30	0.32	0.28	90.4	0.30	0.32	0.37	9.6	0.096	0.069	0.004
PHN5276	3.56	1.04	0.34	0.28	84.9	0.34	0.08	0.44	15.2	0.152	0.109	0.010
FRB1350	3.57	1.29	0.33	0.28	95.3	0.43	0.13	0.42	4.7	0.047	0.034	0.004

*: corrected for recoil-free fractions in garnet after Woodland and Ross (1994).

Table 5
Click here to download Table: Table5_GAG.doc

Table 5. Mössbauer hyperfine parameters (mm/s) and Fe^{2+} and Fe^{3+} percentages for clinopyroxenes

Sample	Fe^{2+} I				Fe^{2+} II				Fe^{3+}				$Fe^{3+}/\Sigma Fe$	err
	QS	IS	HW	%	QS	IS	HW	%	QS	IS	HW	%		
Udachnaya sheared														
U267	2.33	1.30	0.30	16.6	2.02	1.16	0.39	65.8	0.54	0.36	0.57	17.6	0.176	0.035
87-70	2.33	1.14	0.44	11.1	2.06	1.19	0.44	79.6	0.50	0.37	0.68	9.3	0.093	0.021
87-97	2.02	1.19	0.45	14.2	1.87	1.20	0.49	77.2	0.58	0.32	0.52	8.6	0.086	0.014
Dariganga coarse														
8508-6	2.63	1.09	0.38	7.1	2.06	1.16	0.45	70.1	0.64	0.44	0.59	22.8	0.228	0.028
8508-9	2.58	1.13	0.31	11.5	2.04	1.15	0.44	61.0	0.63	0.44	0.65	27.5	0.275	0.064
BY-18	2.54	1.13	0.35	15.2	2.07	1.16	0.48	62.6	0.57	0.47	0.54	22.2	0.222	0.054
BY-19	2.68	1.15	0.32	12.7	2.10	1.16	0.49	61.2	0.66	0.44	0.61	26.1	0.261	0.062
BY-27	2.61	1.13	0.31	15.0	2.05	1.16	0.44	56.7	0.66	0.41	0.60	28.4	0.284	0.045
BY-33	2.72	1.16	0.34	14.2	2.08	1.16	0.46	64.6	0.69	0.46	0.53	21.2	0.212	0.042
Canil and O'Neill (1996) refitted														
89-719	2.67	1.16	0.39	9.8	2.05	1.14	0.44	62.5	0.41	0.31	0.53	27.7	0.277	0.075
BD1150	2.61	1.15	0.42	16.2	2.03	1.15	0.44	51.8	0.48	0.41	0.59	32.0	0.320	0.065
BD1140	2.70	1.18	0.42	8.8	2.05	1.15	0.44	58.4	0.50	0.37	0.67	32.8	0.328	0.078
BD1201	2.55	1.13	0.46	18.9	2.03	1.14	0.41	43.9	0.42	0.37	0.54	37.3	0.373	0.082
BD1354	2.44	1.19	0.51	21.8	2.03	1.15	0.40	53.7	0.51	0.39	0.47	24.5	0.245	0.022
PHN5276	2.08	1.14	0.36	74.0	1.82	1.10	0.22	14.7	0.51	0.30	0.48	11.3	0.113	0.013
FRB1350	2.66	1.12	0.47	11.7	1.99	1.16	0.42	76.5	0.74	0.39	0.44	11.8	0.118	0.037

Table 6
Click here to download Table: Table6.doc

Table 6. Effect of changing redox conditions on Opx–Grt thermometry for mantle xenoliths equilibrated under 'average' redox conditions.

Sample	Redox conditions	$\Delta\log f_{O_2}$ (QFM)*	Fe^{3+}/Fe_{tot} Grt§	Fe^{3+}/Fe_{tot} Opx#	PNG85 GPa (at TTA98)	TNG10 °C (at PNG85)†	PNG85 GPa (at TNG10)‡	TNG10 °C (at PNG85)‡
FRB1350	original	–0.67	0.034	0.021	2.08	724	2.47	761
	lowest	–2.50	0.012	0.007	2.08	729	2.42	762
	highest	+1.02	0.085	0.055	2.08	713	2.60	763
FRB135	original	–1.79	0.057	0.048	3.57	961	4.03	1009
	lowest	–3.42	0.023	0.019	3.57	965	3.90	1000
	highest	+0.21	0.162	0.140	3.57	946	4.69	1062
Bo-08	original	–2.27	0.071	0.053	4.59	1114	5.18	1178
	lowest	–4.02	0.027	0.020	4.59	1125	4.87	1156
	highest	–0.30	0.194	0.149	4.59	1082	7.20	1364
22-7	original	–2.59	0.085	0.020	5.58	1124	5.63	1129
	lowest	–4.49	0.030	0.007	5.58	1162	5.87	1193
	highest	–0.75	0.214	0.056	5.58	1036	5.15	996
U183	original	–3.42	0.077	0.018	6.40	1237	6.52	1250
	lowest	–4.97	0.033	0.007	6.40	1270	6.67	1299
	highest	–1.15	0.238	0.064	6.40	1118	6.17	1096

*: "original" calculated from natural compositions with the oxybarometer of Stagno et al. (2013); "lowest" and "highest" bracket the maximum range for mantle peridotites at respective depth (cf. Fig. 8);
§: "original" measured on natural samples; "lowest" and "highest" calculated by reversing the oxybarometer of Stagno et al. (2013) at "lowest" and "highest" fO_2;
#: calculated from garnet composition using Equation (6);
†: *T* (Nimis and Grütter 2010) calculated at *P* given by combination of Nickel and Green's (1985) barometer (PNG85) and Taylor's (1998) thermometer (TTA98);
‡: *T* (Nimis and Grütter 2010) and *P* (Nickel and Green 1985) calculated by iteration.
Sources of compositional data: FRB1350 – Pearson et al. (1994) and this work; FRB135 – Luth et al. (1990); Bo-08 – Creighton et al. (2009); 22-7 – Kopylova et al. (1999a) and McCammon and Kopylova (2004); U183 – Ionov et al. (2010) and this work.

Fe^{3+} partitioning systematics between orthopyroxene and garnet in mantle peridotite xenoliths and implications for thermobarometry of oxidized and reduced mantle rocks

Paolo Nimis[1,*], ~~Aleksey~~ Alexey Goncharov[2], Dmitri A. Ionov[3], Catherine McCammon[4]

[1] Dipartimento di Geoscienze, Università di Padova, Italy

[2] ~~Faculty of Geology~~Institute of Earth Sciences, Saint-Petersburg State University & IPGG RAS, Saint-Petersburg, Russia

[3] Géosciences Montpellier, CNRS-UMR 5243 - Université Montpellier II, 34095 Montpellier, France

[4] Bayerisches Geoinstitut, Universität Bayreuth, D-95440 Bayreuth, Germany

*: Corresponding author

e-mail: paolo.nimis@unipd.it

tel: +39-0498279161

fax: +39-0498279134

Abstract We have investigated the partitioning of Fe^{3+} between orthopyroxene (Opx) and garnet (Grt) in well-equilibrated mantle xenoliths using Mössbauer spectroscopy. The samples cover a wide range of *P*–*T* conditions (2.1–6.6 GPa, 690–1,412 °C) and geothermal gradients, and are thus representative for Earth's upper mantle in both on-craton and off-craton continental settings. Garnet has Fe^{3+}/Fe_{tot} ratios of 0.03–0.13 and Fe_2O_3 contents of 0.24–1.00 wt%. Orthopyroxene has, on average, lower Fe^{3+}/Fe_{tot} ratios (0.01–0.09) and Fe_2O_3 contents (0.05–0.63 wt%). In low-pressure, high-temperature samples, however, Opx is systematically richer in Fe_2O_3 than the coexisting Grt. The Fe^{3+} Opx/Grt partition coefficient ($D_{Fe^{3+}}^{Opx/Grt}$) shows no obvious relationship with temperature, but increases ~~a negative correlation~~ with decreasing pressure and ~~a positive correlation~~ with increasing ~~the~~ Na_2O^{Opx}. The observed Opx/Grt Fe^{3+} systematics imply that the Opx–Grt Fe–Mg exchange thermometer is not robust against redox changes if total Fe is treated as Fe^{2+}. An approximate evaluation of errors on *T* estimates due to redox effects predicts negligible deviations for strongly reduced conditions (< 65 °C), but potentially large deviations (> to >> 100 °C) for strongly oxidized conditions, especially at very high pressure and when both *P* and *T* are calculated by iteration.

Keywords Ferric iron, Orthopyroxene, Garnet, Mantle xenoliths, Thermobarometry

Introduction

Studies of the distribution of ferric iron in mantle minerals have provided important insights into the redox state and geochemical processes in the Earth ~~(Frost and McCammon 2008)~~. Measured Fe^{3+}/Fe_{tot} ratios in garnet and spinel from xenoliths have been used to derive oxygen fugacity profiles for several upper mantle sections (e.g., Luth et al. 1990; Luth and Canil 1993; Woodland and Peltonen 1999; Woodland and Koch 2003; McCammon and Kopylova 2004; Lazarov et al. 2009; Yaxley et al. 2012; Creighton et al. 2009, 2010; Goncharov and Ionov 2012; Goncharov et al. 2012). These data are of paramount importance for our understanding of processes involving volatile-bearing metasomatic fluids and melts active in the lithosphere today and during its evolution, including those involved in diamond formation and Earth's degassing (Woodland and Koch 2003; Shirey et al. 2013; Stagno et al. 2013).

A large number of Fe^{3+} analyses are now available for garnet, pyroxenes and spinel, which are the most important carriers of Fe^{3+} in the upper mantle. The contents and distribution of Fe^{3+} among these minerals are controlled by crystal-chemical constraints and *P*–*T* conditions and are affected by partial melting and metasomatism (Frost and McCammon 2008). It was recognized that in sub-cratonic mantle sections garnet Fe^{3+}/Fe_{tot} ratios and garnet/clinopyroxene Fe^{3+} partition coefficients tend to increase with temperature (Woodland and Koch 2003; Canil and O'Neill 1996; Woodland 2009). In addition, owing to stabilization of the $Fe^{2+}{}_3Fe^{3+}{}_2Si_3O_{12}$ ("skiagite") component in garnet with pressure, oxygen fugacity has been shown to be driven to lower values relative to the FMQ buffer with increasing depth (Gudmundsson and Wood 1995).

Despite the large amount of data on Fe^{3+} distribution in mantle rocks, specific information on the partitioning of Fe^{3+} between orthopyroxene (hereafter Opx) and garnet (hereafter Grt) is still very scarce. Predictive theoretical modeling of this partitioning is hampered by the lack of accurate thermodynamic data for Fe^{3+}-bearing Opx. Empirical modeling is also problematic due to the paucity of analytical data for Opx. To our knowledge, reliable partitioning data for Opx–Grt pairs are restricted to a set of eight mantle xenoliths, which were analyzed by conventional Mössbauer spectroscopy by Canil and O'Neill (1996), and two compositionally zoned Opx–Grt pairs from metasomatized xenoliths, which were analyzed by high-spatial-resolution Mössbauer spectroscopy by McCammon et al. (2001). Two additional pairs were reported for orogenic garnet peridotites by Malaspina et al. (2012), who used complementary analytical techniques for the determination of ferric iron, i.e., flank-method electron probe micro-analysis (EPMA) for Grt and electron energy-loss spectroscopy for Opx.

Nimis and Grütter (2010) showed that the distribution of Fe^{3+} between Opx and Grt in Canil and O'Neill's (1996) xenoliths is dependent on equilibrium *P*–*T* conditions, implying a significant effect of mantle redox state on Opx–Grt Fe–Mg-exchange thermometry. Unfortunately, the strong correlation between *P* and *T* in these samples did not allow discrimination of the net effects of *P* and *T* on Fe^{3+} partitioning. More recently, Matjuschkin et al. (2014) performed experiments in the CFMAS peridotitic system at 5 GPa and 1,100–1,400 °C under strongly oxidized conditions and measured Fe^{3+} contents in the garnets with the flank method. These authors observed a marked improvement of Opx–Grt temperature estimates using the Harley (1984) Fe–Mg exchange thermometer

when the significant Fe^{3+} contents in the garnets were accounted for and suggested that Fe^{3+}/Fe_{tot} ratios in the coexisting orthopyroxenes should be comparatively small.

To gain a better insight into the partitioning systematics of ferric iron between Opx and Grt under conditions relevant to Earth's upper mantle, we have undertaken a Mössbauer study of Opx–Grt pairs in well-equilibrated ~~mantle~~ xenoliths from both on-craton and off-craton mantle sections, covering a wide *P*–*T* field. The results provide new ~~constraints~~ indications on the mechanisms of incorporation of Fe^{3+} in Opx and have significant implications for mantle thermobarometry.

Materials and methods

Sample selection, microstructures and compositions

The samples used in the present work were selected among well-studied peridotite xenoliths to cover a range of *P*–*T* conditions representative of garnet-facies lithospheric mantle in cratonic and off-craton regions (Table 1). All selected samples show well-equilibrated microstructures. We avoided using samples showing significant alteration or any evidence of chemical disequilibrium, such as significant compositional variations in any minerals, poor consistency between thermometric estimates using independent, mutually-consistent thermometers (cf. Nimis and Grütter 2010) or poor consistency between f_{O_2} estimates using independent, garnet-based and spinel-based oxybarometers (cf. Goncharov and Ionov 2012).

The selected off-craton peridotites (N = 6) are from the Barun-Yargait eruption center within the Late Cenozoic Dariganga alkali basaltic field in SE Mongolia (Ionov et al. 1999; Ionov 2002). The peridotites are fertile to moderately refractory garnet lherzolites (2.67–3.9 wt% Al_2O_3 in whole-rocks) containing 534–66% olivine, 198–2667% Opx, 6–123% clinopyroxene (hereafter Cpx) and 4–1011% Grt; one sample (BY-1918) contains accessory spinel (Table 1). They are coarse- to medium-grained rocks with protogranular textures. The grain size is similar for all silicate minerals. The mineral grains typically have curved boundaries and irregular shapes. Pyroxenes show no optical zoning or unmixing. Garnets have thin kelyphite rims. No volatile-bearing minerals (mica, amphibole, apatite) or silicate glass have been found. Veined peridotites or pyroxenite xenoliths are very uncommon in the whole xenolith suite. The peridotites are fresh and have positive loss on ignition (LOI) values, indicating that the gain of mass due to oxidation of FeO to Fe_2O_3 on heating is greater than the loss of volatiles introduced by alteration.

The selected cratonic peridotites (N = 12) are from the Udachnaya-East kimberlite pipe in the central Siberian craton. The samples are a subset of the xenolith collection described by Doucet et al. (2013, 2014), Goncharov et al. (2012) and Ionov et al. (2010), and were collected in the 420–640 m depth range in the diamond mine pit from unusually fresh kimberlites. Details on petrographic features, major and trace element compositions of whole-rocks and minerals, and oxygen fugacity estimates can be found in the quoted papers. The rocks range in composition from ~~refractory~~Cpx-bearing harzburgite to ~~clinopyroxene-poor~~ lherzolite to Opx-bearing wehrlite (Table 1), and show no or little alteration (commonly with positive LOI). Four samples (U29, U64, U283, U501) are coarse (undeformed), seven (U70, U183, U267, Y-10, Y-19, 87/70,

87/97) are sheared and one (U10) is transitional (incipient deformation with ≤10% of olivine as neoblasts). One of the coarse xenoliths (U283) contains accessory spinel.

Chemical analysis

Major element compositions of minerals used in the present study were determined by wavelength-dispersive spectroscopy electron microprobe analysis at different laboratories. The minerals were analyzed in grain mounts or thin sections. Samples from Dariganga were analyzed at Macquarie University (Sydney) with a Cameca SX-50 instrument at 15 kV voltage and 20 nA current, using natural and synthetic oxide and silicate minerals as standards and the PAP matrix correction. Analyses for U-series samples from Udachnaya are the same as those reported in Ionov et al. (2010) and were obtained at the Laboratoire Magmas et Volcans (Clermont-Ferrand) on a CAMECA SX-100 using 15 kV voltage, 15 nA current and counting times of 10–20 s for peaks and 5–10 s for background; standards were natural and synthetic minerals; the ZAF correction was applied. The other samples from Udachnaya were analyzed or re-analyzed at Padova IGG-CNR with a CAMECA SX-50 and at Clermont-Ferrand with a CAMECA SX-100 using higher currents (20 kV, 40 nA) and longer counting times for Al, Cr, Ca and Na in pyroxenes (40 s peak, 40 s background) in order to minimize propagation of analytical errors on thermobarometric estimates and optimize the analysis of Na in Opx. No systematic decrease in measured Na contents was observed using the higher currents and longer counting times, which excludes significant underestimation due to migration of this element under the electron beam. Analytical standards for pyroxenes and olivine were diopside (for Si and Ca), albite (for Na), orthoclase (for K) and pure oxides (for

Mg, Al, Cr, Fe, Mn and Ti). For garnet, pyrope was used as a standard for Mg and Si. The CAMECA-PAP program was used to convert X-ray counts into weight percent oxides. The analyses are reported in Table ~~1~~2.

Mössbauer analysis

Pure Grt, Opx and Cpx grains were handpicked under a microscope from 0.5 to 2.0 mm size fractions of crushed and sieved rock material. Owing to the small size of some xenoliths and low modal proportions of Cpx, sufficient Cpx separates for Mössbauer analysis could be obtained only for nine of the investigated samples. The valence state of iron and its structural position in ~~Opx and Grt~~the minerals were determined using a SM-1201 Mössbauer spectrometer at the IPGG RAS (Saint-Petersburg, Russia) at room temperature in a constant acceleration mode over a velocity range of ±7 mm/s with a nominal 50 mCi ^{57}Co source in a Rh matrix. The spectrometer was calibrated relative to metallic iron at room temperature. ~~Pure Grt and Opx grains were handpicked under a microscope from 0.5 to 2.0 mm size fractions of crushed and sieved rock material.~~ The minerals were crushed in an agate capsule filled with acetone to avoid iron oxidation in contact with air, pressed in plastic discs and fixed on a special aluminum holder, ensuring an angle between gamma rays and absorber of 54.7°, to avoid asymmetry of the spectra due to preferred orientation of mineral grains. The density of the natural iron in the absorber was about 5 mg/cm^3.

The spectra were approximated by a sum of Lorentzian lines using the MOSSFIT© software. The relative amounts of Fe^{2+} and Fe^{3+} and their site positions in the crystal lattice were determined from integral doublet intensities and hyperfine parameters,

assuming equal Mössbauer effect probabilities for Fe^{2+} and Fe^{3+} at different sites for Opx and different recoil-free fractions of Fe in octahedral and dodecahedral sites for Grt. Constraints on the equality of halfwidths (HW) and integral intensities of the lines in each doublet component of quadrupole splitting (QS) were imposed during spectra fitting. The quality of experimental spectra was assessed by background intensity and the quality of fitting by chi-square distribution.

The fitting model for Grt included a single QS doublet for Fe^{2+} and Fe^{3+}. The relative peak widths and areas of the Fe^{2+} doublet, assigned to dodecahedral (distorted cube) site occupancy, were left unconstrained to account for spectra asymmetry (Amthauer et al. 1976). The doublet attributable to octahedrally coordinated Fe^{3+} was constrained to have components with equal widths and intensities. The Fe^{3+}/Fe_{tot} values obtained were corrected for different recoil-free fractions (Woodland and Ross 1994).

The fitting model for Opx and Cpx included two QS doublets for Fe^{2+} and one for Fe^{3+}. ~~In~~Although previous studies (e.g. Luth ~~&~~and Canil 1993; Canil ~~&~~and O'Neill 1996), used three QS doublets for Fe^{2+} in opx ~~were used~~ in the fitting procedure, ~~but at~~ this approach led to unreasonably small ~~half-weightidths~~HW ~~of lines are very low~~. Addition of the extra doublet is not statistically justified when the lines overlap by more than their ~~halfwidth~~HW, where the ~~Adding the third doublet for Fe^{2+} did not alter Fe^{3+}/Fe_{tot} ratios, but raises~~ errors of hyperfine parameters increase dramatically (~~Goncharov, 2009~~Dollase, 1975). We also note that adding the extra doublet for Fe^{2+} did not alter Fe^{3+}/Fe_{tot} ratios. Therefore, to reach best fitting results, exclude peaks overlap and minimize errors, only two QS doublets for Fe^{2+} were ~~added~~used to fit ~~o~~Opx spectra. ~~The QS doublet components, correlated to Fe^{2+} and Fe^{3+}, assigned to the octahedral site were constrained to have equal widths and intensities.~~

The hyperfine parameters and calculated proportions of Fe^{2+} and Fe^{3+} at different sites, calculated from HW and integral intensities of lines in QS doublets, are reported in Tables ~~2~~ 3 ~~and~~ to ~~3~~5. The hyperfine parameters of Fe^{3+} doublets in Opx are consistent with octahedral coordination (Annersten et al., 1978). No additional lines were observed in any of the spectra, which confirms the absence of other mineral phases, including ~~excluding~~ possible exsolutions ~~of other mineral phases.~~ The absolute errors on the Fe^{3+}/Fe_{tot} ratios varied from 0.003 to 0.017 for Opx, ~~and~~ from 0.009 to 0.024 for Grt, and from 0.01 to 0.06 for Cpx. Two examples of spectra pairs showing different partitioning of Fe^{3+} between Opx and Grt are shown in Figure 1.

Mössbauer spectra of Opx, Cpx and Grt from mantle xenoliths that had been obtained by conventional Mössbauer spectroscopy by Canil and O'Neill (1996) were reprocessed for this study using the same software and fitting approach used for our samples to ensure robust comparison of the new and old data. Seven set~~pair~~s of spectra could be retrieved from the original Canil and O'Neill (1996) files. We obtained similar results to Canil and O'Neill (1996) using their fitting approach; however, for several Opx spectra we observed that the fitting residuals were larger than the baseline scatter and indicated unequal areas of the main doublet components. This asymmetry is likely caused by a slight preferred orientation of crystallites arising from the nature of the sample mount; therefore the Opx spectra were re-fitted allowing the two Fe^{2+} doublets to have components with equal HW but unequal intensity according to the fitting approach of McCammon et al. (2000). One of the spectra (sample FRB1350) showed a contribution from ~~clinopyroxene~~olivine, which was estimated to be roughly ~~8~~13% of the total area based on the intensity of the high QS impurity. Accordingly, an empirical correction was made to the Fe^{3+}/Fe_{tot} ratio in Opx based on the ~~reported Fe^{3+}/Fe_{tot} value~~

~~of 12% in the clinopyroxene~~well established observation that olivine contains no Fe^{3+}.

For the garnets, the same fitting model used for our samples produced Fe^{3+}/Fe_{tot} values within 0.01 of the data reported in Canil and O'Neill (1996), provided the latter were corrected for different recoil-free fractions. Most of ~~For the clinopyroxenes, the differences~~ our refitted Fe^{3+}/Fe_{tot} data for the clinopyroxenes were within 0.02 of those~~from the Fe^{3+}/Fe_{tot} data~~ reported in Canil and O'Neill (1996), with only two samples at 0.03–0.04 of the originally reported values~~ were within 0.04~~. The results of the refitting are reported in Tables ~~2~~ 3 ~~and 3~~to 5. We emphasize that the change in Fe^{3+}/Fe_{tot} values from our reprocessing of the Canil and O'Neill (1996) data compared to their original values is minor and does not alter ~~any~~ the general conclusions presented in their paper.

Thermobarometry

The pressures and temperatures of equilibration of the studied xenoliths and of the reprocessed Canil and O'Neill (1996) data (Table 1) were calculated using a combination of the Taylor (1998) two-pyroxene thermometer and Nickel and Green (1985) Opx–Grt barometer recommended by Nimis and Grütter (2010). Given the presence of a few sodium-rich Opx in our data set, we adopted the modified version of the Nickel and Green (1985) barometer proposed by Carswell (1991). This modification was neither expressly favored nor disfavored by Nimis and Grütter (2010), who showed that both versions of the barometer are consistent with constraints imposed by natural xenoliths and experiments in peridotitic systems. Carswell's (1991) version only diverges from the original Nickel and Green (1985) for Opx with $Na > Cr + Fe^{3+} + Ti$,

for which it yields somewhat higher pressures (up to 1.2 GPa higher in our data set; Table 1) and is claimed to be more robust. Owing to the large relative uncertainties in the determination of the small Fe^{3+} contents in Opx, Fe^{3+} was neglected ~~infor~~in the application of Carswell's (1991) correction.

Only two samples from Udachnaya (U267 and 87/70) showed discrepancies between Opx–Grt (Nimis and Grütter 2010) and two-pyroxene (Taylor 1998) temperatures slightly larger than the assumed safety threshold of ±70 °C proposed by Nimis and Grütter (2010), i.e., +96 °C and –77 °C, respectively. Neither of these two samples, however, showed anomalous behavior in terms of Opx/Grt Fe^{3+} distribution compared with the other samples.

Three of the samples from the Canil and O'Neill (1996) set for which the Mössbauer spectra were refitted, i.e., BD1140, BD1150 and BD1354, show less than optimal agreement between internally-consistent clinopyroxene-based (Taylor 1998 or Nimis and Taylor 2000) and Opx-based thermometers (Brey and Köhler 1990, with correction in Nimis and Grütter 2010) (ΔT = 100–165 °C). *P–T* estimates for these samples should thus be used with caution. Therefore, these three samples will be used for general comparative purposes, but not for quantitative evaluation of Fe^{3+} systematics.

Results

The samples studied in this work cover a wide range of estimated *P–T* conditions (2.1–6.6 GPa, 690–1,412 °C) and geothermal gradients, and are thus representative for Earth's upper mantle in both on-craton and off-craton continental settings (Fig. 2). Garnet has

281 Fe^{3+}/Fe_{tot} ratios of 0.03–0.13 and Fe_2O_3 contents of 0.24–1.00 wt%. Orthopyroxene has,
282 on average, lower Fe^{3+}/Fe_{tot} ratios (0.01–0.09) and Fe_2O_3 contents (0.05–0.63 wt%). In
283 the low-pressure, high-temperature Dariganga suite, however, Opx is systematically
284 richer in Fe_2O_3 than the coexisting Grt (Table ~~1~~2). Such systematic Fe^{3+}-enrichment
285 appears to be unrelated to the abundance of other phases competing for Fe^{3+}, since the
286 modal ranges of Cpx (6–13 vol%) and Grt (3.5–11 vol%) in Dariganga xenoliths overlap
287 those in the other investigated samples (Cpx = 1.4–16 vol%; Grt = 2.1–13 vol%), and
288 spinel only occurs in minor amounts (< 0.5 vol%) in one Dariganga and one Udachnaya
289 sample (Table 1). The main reason for the enhanced partitioning of Fe^{3+} in Opx must
290 therefore be found in the specific *P*–*T* conditions recorded by the off-craton Dariganga
291 xenoliths and, possibly, in specific compositional controls.
292 The higher Fe^{3+} contents in Dariganga Opx are coupled with higher $^{[4]}Al$ contents
293 (Fig. 4a). The latter essentially reflects the low-*P* and relatively high-*T* conditions of
294 equilibration of these samples, which are typical of the garnet-facies off-craton
295 lithospheric mantle (Fig. 2). The association of high Fe^{3+} and high $^{[4]}Al$ suggests a major
296 role of Tschermaks-type substitution in the incorporation of Fe^{3+} in Opx. In addition, the
297 three most Fe^{3+}-rich samples in the low-$^{[4]}Al$ Opx group are those with the highest Na
298 content, and a ~~similar~~ correlation of Fe^{3+} with Na is also shown by all ~~bar~~of the ~~one~~
299 Dariganga samples except for one, which contains spinel (Fig. 4b). This indicates that an
300 additional minor aegirine component $NaFe^{3+}Si_2O_6$ may also have contributed to the
301 incorporation of Fe^{3+} in Opx.
302 The Fe^{3+} Opx/Grt partition coefficient ($D_{Fe^{3+}}^{Opx/Grt} = \frac{(Fe^{3+})^{Opx}}{(Fe^{3+})^{Grt}}$, at. per 4-cation
303 formula unit) shows no obvious relationship with temperature and a roughly negative

correlation with pressure (Fig. 3a,b). Detailed examination of the relationships between ln $D_{Fe^{3+}}^{Opx/Grt}$ and P showed that the scatter in Figure 3b was at least in part correlated with changes in the Na content of Opx. This ~~can be~~is illustrated by a plot of ~~This partitioning behavior is in contrast with what has been reported for natural mantle and experimental clinopyroxene–garnet pairs, which show enhanced partitioning of Fe^{3+} to Grt with increasing temperature (Woodland 2009; Purwin et al. 2013). T~~the residuals of ~~the~~ a ln $D_{Fe^{3+}}^{Opx/Grt}$ vs. P linear regression, which show a positive correlation with the Na_2O content in Opx (Fig. 3c). Such a correlation is consistent with the inferred contribution of aegirine component to Fe^{3+} incorporation and suggests an ~~, suggestings a~~additional ~~second-order~~ compositional control on the ~~incorporation~~ partitioning of Fe^{3+} ~~in~~ between Opx and Grt. The original data of Canil and O'Neill (1996) are systematically shifted to higher $D_{Fe^{3+}}^{Opx/Grt}$, but the refitted data are in good agreement with our data if the effect of Na_2O and the uncertainties in P, $D_{Fe^{3+}}^{Opx/Grt}$ ~~is~~ and Na content~~2~~O are taken into account (Fig. 3c).

The partitioning behavior observed in our Opx–Grt pairs is in contrast with existing ~~what has been~~ report~~s~~ed for natural mantle and experimental Cpx–Grt pairs: these show enhanced partitioning of Fe^{3+} to Grt with increasing temperature (Canil and O'Neill 1996; Woodland 2009; Purwin et al. 2013), a tendency which is confirmed also by our ~~data~~Cpx–Grt pairs (Fig. 5a). A correlation between Fe^{3+} and Na in Cpx is also apparent in our data (Table 2), in line with previous observations in garnet peridotites (Woodland 2009; Malaspina et al. 2012). Owing to the complex combination of P–T and compositional effects, the distribution of Fe^{3+} between the pyroxenes varies significantly

among different samples ($D_{Fe^{3+}}^{Opx/Cpx}$ = 0.1–0.8; Fig. 5b). In particular, the high $D_{Fe^{3+}}^{Opx/Cpx}$ in Dariganga xenoliths (0.5–0.7) is probably ~~mostly~~ due mostly to a combination of relatively high *T*, low *P* conditions and moderate Na^{Cpx} contents. Quantitative evaluation of Opx/Cpx Fe^{3+} partitioning systematics is beyond the scope of the present work. We only emphasize that estimates of Opx Fe^{3+} contents from ~~measured~~ Fe^{3+} measured in Cpx, based on linear regression of data extracted from limited sets of samples from on-craton mantle settings (cf. Canil and O'Neill 1996), are probably unreliable when applied to Opx–Cpx pairs from different mantle environments.

Discussion

Because the thermodynamic properties of Fe^{3+}-bearing Opx end-members are unknown, a rigorous thermodynamic treatment of the equilibria involved in the Fe^{3+} partitioning between Opx and Grt is not possible. However, the topology of the possible relevant reactions and a few approximations allow us to make some qualitative predictions, which may explain the observed partitioning systematics.

Assuming Fe^{3+} enters into Opx in octahedral coordination, in line with our Mössbauer data, the equilibrium controlling Fe^{3+} partitioning at constant f_{O_2} can be expressed by an Fe^{3+}–Al exchange reaction of the type

$$\underset{\text{Grt}}{½M_3Fe^{3+}{}_2Si_3O_{12}} + \underset{\text{Opx}}{MgAl_2SiO_6} \rightarrow \underset{\text{Opx}}{MgFe^{3+}AlSiO_6} + \underset{\text{Grt}}{½M_3Al_2Si_3O_{12}}, \quad (1)$$

where M represents a divalent cation (essentially, Mg, Fe^{2+} or Ca). At equilibrium,

$$-\frac{\Delta G^\circ}{RT} = \ln K_{Fe^{3+}-Al}^{Grt-Opx} = \ln\left(K_D \cdot K_\gamma\right) = \ln \frac{\left(Fe^{3+}\right)^{Opx}}{\left(Fe^{3+}\right)^{Grt}} - \ln \frac{\left(Al_{M1}\right)^{Opx}}{\left(Al\right)^{Grt}} + \ln K_\gamma, \quad (2)$$

where elements are atomic fractions in octahedral sites and $\ln K_\gamma$ includes all non-ideal terms. Since reactants and products in reaction (1) are the same and the coordination number of the exchanged cations does not change in the reaction, the volume change of the reaction should be small. Large extrapolation of Domeneghetti et al.'s (1995) data for Pbca orthopyroxenes allows us to predict a molar volume of ~6.1 J/bar for the $MgFe^{3+}AlSiO_6$ end-member. As expected, the calculated ΔV° of reaction (1) is small (ca. –0.1 J/bar), hence the *P* dependency of the reaction should also be small. Since the Al term in Equation (2) typically decreases with pressure in garnet peridotites, owing to the net-transfer reaction

$$MgAl_2SiO_6 + Mg_2Si_2O_6 \rightarrow Mg_3Al_2Si_3O_{12}, \quad (3)$$

Opx Opx Grt

the sum of the other right-hand terms in Equation (2) should also do so in order to maintain the *P* dependency of $\ln K_{Fe^{3+}-Al}^{Grt-Opx}$ small. If the $\ln K_\gamma$ term is sufficiently small or does not vary significantly with *P*, then the $\frac{\left(Fe^{3+}\right)^{Opx}}{\left(Fe^{3+}\right)^{Grt}}$ ratio~~,~~ (i.e.,~~and thus~~ $D_{Fe^{3+}}^{Opx/Grt}$ ~~,~~), should decrease with increasing pressure.

An alternative equilibrium, again with Fe^{3+} in octahedral coordination, is

$$M\mathrm{Fe}^{3+}\mathrm{AlSiO_6} + M_2\mathrm{Si_2O_6} \rightarrow \tfrac{1}{2}M_3\mathrm{Fe}^{3+}{}_2\mathrm{Si_3O_{12}} + \tfrac{1}{2}M_3\mathrm{Al_2Si_3O_{12}}. \quad (4)$$

Opx Opx Grt Grt

This net-transfer reaction involves an increase of mean coordination number for both divalent and trivalent cations and is therefore expected to be favored by pressure. In fact, a similar equilibrium, with Cr in lieu of Fe^{3+}, was experimentally calibrated as a geobarometer by Nickel (1989).

If Fe^{3+} is assumed to enter Opx to a minor~~some~~ extent also in tetrahedral coordination (cf. Annersten et al. 1978), then the following net-transfer reaction may become relevant:

$$M\mathrm{Fe}^{3+}{}_2\mathrm{SiO_6} + M_2\mathrm{Si_2O_6} \rightarrow M_3\mathrm{Fe}^{3+}{}_2\mathrm{Si_3O_{12}}. \quad (5)$$

Opx Opx Grt

The topology of this reaction is similar to that of equilibrium (3) (with Al instead of Fe^{3+}), on which the Opx–Grt barometer is based (e.g., Nickel and Green 1985). Therefore, regardless of the mechanisms of incorporation of Fe^{3+} in Opx, the $D_{Fe^{3+}}^{Opx/Grt}$ partition coefficient can be predicted to be negatively correlated with pressure, which is in line with our results (Fig. 3).

The positive correlation of the residuals of the $\ln D_{Fe^{3+}}^{Opx/Grt}$ vs. P regression with the Na_2~~O~~ content in Opx (Fig. 3c) suggests that Na also favors incorporation of Fe^{3+} in Opx, probably as an ~~acmite~~ aegirine component ~~$NaFe^{3+}Si_2O_6$~~. In our data set, no

compositional variable other than the Na content was found to have a significant relationship with ~~$D^{Opx/Grt}_{Fe^{3+}}$~~ these residuals. Weighted regression of our data plus the refitted Canil and O'Neill's (1996) data yielded the following expression for $D^{Opx/Grt}_{Fe^{3+}}$ as a function of P and Na^{Opx}_2O ~~(Fig. 4)~~:

$$\ln D^{Opx/Grt}_{Fe^{3+}} = \ln \frac{Fe_2O_3{}^{Opx}}{Fe_2O_3{}^{Grt}} = 0.549(53)\cdot P\ (GPa) + 12.3(1.7)\cdot Na_2O^{Opx} - 0.14(26)\ (wt\%), \quad (R^2 = 0.83). \qquad (6)$$

~~An alternative expression is~~

$$\ln \frac{\left(Fe^{3+}\right)^{Opx}}{\left(Fe^{3+}\right)^{Grt}} = -0.5540551(5147)\cdot P\ (GPa) + 12181.5(1.723)\cdot Na_2O^{Opx}\ (wt\%) - 0.8812(2523), \quad (R^2 = 0.8486), \qquad (76)$$

with ~~cations in~~ atoms per ~~64 oxygen~~ cation ~~(Opx) and 12 oxygen (Grt)~~ formula units for both Opx and Grt. The good agreement between measured and calculated ln $D^{Opx/Grt}_{Fe^{3+}}$ (Fig. 6) suggests that most of the observed $D^{Opx/Grt}_{Fe^{3+}}$ variability can effectively be explained by the influence of P and Na^{Opx} on Opx/Grt Fe^{3+} partitioning. Since the partitioning of Na in Opx is favored by ~~*temperature*~~ *T* in Cpx-bearing garnet peridotites (cf. Brey and Köhler 1990), the sodium terms in Equation~~s~~ (6) ~~and (7)~~ may also

Formatted: Italian (Italy)

Formatted: Italian (Italy)

incorporate some minor temperature effect. Attempts to consider explicitly T in the regressions were, however, unsuccessful.

The practical utility of Equation~~s~~ (6) ~~and (7)~~ as a geobarometer~~s~~ is hindered by the relatively small sensitivity of $\ln D_{Fe^{3+}}^{Opx/Grt}$ ~~and $\ln \frac{(Fe^{3+})^{Opx}}{(Fe^{3+})^{Grt}}$~~ to P and by difficult accurate measurement of Fe^{3+} concentrations in both Opx and Grt and of Na_2O in sodium-poor Opx. More interestingly, the equations can be used to estimate Fe^{3+} contents in orthopyroxenes from mantle peridotites in which only garnets have been analyzed for Fe^{3+}. The Fe^{3+} systematics expressed by Equation~~s~~ (6) ~~and (7)~~ may thus be of help in calculations of Fe_2O_3 budgets and fluxes during geochemical processes involving mantle rocks. A detailed investigation of these issues is beyond the scope of the present work. We only note that, given its relatively large modal proportion in Grt peridotites and significant affinity for Fe^{3+}, especially at moderate pressure, Opx may represent one of the most important Fe^{3+} carriers in Earth's ~~upper~~ lithospheric mantle.

Implications for mantle thermobarometry

Opx–Grt Fe–Mg exchange thermometry is based on the equilibrium

$$MgSiO_3 + \tfrac{1}{3}Fe_3Al_2Si_3O_{12} \rightarrow FeSiO_3 + \tfrac{1}{3}Mg_3Al_2Si_3O_{12} \quad (8)$$

Opx Grt Opx Grt

and depends on

$$\ln K_{D\,\mathrm{Fe^{2+}-Mg}}^{\mathrm{Grt-Opx}} = \ln \frac{\left(\mathrm{Fe^{2+}}\right)^{\mathrm{Grt}}}{\left(\mathrm{Fe^{2+}}\right)^{\mathrm{Opx}}} + \ln \frac{\left(\mathrm{Mg}\right)^{\mathrm{Opx}}}{\left(\mathrm{Mg}\right)^{\mathrm{Grt}}}. \quad (8)$$

In common practice, total Fe is treated as Fe^{2+}, therefore variations in ferric iron contents may affect temperature estimates. Following Nimis and Grütter (2010), the difference between the lnK_Ds calculated using total Fe and Fe^{2+} is given by

$$\ln K_{D\,\mathrm{Fe_{tot}-Mg}}^{\mathrm{Grt-Opx}} - \ln K_{D\,\mathrm{Fe^{2+}-Mg}}^{\mathrm{Grt-Opx}} = \ln \frac{\left(\mathrm{Fe_{tot}}\right)^{\mathrm{Grt}}}{\left(\mathrm{Fe_{tot}}\right)^{\mathrm{Opx}}} - \ln \frac{\left(\mathrm{Fe^{2+}}\right)^{\mathrm{Grt}}}{\left(\mathrm{Fe^{2+}}\right)^{\mathrm{Opx}}} = \ln \frac{\left(\mathrm{Fe^{2+}/Fe_{tot}}\right)^{\mathrm{Opx}}}{\left(\mathrm{Fe^{2+}/Fe_{tot}}\right)^{\mathrm{Grt}}} =$$

$$= \ln \frac{1-\left(\mathrm{Fe^{3+}/Fe_{tot}}\right)^{\mathrm{Opx}}}{1-\left(\mathrm{Fe^{3+}/Fe_{tot}}\right)^{\mathrm{Grt}}}. \quad (9)$$

The difference is null only if the $\frac{1-\left(\mathrm{Fe^{3+}/Fe_{tot}}\right)^{\mathrm{Opx}}}{1-\left(\mathrm{Fe^{3+}/Fe_{tot}}\right)^{\mathrm{Grt}}}$ ratio (hereafter, 'the iron ratio') is equal to unity, i.e., if Opx and Grt have the same Fe^{3+}/Fe_{tot} ratio. If this condition is not satisfied, then temperature estimates may be affected by changes in redox conditions, which will affect the Fe^{3+}/Fe_{tot} ratios in both minerals. Therefore, temperature estimates will only be accurate if Fe^{3+} partitioning and redox conditions in the mantle are comparable to those in the samples used to calibrate the thermometer or if the contributions of ferric iron in the two minerals compensate each other. The latter condition seems to hold for the ~~clinopyroxene~~Cpx–~~garnet~~ Grt thermometer, at least in sodium-free systems (Purwin et al. 2013). Based on experimental data at 5 GPa, Matjuschkin et al. (2014) suggested that this condition does not apply instead to the Opx–Grt thermometer, owing to strong preferential partitioning of Fe^{3+} into Grt, but they did not explore the role of pressure. Nimis and Grütter (2010) recalibrated the Opx–Grt thermometer empirically, using well-equilibrated mantle xenoliths as calibrants. They

found that a correction for pressure was needed, which was larger than expected from thermodynamic treatment of the Fe^{2+}–Mg exchange equilibrium, and suggested that this could be due to a systematic increase of the 'iron ratio' with depth. Our results support this hypothesis (Fig. ~~5~~7).

Using our observed Fe^{3+} partitioning systematics, we can now explore the effect of changing redox conditions on Opx–Grt thermometry on a quantitative basis. We have estimated potential variations induced on Opx–Grt temperature estimates (Nimis and Grütter 2010; hereafter TNG10) by fO_2 changes within the typical upper mantle range (Fig. ~~6~~8) for a set of xenoliths recording 'average' redox conditions for their respective depths of provenance (see Appendix for details of the calculations). The results (Table ~~4~~6) show that conditions more *oxidized* than average, within the typical fO_2 range of upper mantle peridotites, will produce negligible (at low *P*) to significant (at high *P*) *T* *underestimation* (over 100 °C), whereas conditions more *reduced* than average will always produce negligible *T* overestimation (< 40 °C).

Nimis and Grütter (2010) suggested that the commonly observed discrepancies between temperature estimates for mantle xenoliths using the Opx–Grt thermometer (TNG10) and the more redox-robust two-pyroxene thermometer of Taylor (1998; hereafter, TTA98), *using the same input P*, could be due either to redox effects (i.e., highly oxidized or highly reduced conditions) or to kinetic decoupling of the fast Fe–Mg and slow Ca–Mg equilibria due to transient heating. Our results now allow us to refine this premise. Figure ~~7~~ 9 shows TNG10 – TTA98 discrepancies for a few sets of xenoliths and the maximum potential bias due to redox effects, as derived from data in Table ~~4~~6. It appears that large *positive* TNG10 – TTA98 discrepancies, such as those shown by some Jagersfontein xenoliths (Fig. ~~7a~~9a), *cannot* be ascribed to redox variations and are most

likely accounted for by short-term thermal perturbations at depth and consequent disequilibrium. Large *negative* TNG10 – TTA98 discrepancies, such as those shown by some Jagersfontein, Slave or Nikos xenoliths (Fig. ~~7a~~9a–c) might in part be explained by a high fO_2, although disequilibrium or inconsistencies of the TNG10 thermometer for specific *P*–*T*–*X* conditions cannot be excluded.

If *P* is not kept fixed and both *T* and *P* are calculated by iteration according to common practice, the bias on temperature estimates can be considerably amplified. Even so, deviations due to strongly *reduced* conditions remain small in all cases ~~(≤~~ (< 65 °C) and both positive and negative in sign (Table ~~4~~6). This is because the increase of Al that is assumed to compensate~~s~~ for the decrease of Fe^{3+} in Opx (see Appendix) determines a decrease in the *P* calculated with the Opx–Grt barometer, which in turn tends to counteract the effect of decreasing total Fe on *T* estimates, owing to the positive dependency of the Opx–Grt thermometer on *P*. The calculated pressures still remain within only 0.3 GPa of those calculated with the original mineral compositions. Owing to the low Al in Opx coexisting with Grt, the Al-dependent *P* estimates may instead be extremely sensitive to the Al → Fe^{3+} substitution imposed by strongly *oxidized* conditions. In this case, the corresponding deviations on both *P* and *T* estimates become erratic, from strongly negative to strongly positive (Table ~~4~~6), depending on even modest differences in the original Al and Na contents in Opx.

The above exercises contain a significant degree of uncertainty, which derives from uncertainties in the oxybarometer of Stagno et al. (2013), which is used to readjust the Fe^{3+}/Fe_{tot} in the Grt, in the calibration of $\left(Fe^{3+}\right)^{Opx}/\left(Fe^{3+}\right)^{Grt}$ dependency on *P* and $Na_{2}O^{Opx}$, in the determination of Na_2O^{Opx} in the test samples, and in the mechanisms of

incorporation of Fe^{3+} in Opx and its effects on the activity of Al-components (see Appendix). Nonetheless, the results cast doubts on the reliability of many existing thermobarometric estimates for ~~clinopyroxene~~Cpx-free garnet harzburgites and Grt–Opx inclusions in diamonds, for which no independent, sufficiently accurate control on *T* and *P* estimates is generally possible (Nimis and Grütter 2010). It is noteworthy that any inconsistency in published *T* estimates for ~~clinopyroxene~~Cpx-free xenoliths based on Opx–Grt thermobarometry will be difficult to recognize, because the *T*–dependency of the Opx–Grt barometer will force the *P*–*T* points to move roughly along the same conductive geotherm on which the 'good' *P*–*T* points will fall (Brey and Köhler 1990).

Conclusions

The partitioning of Fe^{3+} between orthopyroxene and garnet in our set of mantle xenoliths shows no obvious relationship with temperature, but a ~~significant~~ppears to vary with ~~dependency on~~ pressure and ~~on~~ the Na_2O content of the orthopyroxene. This result is unlike previous observations for clinopyroxene–garnet pairs (cf. Woodland 2009; Purwin et al. 2013). As a consequence, the proportion of Fe^{3+} over total Fe in garnet-buffered mantle orthopyroxene is not uniformly low, as commonly assumed, but varies from 1% (in some high-*P* and low-Na orthopyroxenes) to at least 9% (in some low-*P*, relatively high-Na orthopyroxenes equilibrated with garnet). Some low-*P*, high-Na (high-*T*) mantle orthopyroxenes contain more Fe_2O_3 than coexisting garnets.

In common practice, redox conditions for garnet peridotites are estimated assuming that Fe^{3+} in Opx is negligible, so that fO_2 and activity of ferrosilite in Opx can simply be

calculated using total Fe concentrations (Gudmundsson and Wood 1995; Stagno et al. 2013). Recalculating ferrosilite activities in our samples using only Fe^{2+} instead of Fe_{tot}, produces a decrease in the calculated fO_2 of only 0.02 log units. Therefore, although higher than commonly assumed, the observed Fe^{3+}/Fe_{tot} ratios of up to 9% in Opx should not affect fO_2 estimates based on currently available oxybarometers.

The Fe^{3+} systematics observed in the studied xenoliths instead imply that the Opx–Grt Fe–Mg exchange thermometer is not robust against redox changes if total Fe is treated as Fe^{2+}. In particular, variations in Fe^{3+} partitioning with pressure in mantle peridotites may account for some systematic discrepancies observed between experimentally calibrated Opx–Grt and two-pyroxene thermometers (cf. Nimis and Grütter 2010). An approximate evaluation of errors on Opx–Grt temperatures due to redox effects predicts negligible deviations of *P*–*T* estimates for strongly reduced conditions, but potentially large deviations for strongly oxidized conditions, especially at very high pressure and when both *P* and *T* are calculated by iteration. Therefore, comparisons between *P*–*T* estimates derived using Opx–Grt and two-pyroxene thermometers, a common necessity when studying, for instance, both clinopyroxene-bearing and clinopyroxene-free peridotites, may be problematic if redox conditions are unknown. An experimental verification of Fe^{3+} partitioning systematics, e.g., by high-resolution Mössbauer analysis of Opx–Grt pairs re-equilibrated under controlled *P*–*T*–fO_2 and with varying Na_2O contents, would be desirable to derive a more robust evaluation and, hopefully, recalibration of Opx–Grt thermometers for mantle peridotites.

Acknowledgments We are grateful to Dante Canil for providing access to his original dataset. Sula Milani is thanked for her help in retrieving the old Mössbauer files. Formal

reviews by Bob Luth and two anonymous referees helped us to improve the paper. PN acknowledges financial support by MIUR ex60%. DAI thanks Igor Ashchepkov for providing some of the xenoliths used in this study and acknowledges financial support from the French CNRS, including PNP-INSU and PICS grants, and from the Australian Research Council including Research fellowship and grants in 1994-1998.

Appendix

Estimation of maximum bias on Opx–Grt temperature estimates due to changing redox conditions

Figure ~~6~~ 8 shows a compilation of existing fO_2 data for mantle xenoliths worldwide, recalculated using input *P*–*T* values obtained with the thermobarometer combinations recommended by Nimis and Grütter (2010). This choice significantly reduced the scatter of points (especially for Diavik) compared to earlier published versions of this plot (e.g., Stagno et al. 2013). Correction of Canil and O'Neill's (1996) Mössbauer data for different recoil-free fractions in Grt (Table 4) produced a slight decrease in calculated fO_2 of about 0.6 Δlog units. The plot shows the well-known overall decrease of FMQ-normalized oxygen fugacity with increasing mantle depth and a range for fO_2 at each depth.

From this compilation, we selected five xenoliths coming from different depths and recording 'average' redox conditions for their particular depths of provenance (Table ~~4~~6; Fig. ~~6~~8). We calculated the Opx–Grt temperatures for these xenoliths with the thermometer version of Nimis and Grütter (2010) (hereafter TNG10) at *P* given by the thermobarometers combination recommended by the same authors, using total Fe. The TNG10 thermometer was calibrated against a large set of mantle xenoliths from localities worldwide and should therefore be robust when applied to mantle rocks characterized by 'average' redox conditions. ~~Moreover, a~~All selected xenoliths showed very good agreement (ΔT < 60 °C) between thermometric estimates using the internally consistent thermometers recommended by Nimis and Grütter (2010)~~, which~~. This

indicates good equilibrium and also confirms that redox conditions in the xenoliths were indeed 'average' and compatible with the TNG10 thermometer calibration (cf. Nimis and Grütter 2010). ~~, therefore~~ Therefore the calculated *P*–*T* conditions should be reliable.

We then allowed fO_2 for each of the selected xenoliths to vary to the maximum and minimum values expected for the mantle at the corresponding depths, as indicated by our compilation in Figure ~~6~~8. We estimated the Fe^{3+}/Fe_{tot} ratios in the garnets at these maximum and minimum redox conditions by reversing the oxybarometer of Stagno et al. (2013), and those in the coexisting orthopyroxenes by using the Fe^{3+} partitioning systematics obtained in our work (cf. Equation ~~7~~6). The mineral compositions were modified using the new Fe^{3+}/Fe_{tot} ratios while keeping $K_{D_{Fe^{2+}-Mg}}^{Grt-Opx}$ unvaried—the latter depends essentially on *T*, therefore keeping it fixed corresponds to keeping *T* fixed. An increase (or decrease) in the Fe^{3+}/Fe_{tot} ratio thus determined a net increase (or decrease) in the total Fe content (actually Fe^{3+}), which was compensated by varying the Al^{3+} + Cr^{3+} contents by the same magnitude at constant Al/Cr ratio. Since the solid solution model for garnet which is used in the oxybarometer of Stagno et al. (2013) is sensitive to the Al and Cr contents ~~in the garnet~~, the Fe^{3+}/Fe_{tot} ratios had to be readjusted by iteration, although the effect of this correction was found to be minimal.

We then recalculated the TNG10 temperatures using the modified total Fe contents in both orthopyroxenes and garnets, either keeping *P* fixed or recalculating both *P* and *T* iteratively. The *P*–*T* estimates obtained for the selected xenoliths using the original mineral compositions and the compositions modified for their respective maximum and minimum redox conditions are reported in Table ~~4~~6. We emphasize that ~~, since~~ the aim of this exercise wa~~i~~s to assess 'relative' variations on final *P*–*T* estimates, and that

possible small interlab discrepancies in Fe^{3+}/Fe_{tot} ratios for Grt extracted from the literature and from this work ~~can~~do not significantly alter our results.

References

Annersten H, Olesch M, Seifert FA (1978) Ferric iron in orthopyroxene: a Mössbauer spectroscopic study. Lithos 11:301–310

Ballhaus C (1995) Is the upper mantle metal-saturated? Earth Planet Sci Lett 132:75–86

Boyd FR, Mertzman SA (1987) Composition and structure of the Kaapvaal lithosphere, southern Africa. In: Mysen BO (ed.) Magmatic Processes: Physiochemical Principles. Geochem Soc Spec Publ 1:13-24

Brey GP, Köhler T (1990) Geothermobarometry in four-phase lherzolites II. New thermobarometers, and practical assessment of existing thermobarometers. J Petrol 31:1353–1378

Canil D, O'Neill HStC (1996) Distribution of ferric iron in some upper-mantle assemblages. J Petrol 37:609–635

Caro G (2000) Petrography of the Kennedy Lake orangeite and its mantle xenoliths. Unpubl MSc thesis, University of British Columbia, 100 p

Carswell DA (1991) The garnet-orthopyroxene Al barometer: problematic application to natural garnet lherzolite assemblages. Mineral Mag 55:19–31

Cox KG, Smith MR, Beswetherick S (1987) Textural studies of garnet lherzolites: evidence of exsolution origin from high-temperature harzburgites. In: Nixon PH (ed.) Mantle Xenoliths. John Wiley & Sons, pp 537–550

Creighton S, Stachel T, Matveev S, Höfer HE, McCammon C, Luth RW (2009) Oxidation of the Kaapvaal lithospheric mantle driven by metasomatism. Contrib Mineral Petrol 157:491–504

Creighton S, Stachel T, Eichenberg D, Luth RW (2010) Oxidation state of the lithospheric mantle beneath Diavik diamond mine, central Slave craton, NWT, Canada. Contrib Mineral Petrol 159:645–657

Dollase WA (1975) Statistical limitations of Mössbauer spectral fitting. Am Miner 60: 257-264

Domeneghetti MC, Molin GM, Tazzoli V (1995) A crystal-chemical model for PBCA orthopyroxene. Am Mineral 80:253–267

Doucet LS, Ionov DA, Golovin AV (2013) The origin of coarse garnet peridotites in cratonic lithosphere: new data on xenoliths from the Udachnaya kimberlite, central Siberia. Contrib Mineral Petrol 165:1225–1242

Doucet LS, Peslier AH, Ionov DA, Brandon AD, Golovin AV, Goncharov AG, Ashchepkov IV (2014) High water contents in the Siberian cratonic mantle linked to metasomatism: an FTIR study of Udachnaya peridotite xenoliths. Geochim Cosmochim Acta 137:159–187

643 Frost DJ, McCammon CA (2008) The redox state of Earth's mantle. Annu Rev Earth Planet Sci
644 36:389–420
645 Goncharov AG, Ionov DA (2012) Redox state of deep off-craton lithospheric mantle: new data
646 from garnet and spinel peridotites from Vitim, southern Siberia. Contrib Mineral Petrol
647 164:731–745
648 Goncharov AG, Ionov DA, Doucet LS, Pokhilenko LN (2012) Thermal state, oxygen fugacity
649 and C–O–H fluid speciation in cratonic lithospheric mantle: New data on peridotite xenoliths
650 from the Udachnaya kimberlite, Siberia. Earth Planet Sci Lett 357-358:99–110
651 Gregoire M, Bell DR, le Roux AP (2003) Garnet lherzolites from the Kaapvaal craton (South
652 Africa): Trace element evidence for a metasomatic history. J Petrol 44:629–657
653 Gudmundsson G, Wood BJ (1995) Experimental tests of garnet peridotite oxygen barometry.
654 Contrib Mineral Petrol 119:56–67
655 Harley SL (1984) An experimental study of the partitioning of Fe and Mg between garnet and
656 orthopyroxene. Contrib. Mineral Petrol 86:359–373
657 Hops JJ, Gurney JJ, Harte B, Winterburn P (1989) Megacrysts and high temperature nodules
658 from the Jagersfontein kimberlite pipe. In: Ross j (ed) Kimberlites and related rocks, vol 2,
659 Their mantle/crust setting, diamonds and diamond exploration. Geol Soc Aus Spec Publ, vol
660 14, pp 759–770
661 Ionov DA (2002) Mantle structure and rifting processes in the Baikal-Mongolia region:
662 geophysical data and evidence from xenoliths in volcanic rocks. Tectonophysics 351:41–60
663 Ionov DA, Griffin WL, O'Reilly SY (1999) Off-cratonic garnet and spinel peridotite xenoliths
664 from Dsun-Bussular, SE Mongolia. In: Gurney JJ, Gurney JL, Pascoe MD, Richardson SH
665 (eds) Proc 7th Int. Kimb Conf, vol 1. RedRoof Design Cape Town, pp 383–390
666 Ionov DA, Doucet LS, Ashchepkov IV (2010) Composition of the lithospheric mantle in the
667 Siberian craton: New constraints from fresh peridotites in the Udachnaya-East kimberlite. J
668 Petrol 51:2177–2210
669 Kopylova MG, Caro G (2004) Mantle xenoliths from the southeastern Slave craton: evidence for
670 chemical zonation in a thick, cold lithosphere. J Petrol 45:1045–1067
671 Kopylova MG, Russel JK, Cookenboo H (1999a) Petrology of peridotite and pyroxenite
672 xenoliths from the Jericho kimberlite: Implications for the thermal state of the mantle
673 beneath the Slave craton, Northern Canada. J Petrol 40:79–104
674 Kopylova MG, Russel JK, Cookenboo H (1999b) Mapping the lithosphere below the north
675 central Slave craton. In: Gurney JJ, Gurney JL, Pascoe MD, Richardson SH (eds), J. B.
676 Dawson Volume, Proc 7th Int Kimb Conf, Red Roof Design Cape Town, pp 468–479

677 Lazarov M, Woodland AB, Brey GP (2009) Thermal state and redox conditions of the Kaapvaal
678 mantle: A study of xenoliths from the Finsch mine, South Africa. Lithos 112S:913–923
679 Luth RW, Canil D (1993) Ferric iron in mantle-derived pyroxenes and a new oxybarometer for
680 the mantle. Contrib Mineral Petrol, 113:236–248
681 Luth RW, Virgo D, Boyd FR, Wood BJ (1990) Ferric iron in mantle-derived garnets.
682 Implications for thermobarometry and for the oxidation state of the mantle. Contrib Mineral
683 Petrol 104:56–72
684 Malaspina N, Langenhorst F, Fumagalli P, Tumiati S, Poli S (2012) Fe^{3+} distribution between
685 garnet and pyroxenes in mantle wedge carbonate-bearing garnet peridotites (Sulu, China)
686 and implications for their oxidation state. Lithos 146-147:11–17
687 Matjuschkin V, Brey GP, Höfer HE, Woodland AB (2014) The influence of Fe^{3+} on garnet–
688 orthopyroxene and garnet–olivine geothermometers. Contrib Mineral Petrol 167:1–10
689 McCammon C, Kopylova MG (2004) A redox profile of the Slave mantle and oxygen fugacity
690 control in the cratonic mantle. Contrib Mineral Petrol 148:55–68
691 McCammon CA, Tennant WC, Miletich RM (2000) A new method for single crystal
692 measurements: Application to studies of mineral inclusions in diamonds. Hyper Inter 126:
693 241–245
694 McCammon CA, Griffin WL, Shee SR, O'Neill HStC (2001) Oxidation during metasomatism in
695 ultramafic xenoliths from the Wesselton kimberlite, South Africa: implications for the
696 survival of diamond. Contrib Mineral Petrol 141:287–296
697 Nickel KG (1989) Garnet-pyroxene equilibria in the system SMACCR (SiO_2-MgO-Al_2O_3-CaO-
698 Cr_2O_3): the Cr-geobarometer. In Ross J (ed) Kimberlites and related rocks, vol 2, Their
699 mantle/crust setting, diamonds and diamond exploration. Proc 4th Int Kimb Conf, Geol Soc
700 Aus Spec Publ, vol 14, pp 901–912
701 Nickel KG, Green DH (1985) Empirical geothermobarometry for garnet peridotites and
702 implications for the nature of the lithosphere, kimberlites and diamonds. Earth Planet Sci
703 Lett 73:158–170
704 Nimis P, Grütter H (2010) Internally consistent geothermometers for garnet peridotites and
705 pyroxenites. Contrib Mineral Petrol 159:411–427
706 Nimis P, Taylor WR (2000) Single-clinopyroxene thermobarometry for garnet peridotites. Part I.
707 Calibration and testing of a Cr-in-Cpx barometer and an enstatite-in-Cpx thermometer.
708 Contrib Mineral Petrol 139:541–554

O'Neill HStC, Wall VJ (1987) The olivine-orthopyroxene-spinel oxygen geobarometer, the nickel precipitation curve, and the oxygen fugacity of the earth's upper mantle. J Petrol 28:1169–1191

Pearson DG, Boyd FR, Haggerty SE, Pasteris JD, Field SW, Nixon PH, Pokhilenko NP (1994) The characterisation and origin of graphite in cratonic lithospheric mantle: a petrological carbon isotope and Raman spectroscopic study. Contrib Mineral Petrol 115:449–466

Pollack HN, Chapman DS (1977) On the regional variations of heat flow, geotherms and lithospheric thickness. Tectonophysics 38:279–296

Purwin H, Lauterbach S, Brey GP, Woodland AB, Kleebe H-J (2013) An experimental study of the Fe oxidation states in garnet and clinopyroxene as a function of temperature in the system CaO–FeO–Fe_2O_3–MgO–Al_2O_3–SiO_2: implications for garnet–clinopyroxene geothermometry. Contrib Mineral Petrol 165:623–639

Saltzer RL, Chatterjee N, Grove TL (2001) The spatial distribution of garnets and pyroxenes in mantle peridotites: Pressure-temperature history of peridotites from the Kaapvaal craton. J Petrol 42:2215–2229

Schmidberger SS, Francis D (1999) Nature of mantle roots beneath the North American craton: mantle xenolith evidence from Somerset Island kimberlites. Lithos 48:195–216

Shirey SB, Cartigny P, Frost DJ, Keshav S, Nestola F, Nimis P, Pearson DG, Sobolev NV, Walter MJ (2013) Diamonds and the Geology of Mantle Carbon. Rev Mineral Geochem 75:355–421

Smith D (1999) Temperatures and pressures of mineral equilibration in peridotite xenoliths: Review, discussion, and implications. In: Fei Y, Bertka CM, Mysen BO (eds) Mantle Petrology: Field Observations and high pressure experimentation: A tribute to Francis R. (Joe) Boyd. Geochem Soc Spec Publ, vol 6, pp 171–188

Stagno V, Ojwang DO, McCammon CA, Frost DJ (2013) The oxidation state of the mantle and the extraction of carbon from Earth's interior. Nature 493:84–88

Taylor WR (1998) An experimental test of some geothermometer and geobarometer formulations for upper mantle peridotites with application to the thermobarometry of fertile lherzolite and garnet websterite. Neues Jb Miner Abh 172:381–408

Woodland AB (2009) Ferric iron contents of clinopyroxene from cratonic mantle and partitioning behaviour with garnet. Lithos 112S:1143–1149

Woodland AB, Koch M (2003) Variation in oxygen fugacity with depth in the upper mantle beneath the Kaapvaal craton, Southern Africa. Earth Planet Sci Lett 214:295–310

742 Woodland AB, Peltonen P (1999) Ferric iron contents of garnet and clinopyroxene and estimated
743 oxygen fugacities of peridotite xenoliths from the Eastern Finland Kimberlite Province. In JJ
744 Gurney, JL Gurney, MD Pascoe, SH Richardson (eds) Proc 7th Int Kimb Conf, pp 904–911.
745 Red Roof Design Cape Town South Africa
746 Woodland AB, Ross CR (1994) A crystallographic and Mössbauer spectroscopy study of
747 $Fe_3Al_2Si_3O_{12}$-$Fe_3^{2+}Fe_2^{3+}Si_3O_{12}$ (almandine-skiagite) and $Ca_3Fe_2^{3+}Si_3O_{12}$-$Fe_3^{2+}Fe_2^{3+}Si_3O_{12}$
748 (andradite-skiagite) garnet solid solutions. Phys Chem Minerals 21:117–132
749 Yaxley GM, Berry AJ, Kamenetsky VS, Woodland AB, Golovin AV (2012) An oxygen fugacity
750 profile through the Siberian Craton — Fe K-edge XANES determinations of $Fe^{3+}/\sum Fe$ in
751 garnets in peridotite xenoliths from the Udachnaya East kimberlite. Lithos 140–141:142–151

Figure Captions

Fig. 1 Mössbauer spectra for orthopyroxene and garnet in two xenoliths showing different partitioning of Fe^{3+}.

Fig. 2 *P*–*T* estimates for mantle xenoliths studied in this work. Reference geotherms after Pollack and Chapman (1977). CO'N96 *P*–*T* values recalculated using compositional data in Canil and O'Neill (1996) and references therein. The fields of typical on-craton and off-craton garnet peridotites are shown for comparison.

Fig. 3 Opx–Grt Fe^{3+} partitioning systematics in mantle xenoliths. ~~Arrows indicate the effect of a correction for the presence of ca. 8% clinopyroxene in the Opx separate of sample FRB1350 of Canil and O'Neill (1996).~~ Error bars for ln*D*Fe^{3+} and Na_2O are at 1σ. Uncertainties on Na_2O were not reported for the literature samples and were calculated as $0.026 – 0.08 \cdot Na_2O$ (wt%), based on systematic relationships in our analyses using routine analytical conditions. Error bars for *P* and *T* were fixed to 0.4 GPa, 50 °C, and raised to 0.5 GPa, 70 °C for samples equilibrated at $T < 800$ °C and for some samples showing poor agreement between internally consistent thermometers (cf. Nimis and Grütter 2010). Dashed lines indicate unweighted linear regressions through the data.

Fig. 4 Fe^{3+} contents vs. tetrahedral Al (**a**) and Na contents (**b**) in the investigated Opx. The low-$^{[4]}$Al group corresponds to the on-craton xenoliths, the high-$^{[4]}$Al group consists of the off-craton Dariganga xenoliths. The dashed line in **b** separates the two groups. Spinel-bearing sample BY-18 falls off the trend shown by the other Dariganga samples.

Fig. 5 a Variation of Grt/Cpx ln*D*Fe^{3+} with reciprocal *T* in the investigated xenoliths. Shaded field: data for garnet peridotites after Woodland and Peltonen (1999), Woodland (2009), Lazarov et al. (2009), plus additional data from Canil and O'Neill (1996). As already pointed out by Canil and O'Neill (1996), the spinel-bearing, very low-*T* sample FRB1350 falls off the main trend. **b** Fe^{3+} distribution between Opx and Cpx.

Fig. ~~4~~ 6 Calculated (Equation 6) vs. measured Fe^{3+} partitioning between Opx and Grt. Data for Canil and O'Neill's (1996) samples that showed poor agreement between independent thermometric estimates were not considered in the regression. Error bars are at 1σ. Same symbols as in Fig. 2.

Fig. ~~5~~ 7 Variation in the Grt–Opx 'iron ratio' with ~~*T* and~~ *P* in mantle xenoliths. The relationship with *P* mimics that shown by *D*Fe^{3+} (cf. Fig. 3b). Same symbols as in Fig. 2.

Fig. ~~6~~ 8 Estimated fO_2 normalized to the FMQ buffer (Stagno et al. 2013) for garnet peridotite xenoliths worldwide. The EMOG/D curve corresponds to the enstatite–magnesite–graphite/diamond buffer along a cratonic geotherm (Stagno et al. 2013). The Fe–Ni precipitation curve after O'Neill and Wall (1987). Shaded field approximately indicates the diamond stability field. Dashed lines indicate the apparent typical fO_2 range at various mantle depths. Arrows connect five selected well-equilibrated samples recording 'average' fO_2 for their respective depth to corresponding maximum and minimum fO_2 values. Sources of compositional data: Siberia – Yaxley et al. (2012), Goncharov et al. (2012); Kaapvaal – Luth et al. (1990), Lazarov et al. (2009), Creighton et al. (2009), Canil and O'Neill (1996, as revisited in this work); N and SE Slave – McCammon and Kopylova (2004); Diavik – Creighton et al. (2010); Mongolia – this work.

Seventeen data showing poor agreement (>100 °C) between independent, internally consistent pyroxene thermometers (cf. Nimis and Grütter 2010) were excluded.

Fig. ~~7~~ 9 Differences between temperatures calculated with the Opx–Grt thermometer (Nimis and Grütter 2010; TNG10) and the two-pyroxene thermometer (Taylor 1998; TTA98) for mantle xenoliths from different localities. All xenoliths show good equilibrium between pyroxenes based on criteria in Nimis and Grütter (2010). Shaded fields indicate the declared uncertainty (2 standard errors of estimate, ±70 °C) of the TNG10 thermometer. Dashed lines indicate the maximum predicted bias on TNG10 for strongly reducing and, respectively, strongly oxidized conditions. Several xenoliths from Jagersfontein show positive deviations well beyond estimated uncertainties, suggesting disequilibrium due to transient heating. Xenolith data from Nimis and Grütter's (2010) compilation, specifically: Jagersfontein – Boyd (pers. comm. to H. Grütter), Cox et al. (1987), Boyd and Mertzman (1987), Hops et al. (1989), Mofokeng (1998), Smith (1999), Saltzer et al. (2001), Grégoire et al. (2003); Slave – Kopylova et al. (1999a,b), Caro (2000), McCammon and Kopylova (2004), Kopylova and Caro (2004); Nikos – Schmidberger and Francis (1999).